THÈSE

UNIVERSITE DE PAU ET DES PAYS DE L'ADOUR

École doctorale sciences exactes et leurs applications

Présentée et soutenue le 06 Septembre 2019

par **Joselin Deneb Peredo Mancilla**

pour obtenir le grade de docteur
de l'Université de Pau et des Pays de l'Adour
Spécialité : Génie Chimique

Adsorption et Séparation du Dioxyde de Carbone pour la Production du Biométhane : Etude des Performances de Charbons Actifs

MEMBRES DU JURY

RAPPORTEURS

• Simona Bennici	Chargée de Recherche, HDR / Université de Haute Alsace
• Jimmy Castillo	PR / Université Central du Venezuela

EXAMINATEURS

• Lionel LIMOUSY	PR / Université de Haute Alsace
• Daniel BROSETA	PR / Université de Pau et des Pays de l'Adour

DIRECTEURS

• David BESSIERES	PR / Université de Pau et des Pays de l'Adour
• Cécile HORT	MC HDR / Université de Pau et des Pays de l'Adour

UNIVERSITÉ DE PAU ET DES PAYS DE L'ADOUR

"It is change, continuing change, inevitable change,
that is the dominant factor in society today.
No sensible decision can be made any longer
without taking into account not only the world
as it is, but the world as it will be."
-Isaac Asimov

Abstract

Biomethane is a proven source of clean energy, it is one of the most cost-effective and environment-friendly substitute for natural gas and diesel. The European Union primary energy production from biomethane has folded by ∼23 times in a 5 years time period (2011-2016) making necessary to find new and improved solutions for the separation of methane (CH_4) and carbon dioxide (CO_2), main components of biogas.

In this context, the objective of this doctoral thesis is the determination of performance indicators such as the adsorption capacity and selectivity of activated carbons (ACs) for the CH_4/CO_2 separation. This work focuses on the adsorption properties of activated carbons for the methane/carbon dioxide separation. To this end, CH_4 and CO_2 pure gas experimental adsorption isotherms of activated carbons were obtained on a pressure range of 0.1 to 3 MPa) and temperatures ranging from 303 to 323 K. The first part of this thesis project consisted in the analysis of the CH_4 and CO_2 pure gas adsorption properties of 5 commercial activated carbons Using a set of five commercial activated carbons a linear relationship between the adsorbent surface area and the CO_2 adsorption capacity was determined. The micropore volume also showed a direct influence on the adsorption capacity.

The second part of this work consisted in the study of the carbon dioxide and methane adsorption behavior of biomass-based activated carbons. Using a series of 3 ACs that had been obtained from olive stones by different activation methods, the activation technique proved to be of mayor importance as it determines the textural and chemical properties of the adsorbent and thus its gas adsorption capacity.

Lastly, the CH_4/CO_2 adsorption selectivity of the 5 commercial activated carbons was calculated from the equimolar mixture adsorption isotherms. The selectivity factor was proven to be dependent on the sum of textural and chemical properties of the samples. Although, activated carbons with high average pore sizes and surface areas depicted higher adsorbed quantities it was on detriment of their selectivity. The selectivity was found to be better for the activated carbon showing an intermediate surface area and a narrow pore size distribution. In addition, the presence of sulfur functionalities was also found to improve the adsorption selectivity.

Overall, this work shows that activated carbons are competitive materials for the upgrading of biogas, displaying adsorption properties comparable to those of other commercially available materials.

Resumé

Le biométhane est une source d'énergie verte qui, de part son coût et son faible impact environnemental, peut être considéré comme une alternative au gaz naturel et au diesel. La production d'énergie primaire par l'Union Européenne, à partir du biométhane, a été multipliée par 23 en cinq ans (2011-2016), ce qui rend nécessaire et urgent la recherche de nouvelles solutions performantes pour l'épuration du biogaz, notamment la séparation du dioxyde de carbone (CO_2) du methane (CH_4).

Dans ce contexte, l'objectif de ce travail doctoral porte sur la détermination des indicateurs de performances (capacité d'adsoprtion, sélectivité) de charbons actifs (CAs) dans le contexte de la séparation méthane/dioxyde de carbone pour la production de biométhane. A cette fin, les isothermes d'adsorption de CH_4 et CO_2 ont été déterminées à partir d'un dispositif manométrique d'adsorption. Les mesures ont été effectuées à des températures de 303 et 323 K pour des pressions variant de 0.1 à 3 MPa. Dans un premier temps, l'étude a porté sur 5 échantillons commerciaux de CA différents. Les résultats montrent une corrélation entre la surface spécifique et la quantité de dioxyde de carbone adsorbée. En outre, le volume microporeux a un impact significatif lors des processus d'adsorption du CO_2 tandis que le volume des mésopores n'a pas d'effet direct.

Par ailleurs, l'étude complémentaire d'isothermes d'adsorption du CH_4 et du CO_2 purs à l'aide de trois charbons actifs, issus de noyaux d'olive, activés par différentes méthodes de synthèse, révèle que la méthode d'activation est déterminante pour modifier les propriétés chimiques et structurales des charbons actifs et donc accroitre leurs propriétés d'adsorption.

En outre, la sélectivité des CAs commerciaux pour la séparation CH_4/CO_2 a été calculée à partir des isothermes d'adsorption du mélange équimolaire CH_4/CO_2 à une température de 303 K et pour des pressions jusqu'à une pression de 3 MPa. Les résultats obtenus montrent qu'une surface spécifique élevée (<1500 m^2 g^{-1}) facilite l'adsorption du CO_2 mais réduit le facteur de sélectivité. En parallèle, une forte porosité conduit à une séparation moins efficace des deux gaz alors que la présence de groupes basiques en surface favorise les phénomènes d'adsorption du CO_2.

L'ensemble des résultats montre que les charbons actifs, étudiés dans ce travail de recherche, possèdent des propriétés d'adsorption comparables à celles des charbons actifs commerciaux et sont des matériaux compétitifs pour l'épuration du biogaz.

Acknowledgements

I want to express my gratitude to my thesis directors, David Bessières and Cécile Hort for the guidance, encouragement and support they provided me since the beginning of this project.

I would also like to thank the members of the jury for their thorough revision of this manuscript and the very valuable feedback they provided me.

Special thanks to the University of Pau and all the members of the laboratory of complex fluids and their reservoirs for making my time at this institution an extremely positive experience, in particular to Joseph Díaz for his always very valuable support. I am also grateful to my laboratory partners Olga Ortiz and Bich-Ngoc Ho for their help on this project but most importantly for their friendship.

I extend my gratitude to the Mulhouse Materials Science Institute, with special mention to Mejdi Jeguirim and Camelia Matei Ghimbeu for their participation on this work without which this work would have not been what it is.

I would like to thank the national council of science and technology (CONACyT) of México, the national bank of public works (BANOBRAS) and the secretary of energy (SENER) for the fellowship 293897 provided to pursue my PhD degree. I also acknowledge the CARNOT ISIFoR institute for the given research financing through the project EpurBioAdStoc.

I am grateful to my parents for their love, support and encouragement that have made me who I am today. I'm thankful to my partner Robin for making my life better in so many ways and finally, even-though if he can't read, to my dog Jack for filling my hours with joy.

Contents

List of Figures

List of Tables

CHAPTER 1

GENERAL INTRODUCTION

Introduction

The global energy consumption has more than tripled in a 50 years time period going from 3701 million tons of oil equivalent (Mtoe) in 1965 to 13511 Mtoe in 2017 [1]. Most of the energy being currently produce is supplied by fossil fuels, i.e. oil, coal and natural gas are accountable for up to 85% of the total primary energy consumption. As Figure 1.1 show, the increase of energy demand and global industrialization have resulted in a dramatic increase of carbon dioxide emissions with 99% of the total CO_2 emissions originated from the burning of fossil fuels (see Fig. 1.1) [2, 3, 4].

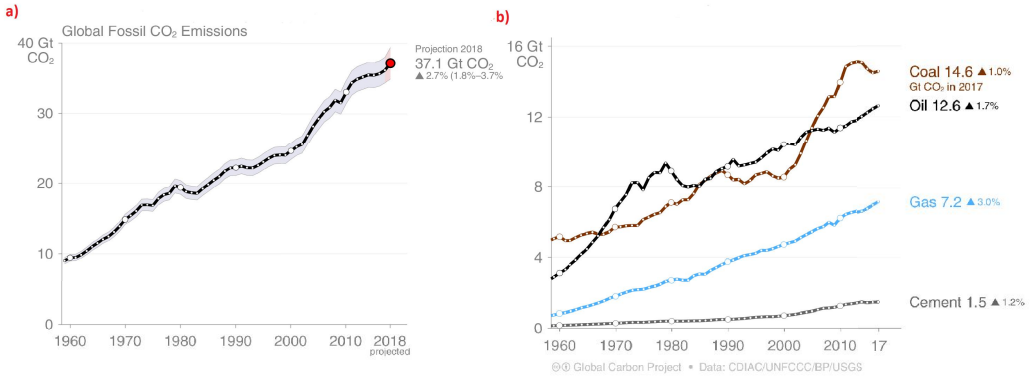

Figure 1.1: Emission of CO_2 from 1959 to 2017: a) Global emissions from fossil flues and industry and b) share of global fossil CO_2 emissions. The Data is reported in billions of tonnes of CO_2 per year ($GtCO_2$) [3].

A linear relationship between cumulative carbon dioxide emissions and projected global temperature change to the year 2100 has been reported [5]. In the efforts to mitigate climate change, strict global regulations of carbon dioxide emissions to the atmosphere have been established. Furthermore, the *Paris Agreement* main goal is to keep the global temperature rise well below 2 °C above pre-industrial levels. To achieve this goal, the emission concentration in the atmosphere of Greenhouse Gases (GHG) has to be decreased until zero net emissions before the end of the 21^{th} century. On this context, the European Union has to reduce its CO_2 emissions by 20% by the year 2020 in addition to increasing by 20% the share of energy production from renewable sources for the same year [6]. Preliminary data indicates a 22% reduction of emmitted CO_2 for the time period 2008-2017 whilst renewable energies share doubled from 8.5 to 17% on the same period of time (see Fig. 1.2) [7].

One of the most attractive renewable energy sources is the *waste-to-energy* pathway. Biogas is the mixture of gases obtained from the anaerobic digestion of organic matter from agricultural wastes, septic tanks, industrial wastewater and municipal

organic residues. The composition of Biogas varies for different subtracts, its main components are methane (CH_4) and carbon dioxide (CO_2) ranging from 44 to 68% and 24 to 40% respectively, it also presents minor impurities (concentration <1%) such as oxygen (O_2), nitrogen (N_2), benzene (C_6H_6), toluene (C_7H_8), hydrogen sulphide (H_2S) and siloxanes (R_2SiO, R=organic radical) [8].

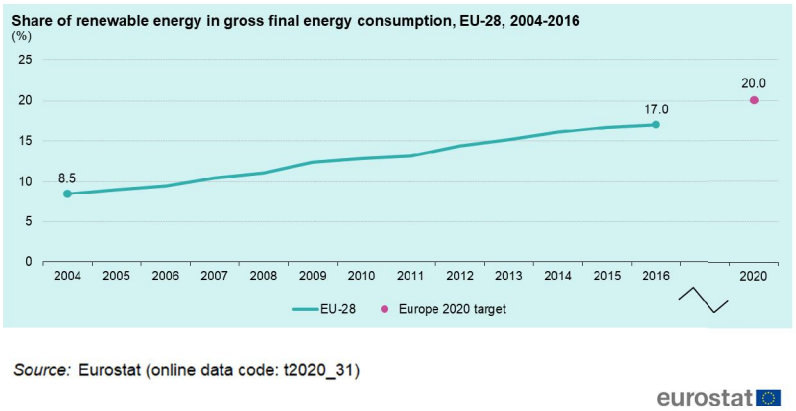

Figure 1.2: Primary production of energy from renewable sources on the EU-28 from 2004 to 2016 [7].

Energy from biogas production in Europe accounted for 16.1 million tons of oil equivalent (Mtoe) in 2016 [9]. The European Commission has evaluated the biogas production to be potentially folded at least 1.9 times by 2030 from that of 2016 [10]. Germany is the world leader in the deployment of biogas production with a primary biogas energy output of nearly 8 Mtoe in 2016, The United Kingdom and Italy produced approximatively 2 Mtoe followed by Czech Republic with 0.61 Mtoe. France ranks 5^{th} biogas energy producing country of the EU with 0.54 Mtoe in the same year [11].

Collected biogas is predominately flared to transform the CH_4 fraction into CO_2 thus reducing its global warming potential from 28 kg of CO_2 eq to 1 kg of CO_2 eq and in a minor degree it is directly burned to generate electricity with an efficiency of 38% [12]. However, the presence of gases other than methane in biogas make its transport and storage expensive and complicated, furthermore, the acid and/or corrosive behavior of some of its impurities lower the possibility to compress the gas while also adding technical difficulties due to possible corrosion and deposition in the combustion engines. Moreover, the calorific value of a biogas mixture containing between 60-65% is approximately 20–25 MJ m^{-3}-biogas whilst the Lower Calorific Value of methane (LCV) is 36 MJ m^{-3}-CH_4 (at STP conditions) [13]. It becomes then evident that an *upgrading process* aiming to remove the undesired compounds from biogas would be advantageous for many technological applications.

The treatment of biogas has two main steps:

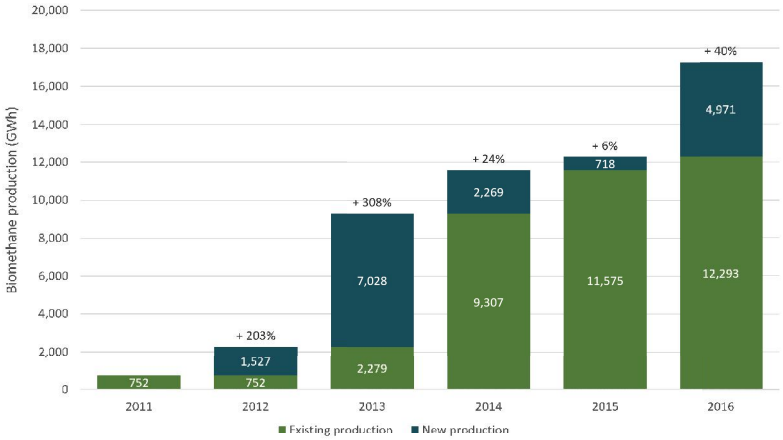

Figure 1.3: Evolution of biomethane production in Europe (GWh)

1. A cleaning process consisting in the removal of harmful and toxic impurities that can damage the grid, appliances or end-users such as hydrogen sulfide, siloxanes and volatile organic compounds (VOCs).

2. An upgrading process targeting the removal of carbon dioxide from biogas. Results in the increase of the biogas energy content.

From this treatment, a highly purified methane stream is obtained (purity >98%) known as renewable natural gas or biomethane. This gas can then be used as a vehicle fuel or more commonly, be inserted in the natural gas grid. The global demand of biomethane has rapidly increased in recent years (see Fig. 1.3) showing an impressive 40% growth on 2016 resulting in the need for cheaper and more efficient biogas treatment technologies [14].

In practice, the cleaning of biogas usually targets only the removal of hydrogen sulphide formed during the digestion process with many biogas plants having removal units based on a biological desulphurization method consisting in introducing a volume of air (or pure oxygen) into the digestor to enhace the biolgical oxidation of H_2S into elemental sulfur by specialized sulphate oxidizing bacteria [15, 13].

There are several available techniques for carbon dioxide removal from biogas including high pressure water scrubbing (HPWS) [16, 17], pressure swing adsorption (PSA) [18, 19], chemical scrubbing with amines (AS) [20, 21], membrane separation [22, 23] and biological upgrading [24, 25]. All of which show good performance for mid-scale applications with similar operational and investment costs. Due to their simplicity, water scrubbing techniques are the most wide spread option (see Fig. 1.4) [26]. On the other hand, chemical scrubbing has the advantage of giving higher purity rates for the produced biomethane with a lower methane slip. Meanwhile, membrane units are gaining terrain due to new studies that allow higher percentages of methane recovery [27]. In comparison, physical adsorption based technolo-

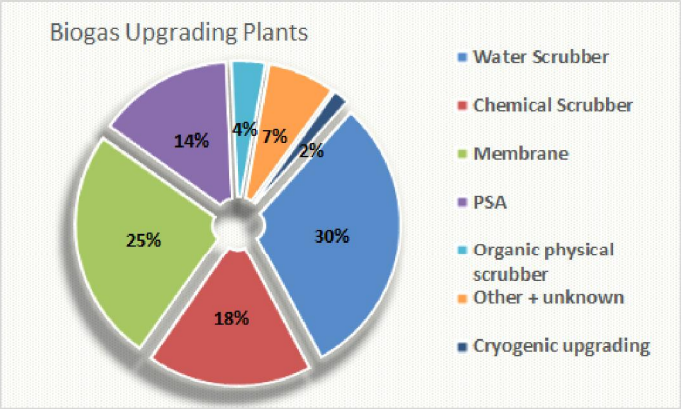

Figure 1.4: Development of biogas upgrading technologies on 2017. Data reported for 11 main biomethane producing countries [29]

gies have the additional advantage of not using watter and/or chemical products, therefore it does not produce any unwanted by-products, ease of regeneration, low investment and operational costs, as well as facility to scale to different volumes of biogas [28]

On Pressure Swing Adsorption the gas mixture enters in contact with a porous material that selectively adsorbs carbon dioxide allowing to subtract the methane stream from the system. To assure a high purity of methane several adsorption and desorption cycles are carried out by pressure shifts. The adsorption of carbon dioxide can be driven by kinetic or equilibrium factors. In the former case, a difference of the diffusing rates of the gas components govern the separation in such manner that the higher diffusing species are adsorbed. Equilibrium selectivity is based on the strength of binding forces between the adsorbent and the gases [30].

The present work is dedicated to the study of activated carbons as kinetic-based adsorbent materials for biogas upgrading. Activated carbons (ACs) are currently seen as a suitable alternative for carbon dioxide separation and capture because of their developed surface area and microporosity, inexpensive production, high CO_2 adsorption and low energy of regeneration [31].

There are several performance indicators of adsorbent materials that determine their applicability for industrial applications. Amongst them, the most important ones are adsorption capacity, selectivity and adsorption heat. The two first ones determine how much a component of a gas mixture will be retain inside the porous matrix while the adsorption heat is used as an indicator of how strongly the molecules are adsorbed and thus of the energy needed for regenerating the adsorbent.

On this context, the present PhD thesis has two main objectives:

1. To establish the factors that influence the first two performance indicators:

Adsorption capacity and selectivity.

2. Apply a chemical modification process to an activated carbon to improve its adsorption properties for biogas upgrading based on the results obtained within the framework of objective 1.

The manuscript, comprising 9 Chapters, is a compilation of published works (Chapters 4-7) and a yet to be published one (Chapter 8):

- Chapter 2 of this work, present the methodology employed for measuring the gas adsorption capacities and selectivities of activated carbons.
- Chapter 3 introduces the studied samples: five commercial and three biomass-based activated carbons. As this chapter shows, the adsorbent were characterized by several analytical and spectroscopic methods including Boehm titration, temperature programmed desorption and scanning electronic microscopy.
- Chapter 4 presents a review on methane and carbon dioxide adsorption on activated carbons. This bibliographic research shines light on the industrial importance of activated carbons for gas adsorption. This type of materials are currently being widely explore as a mean to store natural gas which would allow an alternative vehicular fuel known as adsorbed natural gas (ANG). On the other hand, the adsorption of carbon dioxide is important in the context of capturing industrial flue gas, usually expelled at low partial pressures. The main objective of this Chapter, is to show the importance of choosing an activated carbon with adequate textural and chemical properties for obtaining good adsorption performances for CH_4 and CO_2 adsorption. The presented review was published in the form of a chapter in the book entitled "Char and Carbon Materials Derived from Biomass" edited by *Elsevier Inc* [32].
- Chapter 5 follows with the experimental study of the effect of textural properties (i.e. surface area and micropore volume) on the CH_4 and CO_2 pure gas adsorption of activated carbons. The pure gas adsorption isotherms were obtained for a set of five AC on an extend pressure range (0 to 3 MPa) at two workinf temperatures (303 and 323 K). This work it can also be found as an original research article on the *Journal of Chemical Engineering Data* [33].
- Once the effect of textural properties has been established, Chapter 6 aims to explain these features develop during the activation process of a carbonaceous precursor. The CH_4 and CO_2 adsorption isotherms (0-3 MPa and 303 K) were obtained for three biomass-based (olive-stones) activated carbons synthesized by different activation agents (H_3PO_4, H_2O and C_2O). With this study, adds

up to the literature searching to optimize the production of activated carbons with appropriate porosity for adsorption of carbon dioxide and methane, the results were published on *Energies* [34].

- The second performance indicator is studied on Chapter 7. The selectivity of an adsorbent is a measurement of its preference to adsorb one gas over another from a gas mixture. In the case of biogas upgrading, the ideal material would be highly selective towards carbon dioxide adsorption over methane. For this reason, the CH_4/CO_2 selectivity factor of the 5 commercial ACs from Chapter 5 is here reported. To this end the gas mixture adsorption up to 3 MPa was experimentally measured at 303 K. The role of both textural and chemical properties on the ACs separation capacity is also explored. This work has been published on the *Journal of Environmental Chemical Engineering* [32].

- Chapter 8 covers the second objective of the thesis project. Base on the results gathered on the previous Chapters, the surface chemistry of a commercial activated carbon was modified to enhance its adsorption properties for biogas upgrading. The sample was oxidized with HNO_3 and treated with ammonia (NH_3) for the insertion of nitrogen (N) containing surface groups. The CH_4, CO_2 and CH_4/CO_2 gas adsorption isotherms were obtained for the modified AC (0-3 MPa, 303 K). The results show a reduced pure gas adsorption capacity compensated by a remarkable increase of the selectivity of the adsorbent.

- The final Chapter gives a general outlook of the main results obtained on this work and the conclusions draw from them.

The adsorption experiments here described were carried between August 2016 and June 2019 out at the *Laboratoire des Fluides Complexes et Leurs Reservoirs* (LFC R) in collaboration with the Laboratoire de Thermique Energétique et Procédés (LaTEP), both located at the Université de Pau et des Pays de l'Adour.

Introduction Générale

La consommation mondiale d'énergie a triplé au cours des 50 dernières années. Elle a augmenté de 3701 à 13511 millions de tonnes équivalent pétrole (Mtep) sur la période 1965 à 2017 [1]. La majorité de l'énergie produite est issue des combustibles fossiles (le pétrole, le gaz naturel et le charbon) qui représentent actuellement 85% de la consommation totale d'énergie primaire. Comme l'indique la Figure 1.5, l'augmentation de la demande énergétique ainsi que l'acceleration de l'industrialisation moderne sont la cause d'une forte hausse des émissions de dioxyde de carbone dans l'atmosphere. 99% de ces emissions de CO2 proviendraient de la combustion des carburants fossiles (voir Fig.1.5) [2, 3, 4].

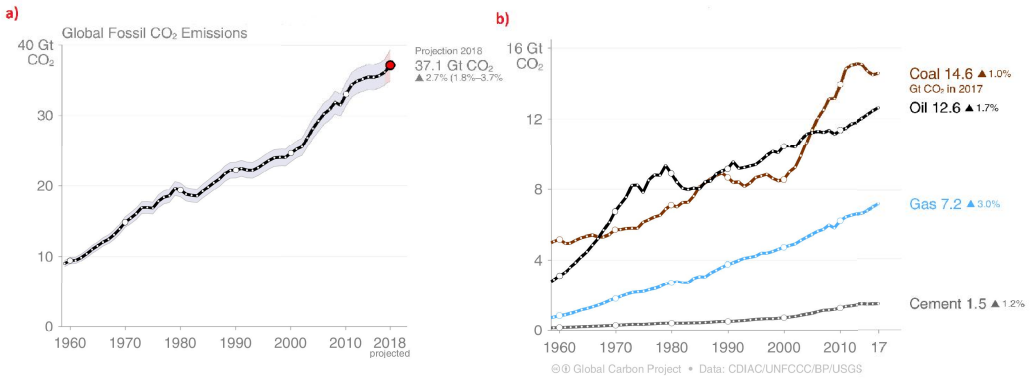

Figure 1.5: Émissions globales de CO_2 dans la période 1959-2017: a) Émissions liés aux combustibles fossiles et aux activités industrielles, b) Principales sources d'émission de CO_2. Les données sont présentées en millions de tonnes de CO_2 par ans ($GtCO_2$) [3].

Il existe une corrélation directe entre les émissions cumulatives du dioxyde de carbone et le changement de la température moyenne de la Terre [5]. Par conséquent, des mesures ont été réalisées pour atténuer ce changement climatique au travers de législations renforcées au niveau international. A titre d'exemple, l'objectif principal de l'Accord de Paris signé en 2008, était de maintenir l'augmentation de température nettement en dessous de 2 °C par rapport aux niveaux préindustriels. Pour y parvenir, il faudrait arriver à zero émission de gaz à effet de serre avant l'année 2100. Dans ce contexte, l'Union Européenne (UE) s'est engagée à réduire ses émissions de CO_2 de 20% (par rapport aux niveaux de 1990) et à porter à 20 % la part des énergies renouvelables dans la consommation d'énergie de l'UE [6]. Des données préliminaires, publiées en 2019 indiquent qu'une réduction de 22% des émissions de CO_2 et une hausse de la production d'énergies renouvelables de 8,5 à 17% à été obtenue entre 2004 et 2016 (voire Fig. 1.6) [7].

La valorisation de déchets pour la production d'énergie est une des voies les plus

prometteuses pour la production d'énergie renouvelable. La fermentation anaérobie de la matière organique produit un mélange gazeux nommé biogaz dont les sources peuvent être constituées de déchets agricoles, de déchets des fosses septiques, d'eau résiduaire industrielle et de déchets organiques ménagers. La composition du biogaz dépend de la source de la matière organique (substrat) utilisé. Le biogas est constitué principalement de méthane (CH_4) et de dioxyde de carbone (CO_2) avec des compositions variant 44 à 60% et 24 à 40% respectivement. Il contient aussi des impuretés comme l'azote (N_2), l'oxygène moléculaire (O_2), le benzène (C_6H_6), le toluène (C_7H_8), le sulfure d'hydrogène (H_2S) et des siloxanes (R2SiO, R= radical organique) [8].

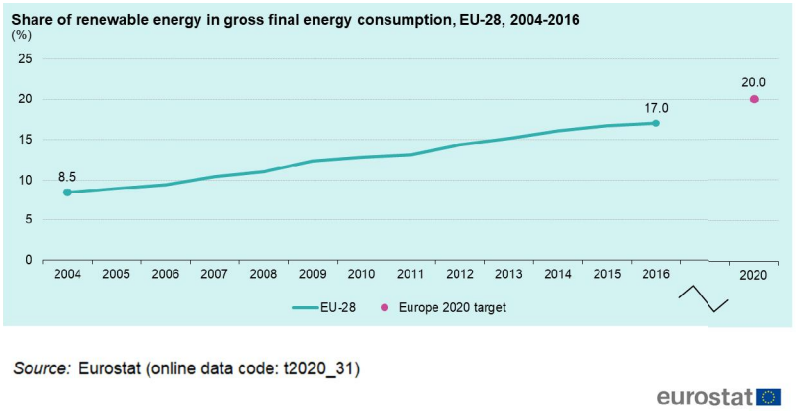

Figure 1.6: Production primaire d'energies renouvelables dans les 28 pays de l'Union Européenne (EU-28) entre 2004 et 2016 [7].

La quantité d'énergie obtenue par la production du biogaz en Europe était de 16,1 millions de tonnes équivalent pétrole (Mtep) en 2016 [9]. Par ailleurs, la Commission Européenne a estimé une augmentation potentielle de la production d'énergie au moyen du biogaz pour 2030 d'au moins 1,9 fois celle de 2016 [10]. L'Allemagne est le leader mondial de la production de biogaz avec 8 Mtep produits en 2016. Elle est suivie par le Royaume Uni et l'Italie avec une production cumulée de 2 Mtep. En quatrième et cinquième position se situent la République Tchèque et la France avec respectivement 0,61 et 0,54 Mtep [11].

Le biogaz collecté est majoritairement brûlé pour transformer le contenu de méthane en dioxyde de carbone, ce qui réduit son potentiel de réchauffement climatique de 28 kg éq. CO_2 à 1 kg éq. CO_2. De façon moins systématique, il est aussi brulé pour produire de l'énergie électrique avec un rendement énergétique de 38% [12]. Cependant, la présence de gaz autres que le méthane dans le biogaz rend son transport et son stockage coûteux et compliqué. En outre, il contient des composés acides et/ou corrosifs qui compliquent sa compression et accroissent les difficultés techniques dues aux risques d'abrasion et d'encrassement dans les systèmes de combustion. Par ailleurs, le pouvoir calorifique d'un mélange de biogaz

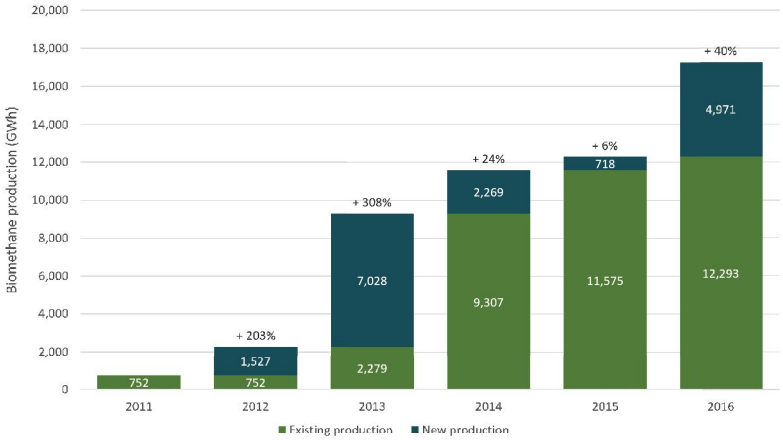

Figure 1.7: Production d'énergie primaire à partir de biogaz en Europe (GWh)

contenant de 60 à 65% de méthane se situe entre 20 à 25 MJ m^{-3}-biogaz tandis que celui du méthane est de 36 MJ m^{-3}-CH_4 dans les conditions de pression et de température normales (TPN) [13]. Il y a donc plusieurs avantages à mettre en œuvre un procédé d'épuration/séparation orienté vers l'élimination des composés indésirables du biogaz pour faciliter sa conversion énergétique.

L'épuration du biogaz produit un méthane hautement purifié (pureté >98%) appelé gaz naturel renouvelable ou biométhane. Celui-ci peut donc être inséré dans le réseau de gaz naturel ou alternativement, utilisé comme carburant automobile. La demande globale de biométhane a explosé au cours de la dernière décade (voir Fig. 1.3) créant ainsi la nécessité de technologies nouvelles et performantes pour l'épuration pour répondre à ce besoin énergétique [14].

Il existe plusieurs techniques disponibles sur le marché pour séparer le dioxyde de carbone du biogaz notamment: le lavage à l'eau [15, 16, 17], l'adsorption par variation de pression [18, 19], le lavage aux amines [20, 21], la séparation membranaire [22, 23], ou encore l'épuration biologique [24, 25]. L'ensemble de ces technologies montre de bonnes performances pour les applications à moyenne échelle avec des coûts d'investissement et d'opération similaires. Cependant, parmi ces procédés de traitement le lavage à l'eau est la méthode la plus utilisée (voire Fig. 1.8), tandis que le lavage aux amines permet une meilleure purification du biométhane. En outre; la séparation membranaire permet l'obtention de pourcentages de récupération très élevés [27]. Néanmoins, l'adsorption physique par variation de pression ou PSA (Pressure Swing Adsorption) possède des avantages supplémentaires tels que la non production de dérivés indésirables, pas d'utilisation d'eau ni de substances chimiques, dépense énérgetique faible et enfin adaptation aisée de ce système pour différents volumes de biogaz [28].

La méthode PSA consiste à séparer le dioxyde de carbone du biogaz en utilisant son affinité chimique ainsi que ses proprietés physiques tels que son diamètre

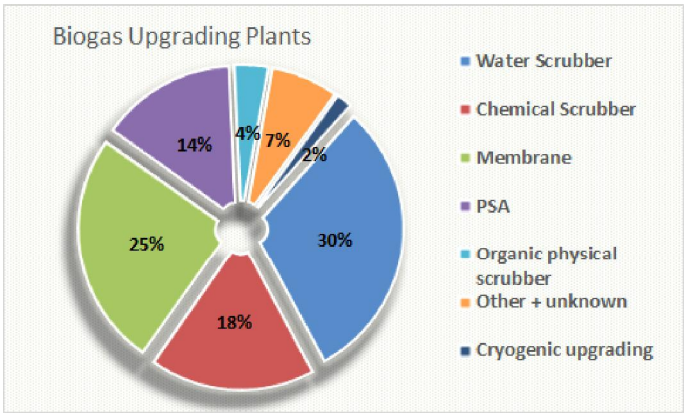

Figure 1.8: Des principales techniques d'épuration de biogaz en 2017 [29].

cinétique et sa polarisabilité vis-à-vis d'un matériau solide poreux. Pour cela, le mélange gazeux du biogaz est introduit sous pression (3 bar) dans un réacteur contentant l'adsorbant, le CO_2 est donc retenu dans la matrice poreuse alors que le méthane traverse le réacteur pour être évacué. Lorsque la pression diminue, le CO_2 est libéré et l'adsorbat est régénéré, ce qui permet le démarrage d'un nouveau cycle d'adsorption/desorption [30].

Ce travail de thèse présente consiste à une analyse approfondie de l'application des charbons actifs dans l'épuration du biogaz par adsorption, grâce à l'étude d'indicateurs de performance d'adsorption (capacité d'adsorption et sélectivité) en fonction des propriétés texturales et chimiques. Les charbons actifs (CAs) sont caractérisés par une grande surface spécifique, une hétérogénéité chimique et des propriétés structurales adaptables (volume de micropores, distribution des tailles de pores). Ils ont l'avantage de pouvoir être fabriqués à partir de tout matériau contenant un fort pourcentage de carbone et par conséquent un faible pourcentage en matière inorganique ce qui permet l'utilisation de déchets tels que les résidus agricoles comme la noix de coco, la coque d'amande, l'écorce de riz, les déchets forestiers tels que le bois et le charbon de bois ou encore les sous-produits industriels et pétroliers [35]. Les CAs sont donc perçus comme des matériaux adsorbants très prometteurs pour la séparation méthane/dioxyde de carbone.

Ce manuscrit de thèse est structuré de la façon suivante :

- le chapitre 2 introduit les dispositifs expérimentaux utilisés durant le développement de ce travail de thèse ainsi que la méthodologie appliquée pour l'obtention des isothermes d'adsorption.
- le chapitre 3 detaille la caractérisation physico-chimique des huit CAs étudiés tout au long de ce travail. Cinq CAs sont des CAs commerciaux et trois autres ont été obtenus par l'activation de noyaux d'olives.
- le chapitre 4 offre un aperçu des facteurs qui affectent l'adsorption et le stock-

age du méthane ainsi que du dioxyde de carbone par des charbons actifs. Ce chapitre a été publié sous la forme d'un chapitre de livre intitulé « Char and Carbon Materials Derived from Biomass » de l'éditeur Elsevier Inc. [32] ;

- le chapitre 5 corrrespond à une étude expérimentale sur l'influence des propriétés structurales des CAs, telles que l'aire superficielle et le volume microporeux des CAs lors de l'adsorption du méthane et du dioxyde de carbone. Ce chapitre a été publié dans le *Journal of Chemical and Engineering Data* [33] ;

- le 6ème chapitre explore l'impact de la méthode d'activation sur les propriétés chimiques et texturales des CAs et par conséquent sur leurs propriétés d'adsorption. Il présente des résultats expérimentaux d'adsorption du CH_4 et du CO_2 purs par des charbons actifs non commerciaux (publié dans la revue *Energies*)[34] ;

- le chapitre 7 montre les isothermes d'adsorption obtenues pour un mélange CH_4/CO_2 50-50% par des charbons actifs commerciaux ce qui permet d'analyser le comportement d'adsorption en présence de ces deux gaz (publié dans le *Journal of Environmental Chemical Engineering* [**?**]) ;

- le chapitre 8 expose des résultats préliminaires concernant la séparation d'un mélange CH_4/CO_2 à l'aide d'un charbon actif modifié par oxydation et traitement à l'ammoniac (NH_3). L'optention des isothermes d'adsorption des gaz purs ainsi que ceux d'un mélange équimolaire CH_4/CO_2 indiquent une augmentation de l'affinité entre le dioxyde de carbone et le CA modifié et donc l'accroissement de la sélectivité. Cet intéressant résultat, en première approximation, peut être corrélé avec l'insertion de groupes basiques à la surface du CA modifié.

- pour conclure, le chapitre 8 récapitule les principaux résultats et conclusions obtenus.

Cette thèse expérimentale a eu pour cadre le groupe Interfaces Systèmes Dispersés du Laboratoire des Fluides Complexes et leurs Réservoirs (LFCR, UMR5150), en collaboration avec le Laboratoire de Thermique, Energétique et Procédés (LaTEP) de l'Université de Pau et des Pays de l'Adour (UPPA). Le LFCR est une unité mixte de recherche (CNRS, Total) dont la majeure partie des activités est centré autour de l'étude des propriétés des énergies fossiles et renouvelables. Le LaTEP développe des activités de recherche axées sur les procédés pour l'environnement et notamment le traitement des gaz ainsi que sur le stockage et la distribution de l'énergie. Cette étude sur la purification des biogaz s'intègre dans ces thématiques.

1.1 Bibliography

[1] Siyi Kan, Bin Chen, and Guoqian Chen. Worldwide energy use across global supply chains: Decoupled from economic growth? *Applied Energy*, 250(February):1235–1245, 2019.

[2] İlhamiYıldız Yıldız. Fossil Fuels. In *Comprehensive Energy Systems Vol. 1*, pages 521–567. 2018.

[3] Global Carbon Project. Carbon budget and trends. Technical report, 2018.

[4] Seul Yi Lee and Soo Jin Park. A review on solid adsorbents for carbon dioxide capture. *Journal of Industrial and Engineering Chemistry*, 23:1–11, 2015.

[5] IPCC. *Climate Change 2014 Synthesis Report. Contribution of Working Groups I, II and III to the Fifth Assessment Report of the Intergovernmental Panel on Climate Change*. Geneva, Switzerland, 2014.

[6] Georgios Amanatidi and S. European policies on climate and energy towards 2020, 2030 and 2050. Technical Report January 2019, Policy Department for Economis, Scientific and Quality of Life Policies, 2019.

[7] eurostat. Statistics Explained. Renewable energy statistics. Technical report, 2020.

[8] S. Rasi, A. Veijanen, and J. Rintala. Trace compounds of biogas from different biogas production plants. *Energy*, 32(8):1375–1380, 2007.

[9] European Biogas Association (EBA). European Biogas Association Annual Report 2018. 2018.

[10] European Comission. Optimal use of biogas from waste streams An assessment of the potential of biogas from digestion in the EU beyond 2020 digestion in the EU beyond 2020 Optimal use of biogas from waste streams. 2017.

[11] EurObserv'er. Biogas Barometer 2017. (November):14, 2017.

[12] Katherine Starr, Gara Villalba, and Xavier Gabarrell. Upgraded biogas from municipal solid waste for natural gas substitution and CO_2 reduction - A case study of Austria, Italy, and Spain. *Waste Management*, 38(1):105–116, 2015.

[13] Irini Angelidaki, Laura Treu, Panagiotis Tsapekos, Gang Luo, Stefano Campanaro, Henrik Wenzel, and Panagiotis G. Kougias. Biogas upgrading and utilization: Current status and perspectives. *Biotechnology Advances*, 36(2):452–466, 2018.

[14] European Biogas Association (EBA). EBA Statistical Report. 2017.

[15] E. Ryckebosch, M. Drouillon, and H. Vervaeren. Techniques for transformation of biogas to biomethane. *Biomass and Bioenergy*, 35(5):1633–1645, 2011.

[16] Bo Cuimei, Guo Wei, Tang Chao, Li Jun, and Lu Xiaohua. Dynamic Control Design and Simulation of Biogas Pressurized Water Scrubbing Process. *IFAC-PapersOnLine*, 51(18):560–565, 2018.

[17] Rimika Kapoor, P. M.V. Subbarao, Virendra Kumar Vijay, Goldy Shah, Shivali Sahota, Dhruv Singh, and Mahesh Verma. Factors affecting methane loss from a water scrubbing based biogas upgrading system. *Applied Energy*, 208(September):1379–1388, 2017.

[18] P. Brea, J. A. Delgado, Vicente I. Águeda, and María A. Uguina. Comparison between MOF UTSA-16 and BPL activated carbon in hydrogen purification by PSA. *Chemical Engineering Journal*, 355(July 2018):279–289, 2019.

[19] Saeed Ghanbari and Catherine H. Niu. Characteristics of oat hull based biosorbent for natural gas dehydration in a PSA process. *Journal of Natural Gas Science and Engineering*, 61(November 2018):320–332, 2019.

[20] S. Sutanto, J. W. Dijkstra, J. A.Z. Pieterse, J. Boon, P. Hauwert, and D. W.F. Brilman. CO2removal from biogas with supported amine sorbents: First technical evaluation based on experimental data. *Separation and Purification Technology*, 184:12–25, 2017.

[21] Nattee Akkarawatkhoosith, Amaraporn Kaewchada, and Attasak Jaree. High-throughput CO 2 capture for biogas purification using monoethanolamine in a microtube contactor. *Journal of the Taiwan Institute of Chemical Engineers*, 98:113–123, 2019.

[22] Sina Gilassi, Seyed Mohammad Taghavi, Denis Rodrigue, and Serge Kaliaguine. Optimizing membrane module for biogas separation. *International Journal of Greenhouse Gas Control*, 83(September 2018):195–207, 2019.

[23] Michal Žák, Helena Bendová, Karel Friess, Jason E. Bara, and Pavel Izák. Single-step purification of raw biogas to biomethane quality by hollow fiber membranes without any pretreatment – An innovation in biogas upgrading. *Separation and Purification Technology*, 203(February):36–40, 2018.

[24] María del Rosario Rodero, Raquel Lebrero, Esteban Serrano, Enrique Lara, Zouhayr Arbib, Pedro A. García-Encina, and Raúl Muñoz. Technology validation of photosynthetic biogas upgrading in a semi-industrial scale algal-bacterial photobioreactor. *Bioresource Technology*, 279(December 2018):43–49, 2019.

[25] Dana Pokorna, Zdenek Varga, Dominik Andreides, and Jana Zabranska. Adaptation of anaerobic culture to bioconversion of carbon dioxide with hydrogen to biomethane. *Renewable Energy*, 142:167–172, 2019.

[26] Christophe E. Wylock and Wojciech M. Budzianowski. Performance evaluation of biogas upgrading by pressurized water scrubbing via modelling and simulation. *Chemical Engineering Science*, 170:639–652, 2017.

[27] Xiao Yuan Chen, Hoang Vinh-Thang, Antonio Avalos Ramirez, Denis Rodrigue, and Serge Kaliaguine. Membrane gas separation technologies for biogas upgrading. *RSC Advances*, 5(31):24399–24448, 2015.

[28] Renju Zacharia, Luis Fernando Gomez, Richard Chahine, Daniel Cossement, and Pierre Benard. Thermodynamics and kinetics of CH4/CO2binary mixture separation by metal-organic frameworks from isotope exchange and adsorption break-through. *Microporous and Mesoporous Materials*, 263(November 2017):165–172, 2018.

[29] D. M. Wall, M. Dumont, and J. D. Murphy. *Green gas - Facilitating a future green gas grid through the production of renewable gas*, volume 2. 2018.

[30] S. W. Rutherford and J. E. Coons. Adsorption dynamics of carbon dioxide in molecular sieving carbon. *Carbon*, 41(3):405–411, 2003.

[31] Supaporn Rattanaphan, Thanyada Rungrotmongkol, and Panita Kongsune. Biogas improving by adsorption of CO2 on modified waste tea activated carbon. *Renewable Energy*, 2019.

[32] Deneb Peredo-Mancilla, Camelia Matei Ghimbeu, Bich-Ngoc Ho, Mejdi Jeguirim, Cecile Hort, and David Bessieres. Comparative study of the CH_4/CO_2 Adsorption Selectivity of Activated Carbons for Biogas Upgrading. *Journal of Environmental Chemical Engineering*, 7(5):103368, 2019.

[33] Deneb Peredo-Mancilla, Cecile Hort, Mejdi Jeguirim, Camelia Matei Ghimbeu, Lionel Limousy, and David Bessieres. Experimental Determination of the CH ₄ and CO ₂ Pure Gas Adsorption Isotherms on Different Activated Carbons. *Journal of Chemical & Engineering Data*, page acs.jced.8b00297, 2018.

[34] Deneb Peredo-Mancilla, Imen Ghouma, Cecile Hort, Camelia Matei Ghimbeu, Mejdi Jeguirim, and David Bessieres. CO2 and CH2 adsorption behavior of biomass-based activated carbons. *Energies*, 11(11):1–13, 2018.

[35] Catherine Ayral. *Elimination de polluants aromatiques par oxydation catalytique sur charbon actif.* PhD thesis, Université de Toulouse, 2009.

CHAPTER 2

METHODOLOGY

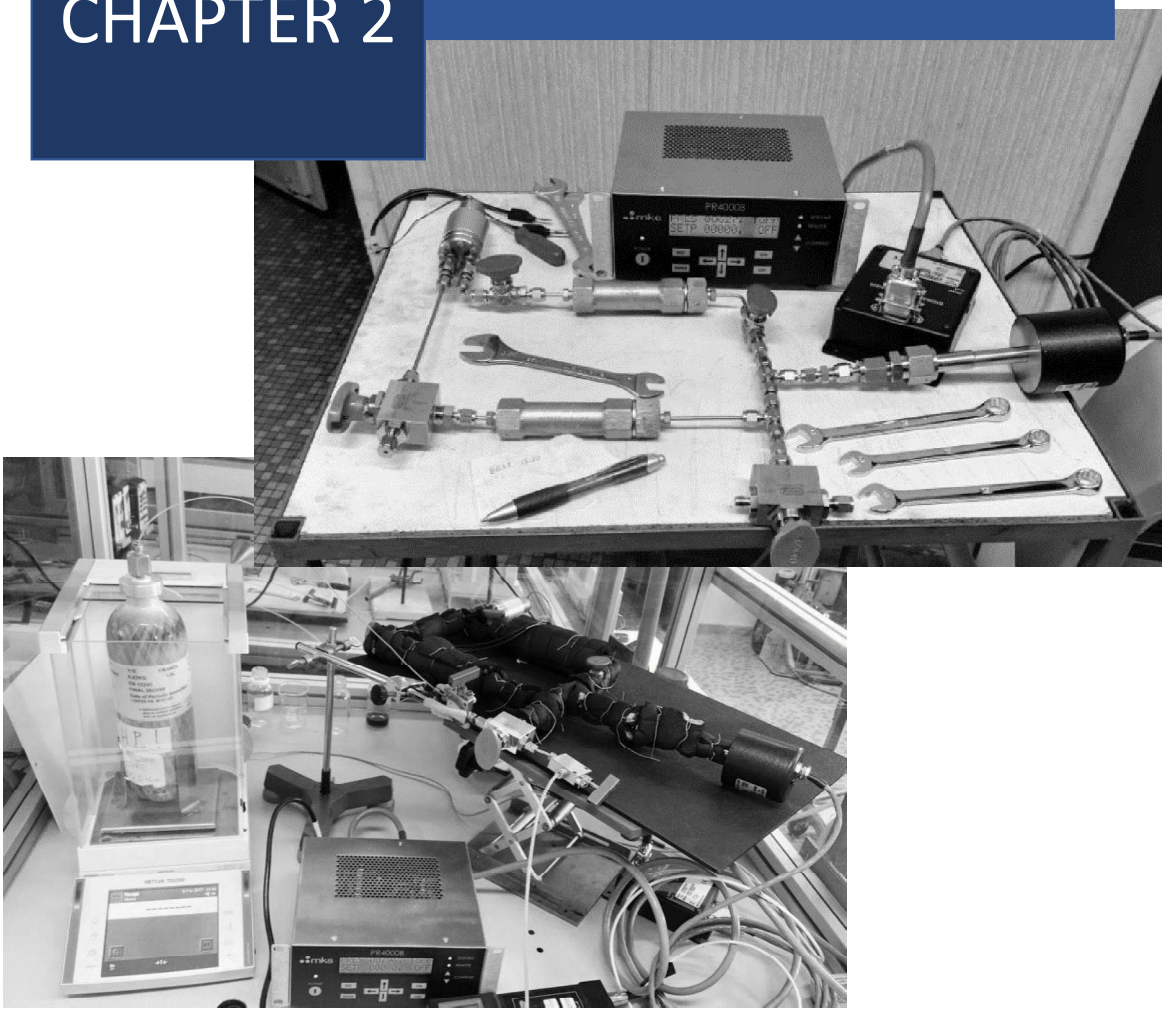

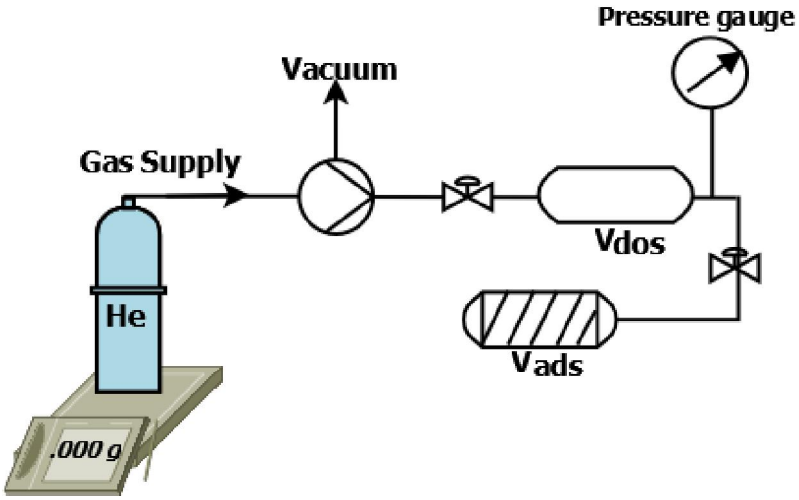

Figure 2.1: Schematization of the gravimetric method for the volume calibration of the adsorption devices.

The gas adsorption behaviour of activated carbons was characterized by means of the adsorption isotherms, they relate the adsorbed amount of gas (n^a) by a mass of solid (m^s) and the equilibrium pressure (p) at constant temperature (T) as expressed by equation 5.5,

$$n^a/m^s = f(p)_T \tag{2.1}$$

On this work, the adsorption isotherms were obtained by gas adsorption manometry, a method based on the measurement of the gas pressure in a known, constant volume at an specific temperature. This technique is one of the most widely thanks to its simplicity and efficacy, all the information needed for the adsorption isotherm is obtained from the pressure transducer. In a general way, it consists on recording the temperature and pressure of each gas dose, afterwards the gas is allowed to enter in contact with the adsorbent. Once equilibrium is established, the change in pressure is used to calculate the amount adsorbed.

As sections 2.1 and 2.2 of the present Chapter will discuss, different *home−made* experimental devices are employed for measuring the adsorption isotherms of pure gases and of gas mixtures. However, in both cases, two preliminary steps are needed [1]:

1. Determination of the volume of the empty system.

2. Assessment of the effective volume occupied by the adsorbent.

The evaluation of the system volume is obtained after the design and assembling of each of the adsorption devices. On this work, a gravimetric calibration method

Figure 2.2: Gravimetric volume calibration test

was chosen, Figure 2.1 shows the schematization of the system used for the volume calibration while 2.2 shows a photo of the experimental installation. The main components of the adsorption device are a reference or dosing cell (V_{dos}), an adsorption cell (V_ads) (top industries, 21 cm^3) and a pressure transducer (MKS model 121 A, pm 0.01 % on the full pressure range from 0 to 3.3 MPa) connected to V_{dos}. For the volume calibration an helium (He) gas bottle is placed on a precision balance (mettler toledo, ± 0,0001 g) and a gas dose is introduced in the dosing volume so that the amount of gas can be calculated from the bottle mass difference. The experiments were carried out on a temperature-controlled room to ensure isothermal conditions during the measurement. The volume of the dosing cell can then be calculated by equation 2.2,

$$V_{dos} = \frac{\Delta m \cdot MM}{\nu_{dos}} \tag{2.2}$$

Where:

- Δm is the difference in the mass of the bottle (g)
- MM is the molar mass of helium (mol g^{-1})
- ν_{dos} is the molar density of helium at the T and P conditions (mol cm^{-3}) taken from the online data of the National Institute od Standards and Technology [2].

The gas was then expanded into the adsorption cell V_{ads} by opening the valve between V_{dos} and V_{ads}, the total volume of the system (V_{tot}) can be calculated with the molar density of the gas at the pressure after expansion (ν_{fin}) as expressed by equation 2.3,

$$V_{tot} = \frac{\Delta m \cdot MM}{\nu_{fin}} \tag{2.3}$$

The volume of the adsorption cell is obtained by the difference of the total volume and the dosing volume (equation 2.4).

$$V_{ads} = V_{tot} - V_{dos} \tag{2.4}$$

In order to ensure a correct calculation of the volume of the system, an outgassing process consisting of applying vacuum conditions for 1 h was carried out before each measurement. The volume calculation was repeated 7 times for each adsorption device and the final value was expressed as the average value. In addition, 3 tests using carbon dioxide CO_2 instead of Helium were done for each system to confirm the results.

The second preliminary steps consists in the determination of the volume occupied by the adsorbent inside the adsorption cell so that the remaining $dead - space$ volume can be assessed. This step has to be carried out every time a new adsorbent sample is places in the adsorption cell.

The methodology starts by introducing a known mass of the adsorbent, typically 1 g, inside the adsorption cell. A heating wire controlled by a PID regulator (Eurotherm 3208) is placed uniformly around the system and its totality is covered in a temperature isolation foam (see Fig. 2.3). In addition, two thermocouples are placed (red wires on 2.3), one on V_{dos} and the other on V_{ads} to monitor the absence of temperature gradients.

The preparation of the sample for the adsorption experiments requires to exit any fluid particles contained in the system, this is achieved by applying vacuum (10^{-2} Pa) and temperature (100 °C) for 8 h. Afterwards, successive expansions of helium from the dosing cell into the adsorption cell are carried out at the temperature of the adsorption experiments: an helium gas dose is introduces in V_{dos}, once equilibrium conditions are reached (depicted by pressure stabilization), the pressure is recorded and the valve connecting the two cells is opened, a new equilibrium is reached and the valve is closed. The $dead - space$ volume (V_{ds}) on the adosption cell at the first step is calculated by equation 2.5.

$$V_{ds} = V_{dos}\left(\frac{P_{dos}}{P_{fin}} - 1\right) \tag{2.5}$$

Where:

- P_{dos} is the pressure at the dosing step (MPa)

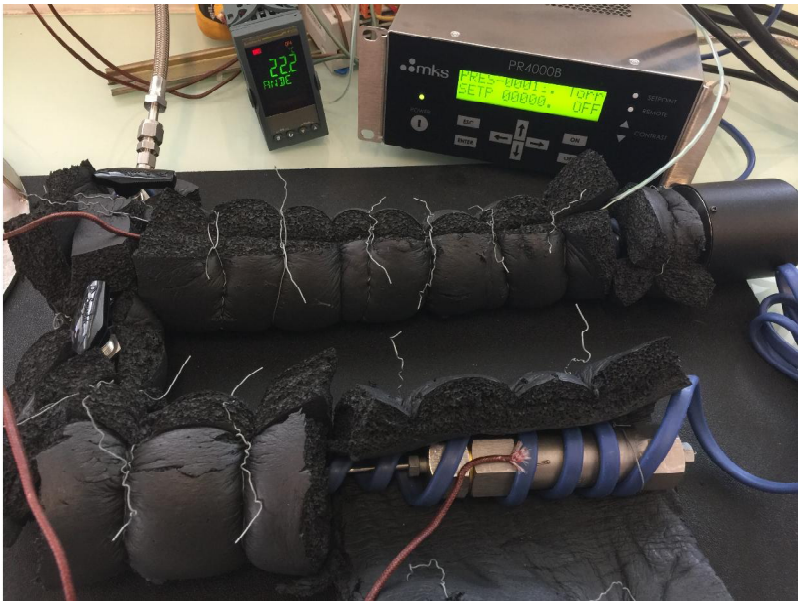

Figure 2.3: Heating system for isothermal conditions of the pure gas adsorption device.

- P_{fin} is the pressure after expansion (MPa)

Consecutive doses of helium are inserted in the dosing cell and expanded in the adsorption cell. The V_{ds} for an i step is calculated by equation 2.6.

$$V_{ds}^{i} = V_{dos}\left(\frac{P_{dos}^{i} - P_{fin}^{i}}{P_{fin}^{i} - P_{fin}^{i-1}}\right) \tag{2.6}$$

The $dead - space$ for a mass of a particular adsorbent is obtained by the average of six consecutive measurements and it can never be bigger than V_{ads} obtained from the gravimetric volume calculation. The helium contained in the system is extracted by vacuum conditions for 2 h, after-what the procedure for obtaining the gas adsorption isotherms can be carried out.

2.1 Pure Gas Adsorption

Figure 2.4 is an schematic representation of the designed pure gas adsorption device. To obtain a pure gas isotherm, a first dose of gas is loaded in the dosing cell (V_{dos}) at a known temperature, once the pressure has stabilized the volume of gas is expanded to the adsorption cell V_{ads}. The amount adsorbed can be calculated by a mass balance after the adsorption equilibrium is reached (constant pressure) [3]. The number of adsorbed moles (n_{ads}^{1}) on this step is calculated by equation 2.7

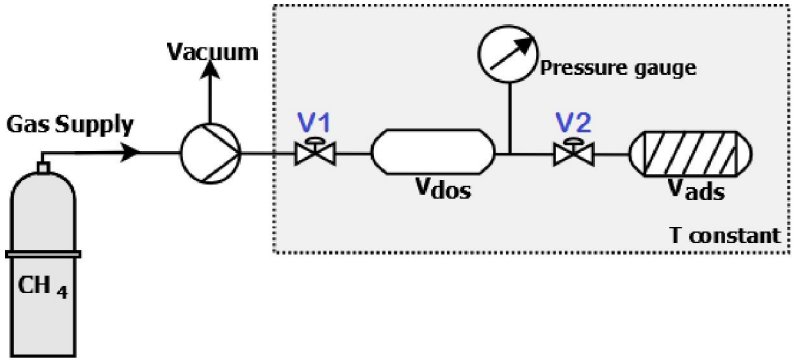

Figure 2.4: Schematization of the $home - made$ pure gas adsorption devide

$$n^1_{ads}(T, p_1) = \frac{V_{dos}}{\nu_0(T, p_0)} - \frac{V_{dos} + V_{ads}}{\nu_1(T, p_1)} \tag{2.7}$$

Where:

- T is the working temperature
- p_0 is the dosing pressure
- ν_0 is the gas molar volume at T and p_0
- p_1 is the pressure after adsorption
- ν_0 is the gas molar volume at T and p_1

The successive points of the isotherm are obtained by an accumulative process, valve $V2$ is closed and a new dose of gas inserted in V_{dos} followed by its pressure equilibration and expansion in to V_{ads}. The procedure is repeated up to a maximum pressure of 3.3 MPa (max. tolerance manometer) at intervals of $\approx$ 0.5 MPa. Equation 2.8 is used for the amount adsorbed at a given step i.

$$n^i_{ads}(T, p_1) = V_{dos}\left(\sum_{k=1}^{i} \frac{1}{\nu_{2k-2}} - \sum_{k=1}^{i} \frac{1}{\nu_{2k-1}}\right) - \frac{V_{ads}}{\nu_{i+1}} \tag{2.8}$$

2.2 Gas Mixture Adsorption

For the study of co-adsorption of gas mixtures, a manometric device coupled with a gas chromatograph (Agilent 7890 A) was developed (see Fig. 2.5). This system was conceived to be cyclic so that the recirculation pump (GK-M 24/02, max. flow: 2.81 L min^{-1}) ensures an homogeneous composition of the gas phase throughout the

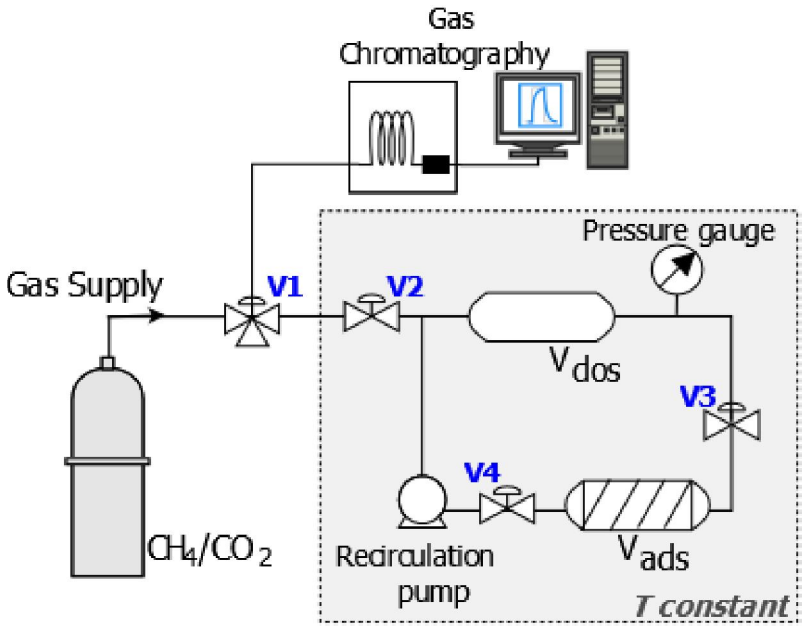

Figure 2.5: Schematization of *home − made* gas mixture adsorption device.

system during the adsorption process [4]. The system volume was calculated by the gravimetric calibration method.

In a consistent way to the pure gas adsorption analysis, the sample was placed inside the adsorption cell (V_{ads}) and out-gassed (vacuum at 100° for 8 h) and the dead sapce volume was calculated by helium expansions.

The equimolar CH_4/CO_2 gas mixture is expanded from the dosing volume V_{dos} to the adsorption cell V_{ads} via a step-by-step method. Upon equilibration of the pressure during the adsorption process, the adsorption volume is isolated by clossing valves $V3$ and $V4$ and a discrete quantity of gas is extracted through $V2$ and analyzed by gas chromatography. The total amount of gas adsorbed at each step is calculated by equation 7.3,

$$n_{ads}^{total} = n_{dos}^{total} - n_{g}^{total} \tag{2.9}$$

where n_{ads}^{total} is the total number of adsorbed gas moles, n_{dos}^{total} is the number of moles introduced in the dosing system and n_{g}^{total} is the number of gas moles remaining in the gas phase after adsorption.

The contribution of each gas to the adsorbed amount is expressed by equation 7.4,

$$n_{ads}^{total} = n_{ads}^{CH_4} - n_{ads}^{CO_2} \tag{2.10}$$

and their contribution to the number of moles in the gas phase after adsorbtion by equation and 7.5 ,

$$n_g^{total} = n_g^{CH_4} - n_g^{CO_2} \tag{2.11}$$

The mole fraction of the first component in the gas phase (y_1), and in the adsorbed phase (x_1) can be obtained from the gas chromatogram as expressed by equations 7.10 and 2.13,

$$y_1 = \frac{n_g^{CH_4}}{n_g^{CH_4} + n_g^{CO_2}} \tag{2.12}$$

$$x_1 = \frac{n_{ads}^{CH_4}}{n_{ads}^{CH_4} + n_{ads}^{CO_2}} \tag{2.13}$$

in such a way that the sum of the mole fractions of both components in each phase is equal to the unity (eq. 2.14 and eq. 2.15),

$$y_1 + y_2 = 1 \tag{2.14}$$

$$x_1 + x_1 = 1 \tag{2.15}$$

For the first gas of dose, the amount adsorbed of each component can be calculated by the following equation,

$$n_{ads}^1 = n_{ads}^{total} \cdot x_1 \tag{2.16}$$

In the step-by-step scheme, the gas is evacuated from the dosing volume after each adsorption step and a new dose of the original equimolar mixture is introduced. The adsorbed amount of each gas at step i is given by equation 2.17,

$$n_{ads,i}^1 = (0.5\ n_{dos}^{total} + y_{i-1}^1 \cdot n_{g,i-1}^{total}) - y_i^1 \cdot n_{g,i}^{total} \tag{2.17}$$

The adsorbent selectivity can then be calculated as a function of pressure as expressed by 2.18

$$Selectivity = \frac{\left(\frac{y_1}{y_2}\right)}{\left(\frac{x_1}{x_2}\right)} \tag{2.18}$$

2.3 Bibliography

[1] Francoise Rouquerol, Jean Rouquerol, and Kenneth Sing. *Adsorption by powders and porous solids*. Academic Press, London, UK, 1999.

[2] National Institute of Standards and Technology. Thermophysical Properties of Helium.

[3] Olga Patricia Ortiz Cancino, Deneb Peredo Mancilla, Manuel Pozo, Edgar Pérez, and David Bessieres. Effect of Organic Matter and Thermal Maturity on Methane Adsorption Capacity on Shales from the Middle Magdalena Valley Basin in Colombia. *Energy and Fuels*, 31(11):11698–11709, 2017.

[4] D Pino, F Plantier, and D Bessieres. Experimental determination of the adsorption isotherms in gas mixtures under extended pressure and temperature range. *Journal of Thermal Analysis and Calorimetry*, 117(3):1469–1477, 2014.

CHAPTER 3

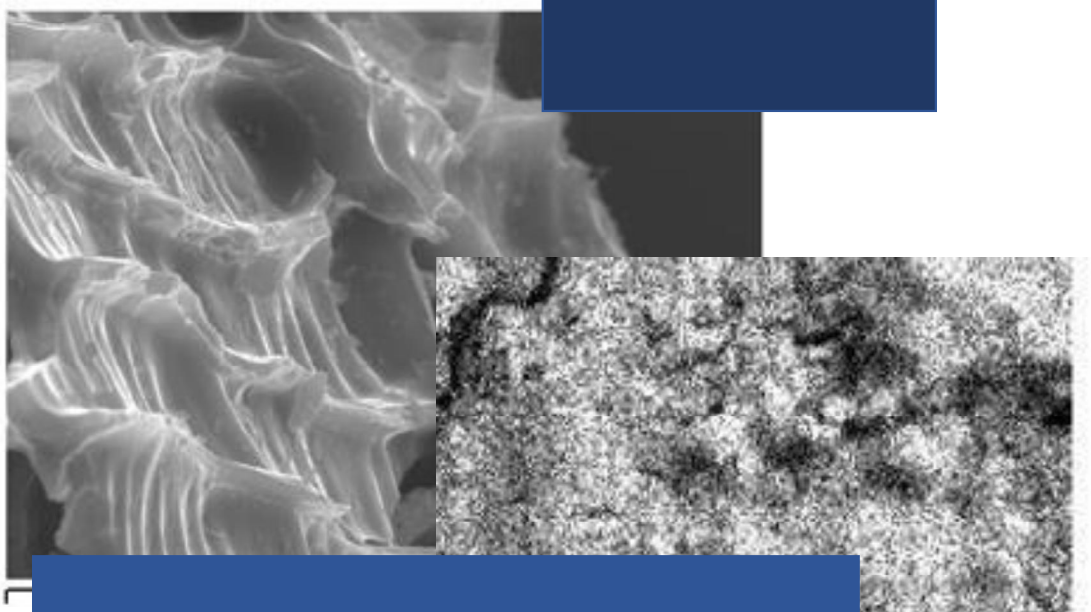

SAMPLES CHARACTERIZATION

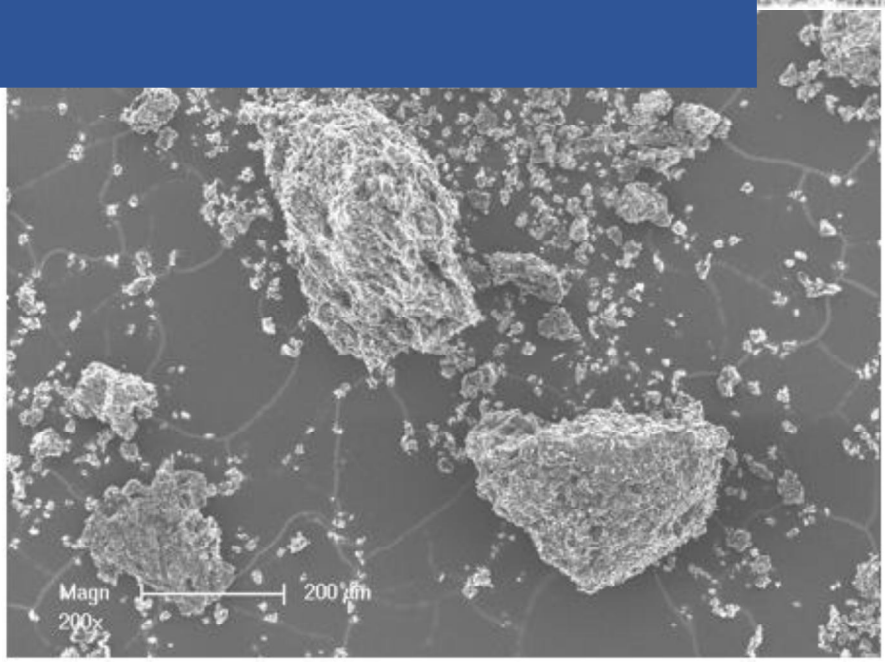

3.1 Chapter Outline

The CH_4 and CO_2 pure gas adsorption as well as the equimolar CH_4/CO_2 mixture adsorption were studied on a set of commercial activated carbons (Chapters 5 and 7 respectively). This comprehensive analysis of the gas adsorption process is highly useful for understanding the effect of both textural and chemical properties on the maximum adsorption capacity of pure gases and on the separation selectivity of the adsorbents. To this end, the samples were fully characterized by a variety of analytical techniques.

Furthermore, the pure gas adsorption isotherms were obtained on three non-commercial activated carbons from olive stones synthesized by different activation techniques (Chapter 6): physical activation with CO_2 and H_2O and chemical activation with HNO_3. The results shine light on the importance of the activation method of activated carbons for adsorption purposes.

The present Chapter summarizes the chemical and textural properties obtained for all the adsorbent materials used throughout this work.

Commercial Activated Carbons

Five commercial activated carbons provided by Cabot Corporation (USA) are studied on this work. Activated carbons CNR-115 and CGran were produced by chemical activation using phosphoric acid (H_3PO_4) as the activation agent, the remaining adsorbents (GAC 1240, RX 1.5 and Rox 0.8) were obtained by physical activation with steam.

The morphology and composition of the materials were examined by scanning electron microscopy (SEM) using a FEI model Quanta 400 equipped with and energy dispersive spectrometer (EDX).

The SEM pictures shown in Figure 3.1, indicate a granular morphology for CNR-115, RX 1.5 and Rox 0.8, and a pallet-like morphology for the other two. Differences in the particle size are depicted, with the largest ones been found for CNR-115 and RX 1.5. At 100 μm magnification a rough porous surface is observed for all of the samples. Furthermore, the presence of big channels is discerned on CGran. These differences can be attributed to variations on the activation method (e.g. temperature, activation time, precursor material and pressure).

A clear contrast between the physically and the chemically activated samples is observed on the chemical composition extracted by EDX spectroscopy (Table 3.1). The carbon percentage of CNR-115 and CGran is $\approx 10\%$ lower than the one found

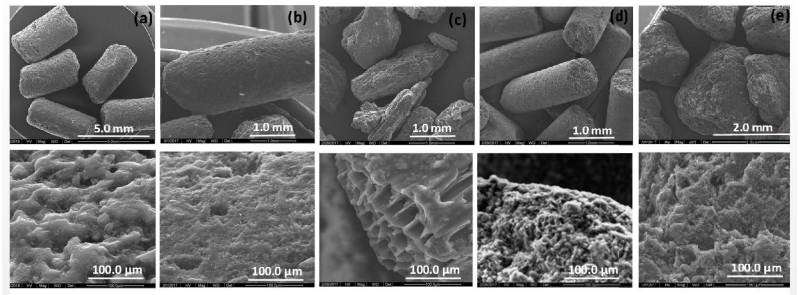

Figure 3.1: SEM images of commercial activated carbons: a) CNR-115, b) RX 1.5, c) CGran, d) Rox 0.8, e) GAC 1240 at two magnifications (>1.0 mm and 100 μm)

Table 3.1: Chemical composition of commercial activated carbons (atomic % of elements) obtained by EDX spectroscopy

Element	**CNR-115**	**CGran**	**Rox 0.8**	**RX 15**	**GAC 1240**
C	84	81.2	94.6	93.3	91.4
O	14	15.6	4.1	6.0	6.6
P	0.53	2.6	x	x	x
Na	0.54	0.6	0.3	x	x
S	x	x	0.5	0.3	0.6
Si	x	x	0.2	0.5	06
Al	x	x	x	x	0.5
Cl	x	x	x	x	0.3
Ca	x	x	x	x	x
F	0.9	x	x	x	x

on the other samples, in fact chemical activation with H_3PO_4 results in an increase of the sample's oxygen and phosphorous content.

To evaluate the structure of the activated carbons, X-ray power diffraction (XRD) was also performed using a D8 ADVANCE A25-Bruker instrument. Figure 3.2 shows the diaffactogram of the samples. The presence of broad peaks on the samples indicates highly disordered materials with low graphitization. The peaks at 24, 44 and 80 ° correspond to the (002), (100) and (110) diffraction planes of graphite. The remaining small peaks are related to crystalline impurities such as SiO_2 tridymite on Rox 0.8 and SiO_2 quartz on GAC 1240.

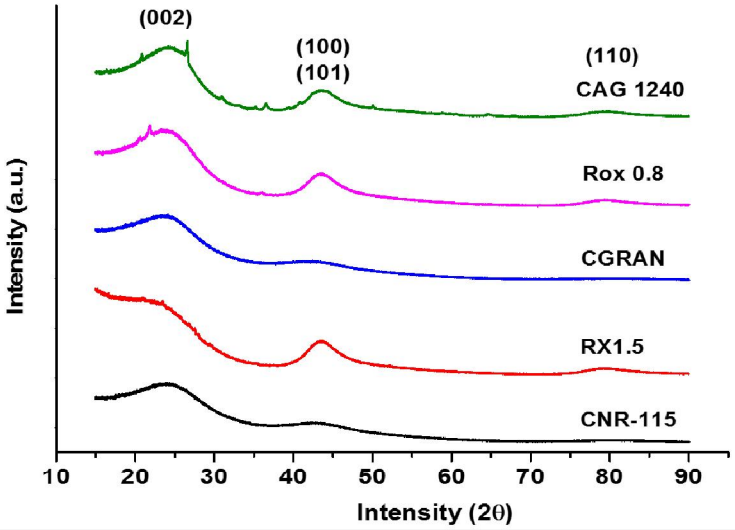

Figure 3.2: XRD patterns of commercial activated carbons

The temperature programmed desorption (TPD) analysis was carried out using a home-made apparatus coupled with an INFINCON Transpector mass spectrometer. The presence of an important amount of oxygen containing surface functionalities on CGran and CNR-115 is depicted on the CO_2 and CO desorption profiles (Fig. 3.3). The peresence of carboxylic and lactones (desorbed at 673 K) is observed on both ACs CO_2 desorption profiles whilst carbonates (1100 K) are perceived only on CNR-115. On the other hand, the CO desorption peaks at 900 K and 1100 indicate the presence of phenols and quinones respectively.

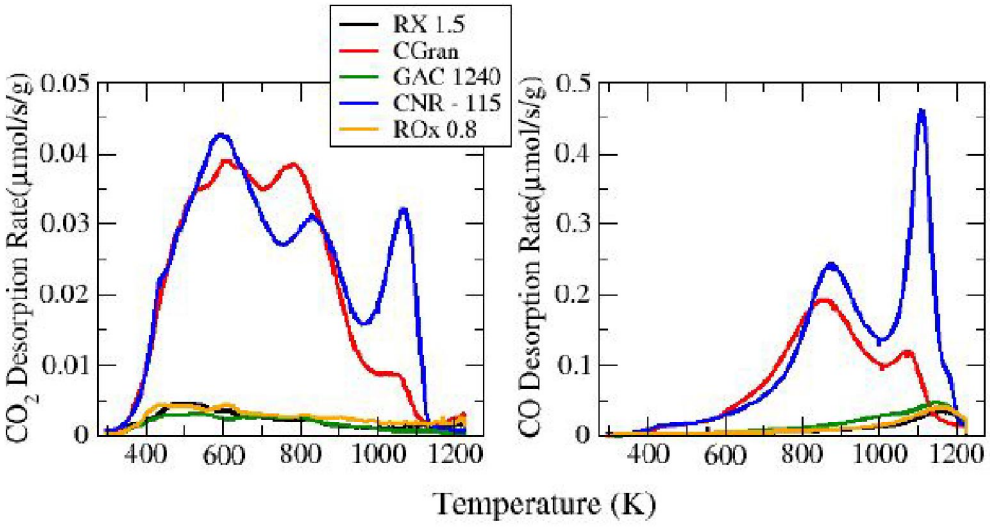

Figure 3.3: CO_2 and CO temperature programmed desorption profiles of commercial activated carbons

The integration of the desorption profiles gives the total desorbed quantity displayed on Figure 3.4. The presence of acidic oxygen containing functionalities (des-

orption on CO_2) is revealed to be lower than that of basic groups (desorption of CO) on the five adsorbents.

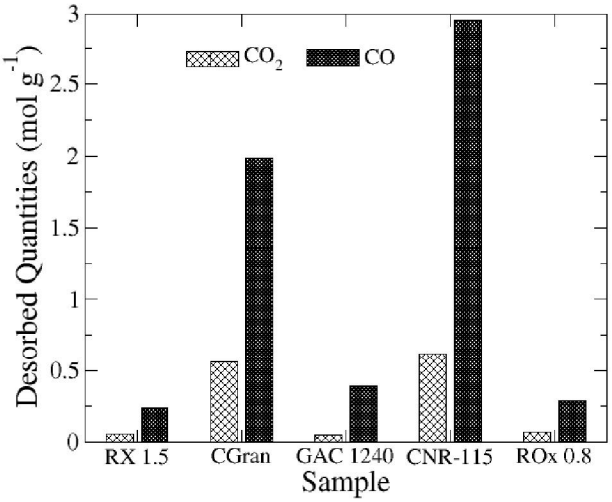

Figure 3.4: Total CO_2 and CO TPD desorbed quantities (mol g^{-1}) of commercial activated carbons

The analysis of the surface chemistry of AC continues with the calculation of their pH at the point of zero charge (pH_{PZC}), that is the point at which the negative and positive charges of the surface of the material cancel each other. The methodology roughly consists on mixing 0.1 g of CA in 5 solutions of different pH ($2<pH<10$) for 72 h under stirring conditions. After this time, the solutions were centrifuged and filtrated and their final pH measured with a Denever Intrument 215 pH meter. Similar pH values are obtained for all the solutions prepared with the same activated carbon, this value correspond to the pH_{PZC}. Once an estimated value was obtained, the same protocol was followed preparing 3 solutions with an initial pH value in the vicinities of the final values of the first set for each AC.

An indirect titration method was followed to determine the quantities of basic and acid oxygen containing functionalities. Samples of 0.2 g was put in contact with 50 mL of NaOH 0.1 N and HCl 0.1 for the quantification of acid and basic groups respectively. The solutions were kept under agitation for 72 h, centrifuged and filtrated. Three aliquots of 10 mL were taken from the fluid phase and each one was titrated with Na_2CO_3 0.1 N. For the indirect measurement of acid functionalities, 10 mL of HCl (0.1 N) were added to the filtrate aliquots prior to titration. The amount of surface group is obtained from the inflection point of the titration curve and as the average of 3 measurements.

Table 3.2 summarize the results for the pH_{PZC} and the basic and acid surface

oxygen functionalities. The chemical activated samples show an acid pH_{PZC}, with an important presence of acid surface groups such as carboxylic acids, phenols and lactones. Steam activation proves to give higher pH_{PZC} values indicating the presence of carbonyles and ethers, this translates in higher exhibit amounts of basic groups.

Table 3.2: Acid-Basic character of commercial activated carbons

Sample	pH_{PZC}	**Total Acid (mmol g^{-1})**	**Total Basic (mmol g^{-1})**
RX 1.5	9.75 ± 0.05	0.18 ± 0.01	0.73 ± 0.04
CGRAN	3.86 ± 0.02	1.74 ± 0.05	0.01 ± 0.01
GAC 1240	8.13 ± 0.04	0.18 ± 0.01	0.49 ± 0.02
CNR-115	6.14 ± 0.03	0.49 ± 0.02	0.61 ± 0.03
ROx 0.8	8.74 ± 0.04	0.21 ± 0.01	0.61 ± 0.03

The textural properties of adsorbent materials are the most defining factor of their adsorption behaviour. For this reason, the nitrogen (N_2) adsorption isotherms (77 K) were acquire using a Micrometrics ASAP 2000 automatic apparatus (see Fig. 3.5). The BET (Brunauer-Emmet-Teller) surface area S_{BET} and total pore volume V_{tot} (cm^3 g^{-1}) were obtained from the linear section of the adsorption isotherm (P/P_0=0.01-0.05) and the amount of adsorbed N_2 at P/P_0=0.95 respectively. The micropore volume V_{micro} was calculated using the Dubinin-Radushkevich equation (10^{-4} <P/P_0 < 10^{-2}). The mesopore volume V_{meso} was calculated as the difference between total and micropore volume.

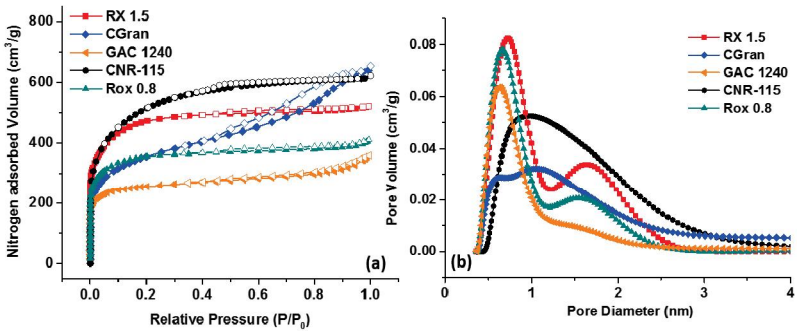

Figure 3.5: a) Nitrogen adsorption isotherms at 77 K and b) NLDFT pore size distribution of commercial activated carbons.

Non liquid density functional theory with a carbon slit pores model was used to reproduce the adsorption isotherm and obtain the pore size distribution (PSD) and thus, the average pore size (L0).

The five ACs are mainly microporous (see Fig. 3.5 and Table 3.3) with a significant presence of mesopores on sample CGran. The samples display an important

range of surface areas: from 982 m^2 g^{-1} of GAC 1240 to 1714 m^2 g^{-1} of CNR-115.

Table 3.3: Textural Characterization of Activated Carbons

Sample	$\mathbf{S}_{BET}$ ($\mathbf{m^2\ g^{-1}}$)	$\mathbf{V}_{micro}$ ($\mathbf{cm^3\ g^{-1}}$)	$\mathbf{V}_{meso}$ ($\mathbf{cm^3\ g^{-1}}$)	$\mathbf{V}_{tot}$ ($\mathbf{cm^3\ g^{-1}}$)	**L0** (**nm**)
RX 1.5	1683	0.61	0.20	0.81	0.93
CGran	1378	0.45	0.54	0.99	1.00
GAC 1240	982	0.36	0.20	0.56	0.76
CNR-115	1714	0.64	0.31	0.95	1.10
Rox 0.8	1323	0.48	0.16	0.64	0.84

The broad span of textural and chemical properties of the set of commercial carbons will be highly beneficial to draw conclusion on their possible effect on the adsorption of methane, carbon dioxide and their mixtures as presented on Chapters 5 and 7.

3.2 Biomass-Based Activated Carbons

The adsorption of carbon dioxide and methane by biomass-based activated carbons is studied on Chapter 6. The adsorbents were synthesized at the Material Science Institute of the University of Mulhouse. To this end, olive stones underwent a carbonization process (873 K for 60 min) followed by activation with H_3PO_4 (AC-H_3PO_4), H_2O (AC-H_2O) or CO_2 (AC-CO_2), a detailed description of the preparation methods can be found on Chapter 6.

Table 3.4 displays the textural properties of the biomass-based ACs, they were obtained following the methodology earlier described for the commercial activated carbons.

Table 3.4: Textural Properties of Carbon Materials.

Sample	**SSA** ($\mathbf{m^2\ g^{-1}}$)	$\mathbf{V}_{\mu}$ ($\mathbf{cm^3\ g^{-1}}$)	$\mathbf{V}_{TOT}$ ($\mathbf{cm^3\ g^{-1}}$)	$\mathbf{V}_{meso}$ ($\mathbf{cm^3\ g^{-1}}$)
AC-H_3PO_4	1178	0.45	0.49	0.04
AC-CO_2	757	0.30	0.32	0.02
AC-H_2O	754	0.28	0.58	0.30

Chemical activation with phosphoric acid results in an increased quantity of micropores as well as higher surface area. In regards of physical activation, similar

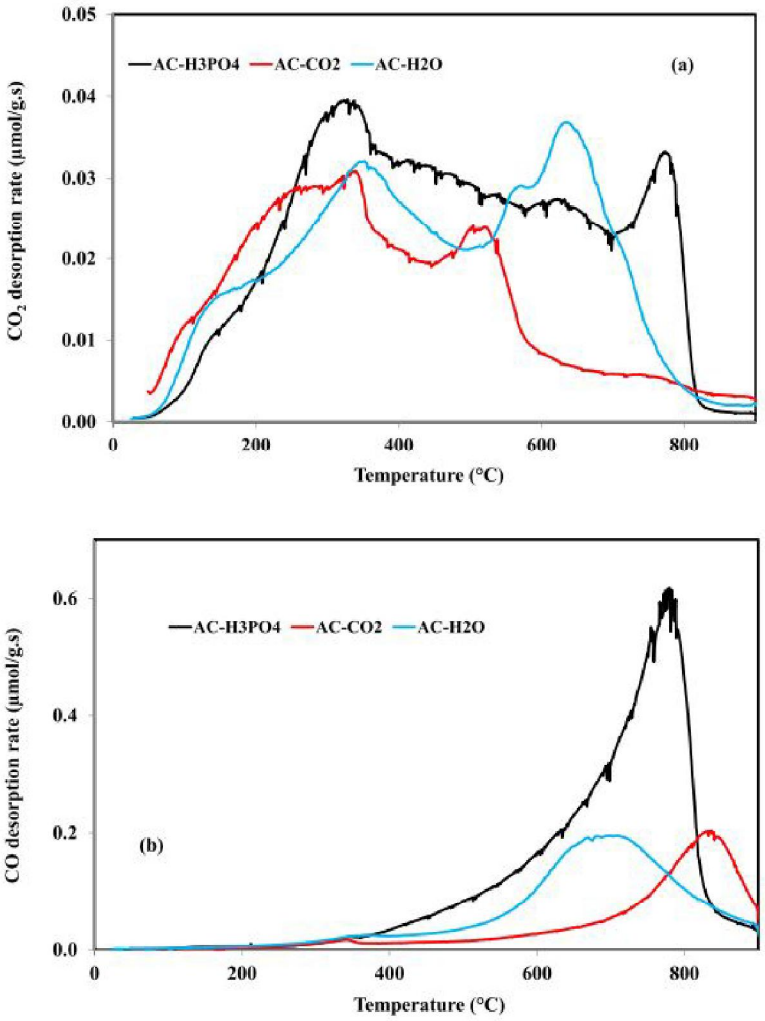

Figure 3.6: TPD desorption profiles of CO2 (a); and CO (b) of biomass-based activated carbons.

microporosity and surface area are found for the steam and the carbon dioxide activated carbons, however a higher gasification of steam activated carbon results in an important formation of mesopores.

Furthermore, a comparison between tables 3.3 and 3.4 shows overall less developed textural characteristics of the non-commercial adsorbents, however, as it will be later discussed, activated carbons obtained from biomass wastes have several economical and environmental advantages.

The CO and CO_2 temperature programmed desorption profiles and total emmited quantities of the three samples are shown on Fig. 3.6 and Table 6.2.

The CO_2 desorption shows the presence of carboxylic groups ($\approx$ 400 °C) on all of the samples, lactones ($\approx$ 520 °C) on AC-CO_2 and anhydride groups (Temp. >600 °C) on both AC-H_3PO_4 and AC-H_2O.

The wide CO decomposition peak of AC-H_3PO_4 can be attributed to phenol,

carbonyl and quinone groups. In contrast the CO peak of the steam activated carbon comes from phenol decomposition, whilst the one found for AC-CO_2 indicates the presence of quinone surface groups.

The adsorbents showed a higher cumulated desorbed amount of basic oxygen-containing surface functionalities (CO_2 desorption) than acid ones (CO desorption) (Fig. 3.5).

Table 3.5: Cumulated Amounts of the Emmited CO and CO_2 During the TPD-MS Analysis of Carbon Materials.

Sample	**CO (mmol g^{-1})**	**CO_2 (mmol g^{-1})**
AC-H_3PO_4	3.43	0.72
AC-CO_2	1.06	0.38
AC-H_2O	1.25	0.39

Peredo-Mancilla, D., et al. (2019).
Gas Storage. In *Char and Carbon Materials Derived from Biomass.*
Amsterdam: Elsevier Inc. 341-382.

CHAPTER 4

A REVIEW ON THE CH_4/CO_2 ADSORPTION BY CARBONACEOUS MATERIALS

ISBN: 978-0-12-814893-8
DOI: https://doi.org/10.1016/C2017-0-02406-0

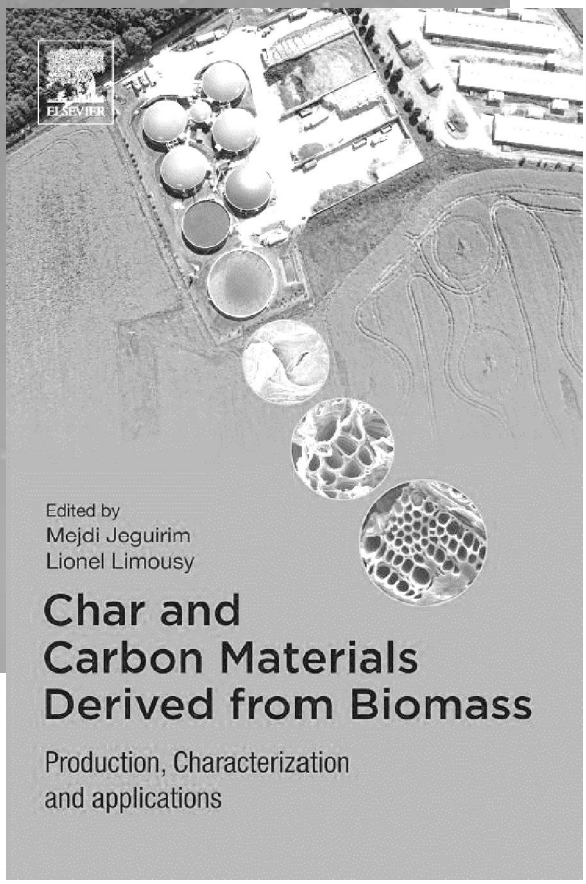

4.1 Chapter Outline

Activated carbons are highly porous materials produced from a carbon-rich precursors by a chemical or physical activation process. They have appreciable surface area ranging from 5 m^2 g^{-1} to well above 2000 m^2 g^{-1} that have made them the most widely used of all-purpose industrial adsorbent.

The present chapter, expressed in the form of a bibliographic review, explores the application of carbonaceous materials and in particular activated carbons for carbon dioxide and methane adsorption and storage. The importance of the precursor material, the activation method and the textural properties of the adsorbent material for gas adsorption applications is here highlighted.

4.2 Introduction

Gases play an important role in our daily life. They are usually found in the form of gas mixtures with the one most known being atmospheric air which is constitute of approximate volumes of 78.08% nitrogen (N_2), 20.95% oxygen (O_2), 0.93% argon (Ar), 0.03% carbon dioxide (CO_2) and traces of methane CH_4, helium (He), neon (Ne), krypton (Kr), xenon (Xe) and ozone (O_3) [1]. Amongst them, CO_2, CH_4 and nitrogen oxides (NO_x) are a product of incomplete burning of fossil fuels (coal, oil, diesel, natural gas) and are the major contributors of global warming (GW) as they are emitted in higher amounts than other greenhouse gases (GHG) such as hydrofluorocarbons (HFCs), perfluorocarbons (PFCs) and hexafluorocarbon (F_6C). As it can be seen in Figure 4.1, the atmospheric concentrations of these three gases have dramatically increases since the pre-indusrtial years ($\sim$1850) thus the reduction of its emissions has become a main target arising a need for new technologies for the selective adsorption and storage of this pollutants [2].

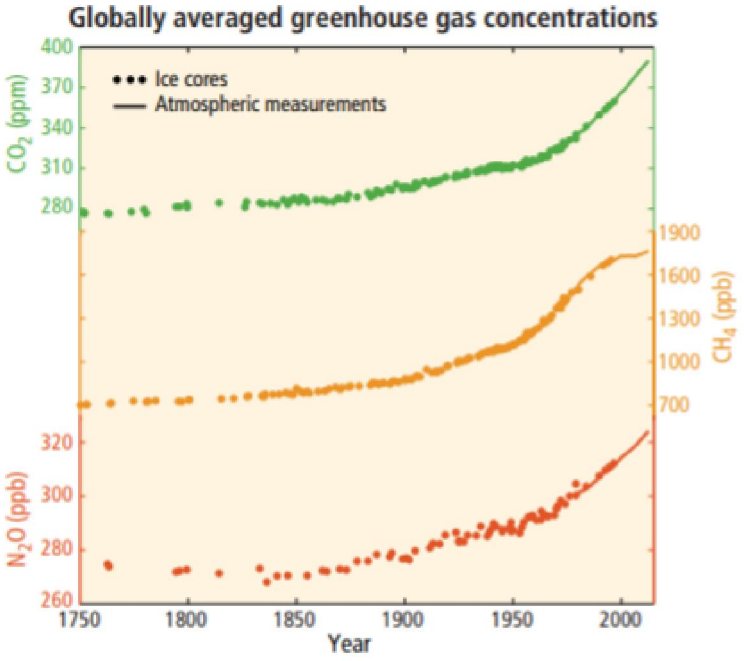

Figure 4.1: Observed changes in atmospheric greenhouse gas concentrations between the years 1750 to 2011. Atmospheric concentrations of carbon dioxide (CO_2, green), methane (CH_4, orange) and nitrous oxide (N_2O, red). Data from ice cores (symbols) and direct atmospheric measurements (lines) are overlaid. Source: Intergovernmental Panel of Climate Change 2014 [2]

Carbon dioxide is a product of many industrial processes with the fossil fuel power plants being the most important emitters (40% of the total CO_2). In order to reduce its emission the solutions include increasing the efficiency of the power plants, demand side conservation and a change towards nuclear and renewable energies, as well as the implementation of carbon capture and storage (CCS) systems [3]. CCS can be used as a strategy to reduce not only the power plants emission but it can also be employed in many industrial sectors such as the petrochemical industry, iron and steel refineries and cement production.

There are many separation technologies available for the separation and storage of CO_2: amine scrubbing, water scrubbing, membranes separation, cryogenic separation, biological and physical adsorption. Most of the commercial CCS use amine or water scrubbing but it has important drawbacks such as production of undesirable bi-products, high energy regeneration, high corrosion and low cost efficiency. On this context, physical adsorption has the advantages of having low energy requirements, cost advantage, no use of water or additional chemicals and being easy to scale to a wide range or temperatures and pressures [4].

For the case of methane, the principal anthropogenic sources are thought to be the production of livestock, natural gas production and distribution, emissions

from landfills and the mining of coal [3]. Due to methane's low volumetric energy density, the store of this gas for its use as a clean energy source involves the use of high pressures to obtain compressed natural gas (CNG) and low temperatures, down to 120 K, for liquefied natural gas (LNG). This methods have a very high energy output as well as various security issues that limits its use. The storage of methane by adsorption in a solid material, known as adsorbed natural gas (ANG) presents advantages over LNG and CNG in terms of energy efficiency and safety. An ANG storage system would have the ability of storing great quantities of methane in small volumes under atmospheric conditions. To compete with other fuels (and other methane storage forms), the department of energy (DOE) of the U.S. has stablished a CH_4 storage capacity of 180 v/v (volume of gas adsorbed at standard temperature and pressure: 298 K, 0.1 MPa per volume of the storage vessel) [5], [6].

The development of porous adsorbent materials compatible with the adsorption of gases such as CH_4 and CO_2 has become then a target issue for researches, with the goals of finding cheap and eco-friendly precursor materials and stablishing the synthesis procedures that will produce better yielding and the required properties of the material. There are a variety of porous materials used for the adsorption of gases such as zeolites [7, 8, 9], carbon nanotubes [10, 11], metal organic frameworks (MOFs) [12, 13, 14] and activated carbons [15, 16][17]. Among this materials, activated carbons are the most widely used in the industry, thanks to the ease of synthesis as well as the possibility of pore tailoring and chemical functionalization of the material. In addition, activated carbons can be produced from biomass as the carbon source which they advantages of low cost, high availability, valorization of agricultural wastes and development of high specific surface area adsorbent [18].

On this chapter the use of activated carbons for the adsorption of key gases with a focus on biomass-derived activated carbons is discussed. The effect of the textural (like surface area and pore volume) and chemical properties (surface groups) upon the adsorption behavior of the adsorbent is evaluated.

4.3 Methane Storage

Methane (CH_4) accounts for about 10% of the total greenhouse gases emissions. Over 60% of total CH4 is generated by human activities such as energy production and, organic waste and the raising of livestock while the other 40% is emitted by natural sources like natural wetlands [19, 20]. As part of the global efforts to mitigate its environmental impact methane is being studied for use as a clean energy in the way of natural gas and biomethane. Natural gas is considered an alternative fuel because of its environmental benefits, its combustion is relatively cleaner than that

of other fossil fuels. Natural gas use results in the production and emission of less pollutants, 29% less carbon dioxide per joule delivered than oil and 44% less than coal [21]. As a vehicle fuel it emits 15 to 20 percent less heat-trapping gases than gasoline. The main component of natural gas is methane (approximately 90% and higher in most cases, it also contains a small portion of heavier hydrocarbons such as ethane (C_2H_6), propane (C_3H_8) and butane (C_4H_{10}). On the other hand, biogas is the product of the anaerobic fermentation of organic matter which main constitutes are CH_4 (50-75%) and CO_2 (25-45%) (see table 4.1). Biogas can be directly burned to generate electricity in a combined heat and power plant (CHP) or alternatively it can be purified to produce biomethane (96% CH_4) [18].

Table 4.1: Composition of natural gas and biogas in volume percentage

Compound	**Natural Gas**	**Biogas**
Methane (CH_4)	88.1 %	50-75 %
Carbon dioxide (CO_2)	0.8 %	25-45%
Ethane (C_2H_6)	4.2 %	*
Hydrogen (H_2)	*	0-2 %
Hydrogen sulfide (H_2)	*	0-1 %

* None detected

The utilization of biomethane as an alternative energy source also presents a variety of environmental benefits that include a decrease of greenhouse gas emissions, cheap organic waste recycling and the formation of nitrogen rich products that can be use as fertilizers. In addition, the similar properties of biomethane and methane make it possible for biomethane to replace or be added to natural gas to be used as a vehicular fuel. However, despite the benefits of using methane-rich fuels, their use is limited due to transportation and storage uses. At normal temperature and pressure methane is in the gaseous state which results on a volumetric energy density of only 0.12% of that of gasoline. Table 4.3 shows the physical properties of methane.

Table 4.2: Physical Properties of methane.[22]

Molar mass (g mol^{-1})	**Boiling point (K)**	**Temperature^c (K)**	**Pressure^c (MPa)**	**Density^c (g cm^3)**
16.043	111.65	190.90	4.64	0.16

Currently, CH4 storage methods are performed by means of compressed natural gas (CNG) or liquefied natural gas (LNG). These methods involve high cost processes (cryogenics and compression), special storage tanks and they also present risks to

safety due to the use of high pressure and/or the refueling of cryogenic liquids that complicate their use in the vehicle sector. A promising alternative that will reduce the costs and safety risks, consists in the storage of natural gas (or biomethane) at low pressure and normal temperature in the adsorbed form (ANG – adsorbed natural gas). According to the US Department of Energy (DOE), in order for the ANG technology to be commercially used a target CH4 storage capacity of 180 v/v at 35 MPa (volume of gas at standard pressure and temperature conditions per volume of the storage vessel) was stablished [23]. In this context, the search of adsorbent materials that can meet the DOE standards has become a hotspot of research. The established value of 180 v/v corresponds to the energy density of CNG at a pressure of 16.3 MPa (Table 3). This value is considered a reference target when searching for new adsorbents, however, the U.S. department of Energy under the program "Methane Opportunities for Vehicular Energy (MOVE)" demands an energy density for the ANG systems equivalent to CNG under 25 MPa (266 v/v) [24].

Table 4.3: Energy Densities of Methane and Conventional Fluids (1 L of CH_4=0.0345 MJ) [25].

Pressure (MPa)	**Volumetric storage capacity (v/v) at STP**	**Energy density (MJ/L)**
CNG (15 Mpa)	168	5.80
CNG (20 Mpa)	222	7.68
CNG (25 Mpa)	266	9.2
LNG (110 K and 0.1 MPa)	600	22.2
Gasoline	*	34.2
Diesel	****	**37.3**

* Required density of methane in a CNG tank to make it equivalent to gasoline

** Required density of methane in a CNG to make it equivalent to diesel: 1.0785 g cm^{-3}

It is of general consensus that an efficient adsorbent for the storage of methane must have a high specific surface area (from 1000 m^2 g^{-1} up to 3000 m^2 g^{-1}), with a pore size distribution that ranges around 1.0 to 2.0 nm with a micropore volume of at least 85% of total pore volume [26]. Different class of porous materials have been studied aiming to reach the DOE target including activated carbons, ordered carbonaceous materials, zeolites and MOFs. Among all the available adsorbent materials, activated carbons present advantages that make them suitable materials for gas storage such as high surface area, large pore volume and light weight. In particular, for the methane storage process they have the benefits of not being sensitive to humid conditions, they tend to have reasonable prices as well as good

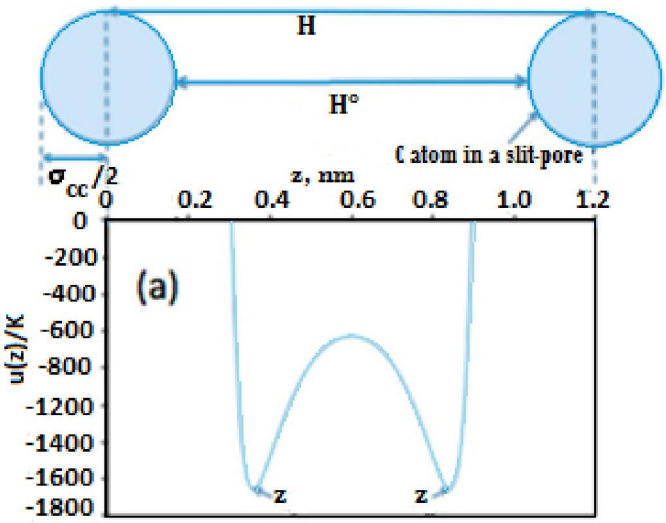

Figure 4.2: Potential energy, $u(z)$, for a spherical methane Lennard-Jones (LJ) site interacting with walls of a slit pore of width $H = 1.2$ nm in terms of the distance z (distance between the center of the methane molecule and the center of a wall carbon atom) [25]

adsorption properties at atmospheric pressure. The adsorption capacity of activated carbons (ACs) is highly related to the textural properties. They present a wide range of pore sizes that go from the micropore to macropore region and a surface area between 400 and 3000 m^2 g^{-1}. Furthermore, their textural properties can be controlled by various activation factors. The CH_4 molecule is symmetrical and therefore it does not present a dipole or quadripole. It is difficult then, to increase the storage capacity of the adsorbent by surface modification. However, the gas storage capacity of ACs can be enhanced by controlling the pore structures. For the methane adsorption it has been found that the presence of high microporosity with no macropore volume is optimal since the size of the methane molecules are equivalent to the size of micropore. An average pore volume of at least 0.8 nm (diameter greater than two molecules of methane) is wished [27, 28]. In fact since the interaction of the methane molecules with activated carbons is governed by van der Waals interactions, the attractive force of the pore walls of the adsorbent are a function of the distance z between the center of the methane molecule and the center of a carbon atom on the pore wall, this interaction can be described by the Lennard-Jones potential (Fig. 4.2).

The attraction force becomes stronger when z is equivalent to one methane molecular diameter (0.36 nm), at longer distances the attraction energy becomes too week and thus the formation of a second adsorbed layer is impeded, the rest of the methane molecules will filled the empty pore space with a low gas-like density. A linear relationship between the micropore volume (up to 1.6 cm^3 g^{-1}) and the methane adsorption capacity of different activated carbons at 35 bars and 298

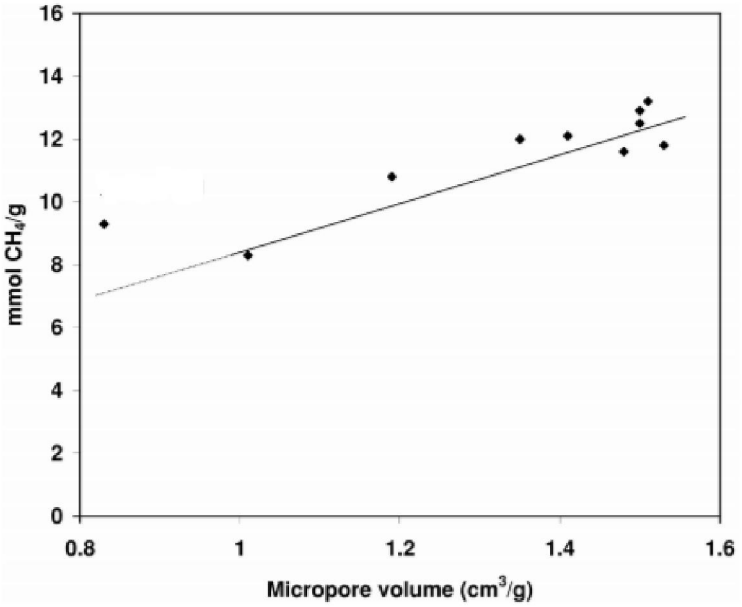

Figure 4.3: Relationship of the methane adsorption capacity at 35 bar and 298 K with the micropore volume for a series of activated carbons calculated by N_2 adsorption isotherms [29].

K Fig. 4.3) could be established. However, a large portion of pores that have an optimal size of around 0.8 nm plays a major role in the adsorption of methane [29]. Furthermore, it has been reported that the presence of pores larger than 0.8 nm is needed in order to facilitate the access and adsorption of the gas molecules. For example, García-Blanco et al. [30] showed that the Maxorb activated carbon, with a surface area of 3090 m^2 g^{-1} and a pore size distribution from pores between 0.5 and 3 nm showed a micropore filling of only 59% when adsorbing methane at 298 K and 3500 kPa. However, even if the micropore filling was low, the narrow micropore (<0.8 nm) filling is total, indicating that methane is not only adsorbed in the narrow micropores but also of pores of larger size. This need of larger pores for the methane adsorption was also evidenced by Casco et al. [14] when comparing a set of activated carbons with different pore volumes (Fig .4.4) . Samples with pure micropororous network (F400 and Maxsorb) showed a maximum adsorption capacity at moderate working pressures ($6 - 8$ MPa), by contrary, samples that combine micropores with mesopores (pore size <2 nm) such as the activated carbons RGC30, LMA738, LMA405 and LMA726, there was a continuous increase of the adsorbed quantity. Furthermore, they found that the correct design of activated carbons can result in materials that meet both the DOE and DOE MOVE requirements set by the U.S. department of energy.

As it was previously mentioned, the feasibility of using ANG instead of CNG and LNG relays on the ability of the adsorbent to store a high amount of gas inside the fuel tank, which means that the porous adsorbent must present a high packing

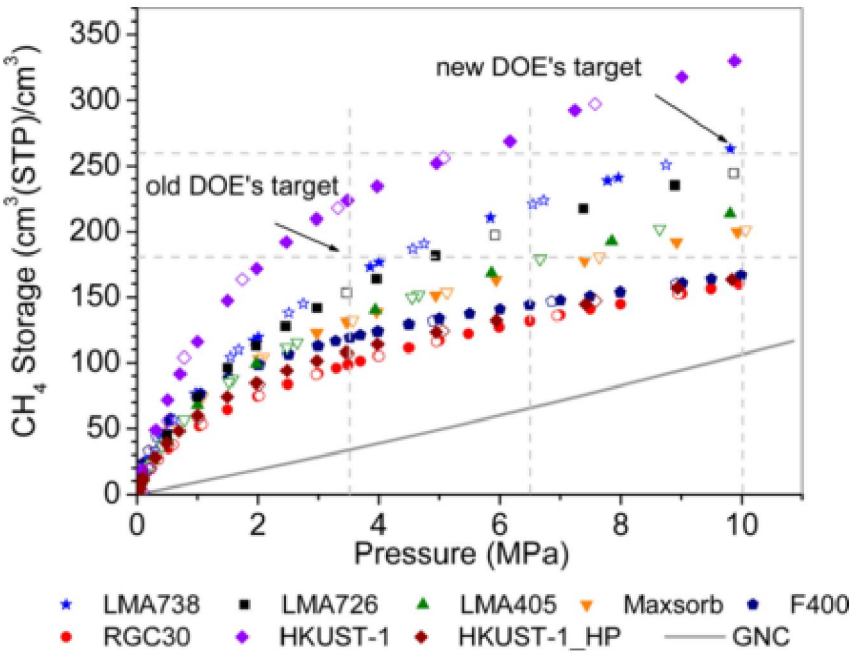

Figure 4.4: Methane storage capacity for different activated carbons at 298 K and up to 10 MPa. MOF sample HKUST-1 has been included for the sake of comparison (closed symbols represent adsorption data, open symbols represent desorption data) [14].

density ensuring that the storage capacity and the energy density, on volumetric basis is high. Since the microporosity of ACs is created by removal of carbon atoms during the activation process, after a certain microporosity volume further activation is followed by the creation of macropores translating into a useless volume for gas storage and thus a decrease of the packing density. Hence, carbons with high CH4 uptake might result in a lower volumetric storage capacity of methane than some with lower surface area. In this sense is useful to express the adsorption capacities in terms of volumetric quantities instead of gravimetric basis (Fig. 4.5) [31].

Along with a high micropore volume, the activated carbon is required to have a high packing density, thus presenting a high energy density on volumetric basis. Optimization of the packing density can be done by means of improving the bulk density, monolith preparation and particle size design. It is strongly related to the activation degree of the adsorbent, the higher the surface area and pore volume are the lower the packing density is. Byamba-Ochir et al. [15] showed the importance of the activation conditions for the preparation of ACs for methane storage, they found that the BET surface area increased with an increase of the ratio of activating agent and the Mongolian raw anthracite, however, the packing density gradually decreases and therefore does the volumetric capacity (Table 4.4).

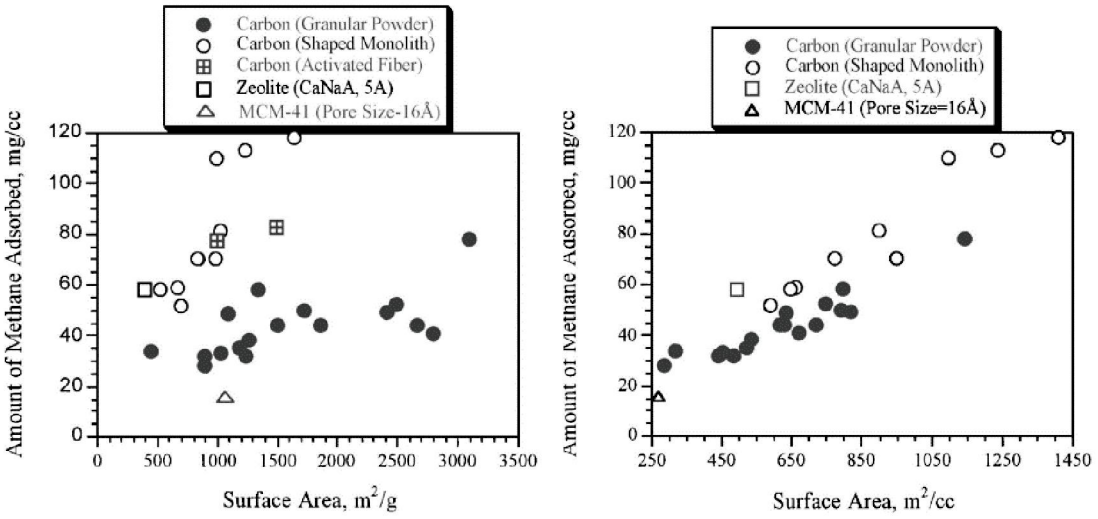

Figure 4.5: Effect of expressing the methane adsorption capacity in terms of gravimetric surface (m^2 g^{-1}) area vs volumetric surface area (m^2 cm^{-3}) for different porous materials at 3.447 MPa and 298 K. A suited adsorbent for the ANG storage presents a maximum volumetric surface area [31].

Table 4.4: Effect of activating agent/Mongolian raw anthracite radio in the volumetric methane adsorption capacity [15].

Carbon monoliths	**SBET (m^2 g^{-1})**	**v/v ($cm^3{}_{CH4}/cm^3{}_{AC}$)**
PMAC2/1-C3-65	622	43.6
PMAC1/1-C3-65	845	60.1
PMAC1/2-C3-65	1460	162.2
PMAC1/3-C3-65	1757	147.8

To further investigate the effect of the adsorbent design parameters and the volumetric storage capacity, Kumar et al. [25] plotted the volumetric adsorption capacity versus the product of the packing density (PD) and the specific surface area of the adsorbents (Fig. 4.6) finding a logarithmic relationship. They determined that in order to achieve the volumetric methane adsorption capacity of 180 v/v, the adsorbents must have a surface area of 2463 m^2 cm^{-3} and packing density of about 1.2 g cm^{-3}. This are just guidelines since consideration of pore volume and distribution must be made.

One important advantage of using activated carbons as adsorbent materials for gas separation and storage is the possibility of using different organic materials rich in carbon contents as precursors with coal and wood being the most employed ones. However, in recent years there has being an increasing interest on the production of AC from agricultural wastes. The use of this type of materials as precursors can

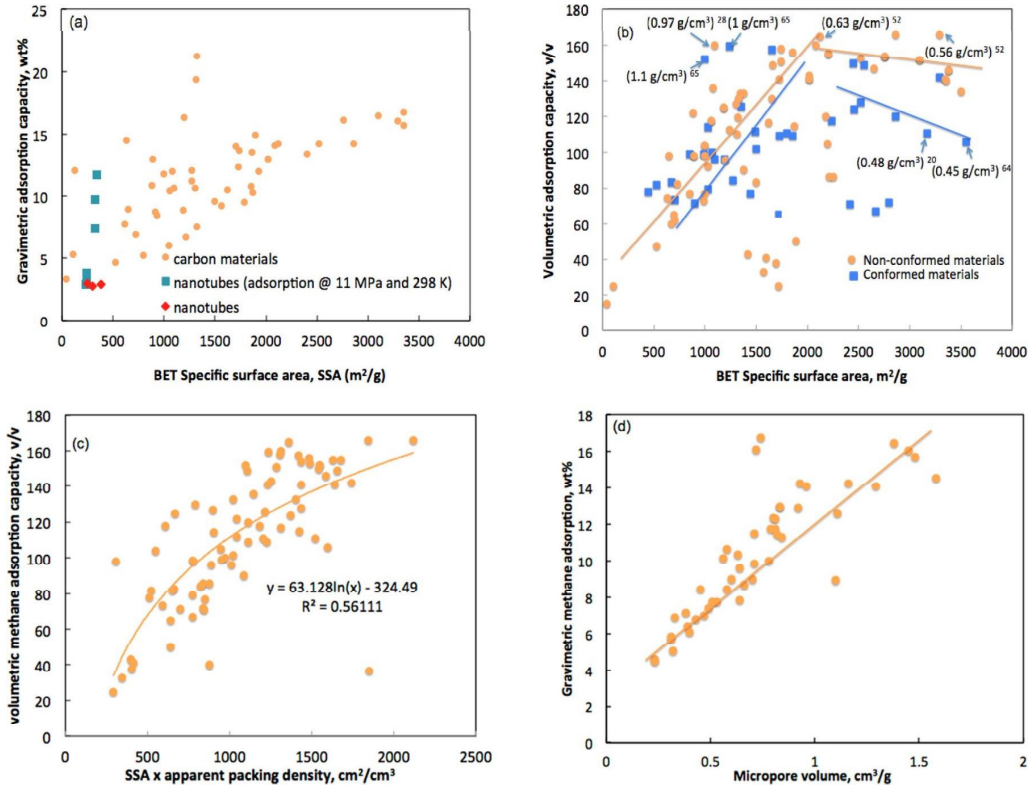

Figure 4.6: Volumetric adsorption capacity (v/v) of carbon structures versus the product of the BET specific surface area (SSA) and packing density [25]

reduce the pressure on mines and forests while valorizing products that otherwise result in waste production with economic and environmental impacts [32]. Examples of such precursor materials include rubber seed coat, olive seed, coconut shell, oil pal fiber and almond shell-derived [33]. Some of the results obtained using low-cost lignocellulosic biomass activated carbons for methane adsorption and storage are described in table 4.5.

Table 4.5: Biowaste precursors used to prepare activated carbons along with their specific surface area and CH_4 storage [34].

Precursors	**Activating Agent**	**Surface Area (m^2 g^{-1})**	**Storage Capacity**
Sugarcane molasses	KOH	2202	197.23 mg g^{-1}
Oil palm Shell	$ZnCl_2$	870	13 cm^3 g^{-1}
Corncob	KOH	3227	273.4 cm^3 g^{-1}
Corn cobs	KOH	1320	120 v/v
Palm shell	H_3PO_4	25.7	cm^3 g^{-1}
Olive stones	H_3PO_4	1014	4.69 mmol g^{-1}

Activated carbons can be optimized for methane storage by testing several activation conditions, such as activation method, activation temperature, activation

agent, activation agent to char ratio. Bagheri et al. [35] studied the effect of activation conditions on a corn cobs based AC, showing that the methane adsorption capacity can be increased from a low 25 v/v to up to 120 v/v at 298 K and 3.44 MPa when using optimal activation conditions. Using a similar optimization process Policicchio et al. [36] were able to obtain a CH_4 adsorption capacity of 150 v/v at 298 K and 3.5 MPa for a cellulose based AC. This optimization relays on the change of the textural parameters of the adsorbent (such as BET surface area and pore size distribution) upon different activation conditions. Ruiz et al. tested the effect of different activation temperatures, activation agent/precursor weight and inner flow gas on the pore size distribution (Fig. 4.7) [37]. Overall the best methane storage capacities were found when the activation method produced samples with high BET surface area. In the case of physical activation methods a higher activation degree resulted in a development of the porosity thus resulting in a higher surface area. In the case of chemical activation, a low activation temperature (between 700 and 800 °C) and a higher activation ratio/precursor resulted in a higher narrow micropore (<0.8 nm) volume. All the hitherto present studies show that the new DOE MOVE requirements are difficult to achieve by activated carbons and its feasibility is questionable. Furthermore, using Monte Carlo simulations a maximum methane storage capacity of activated carbons has been predicted to be 209 v/v at 3.4 MPa [38]. Thus this implies for researchers working in the design of new materials for the methane storage to reconsider this targets and/or changing the operating conditions (i.e. using higher pressures).

4.4 Carbon Dioxide Adsorption

Reducing carbon dioxide (CO_2) emissions is a key factor to fight global warming since among the greenhouse gases is the one emitted in higher volume. It is estimated that in 2006, CO_2 alone accounted for 81.6% of the total GHG emissions in the US [39], [40]. The CO_2 atmospheric concentration has increased from a preindustrial value of 280 ppm to 408 ppm in 2018 resulting in an increase of 1°C of the global temperature [40, 2]. The main source of carbon dioxide is the burning of fossil fuels followed by land-use change. Annual fossil fuels emissions increased from an average 6.4 GtC in the 1990s to 7.2 GtC average per year in 2000-2005 (1 gigatonne of carbon or GtC = 1 billion tonnes of carbon) [41]. Fossil fuel combustion is the principal source of anthropogenic carbon dioxide emissions (58% of global GHG emissions) thus they are required to drastically reduce its carbon dioxide emissions [42]. Carbon Capture and Storage (CCS) has been proposed as one of the most promising technologies to reduce carbon dioxide emissions in the short-term while carbon-free processes are implemented. It is believed that by the year 2050 CCS can reduce by 20% the

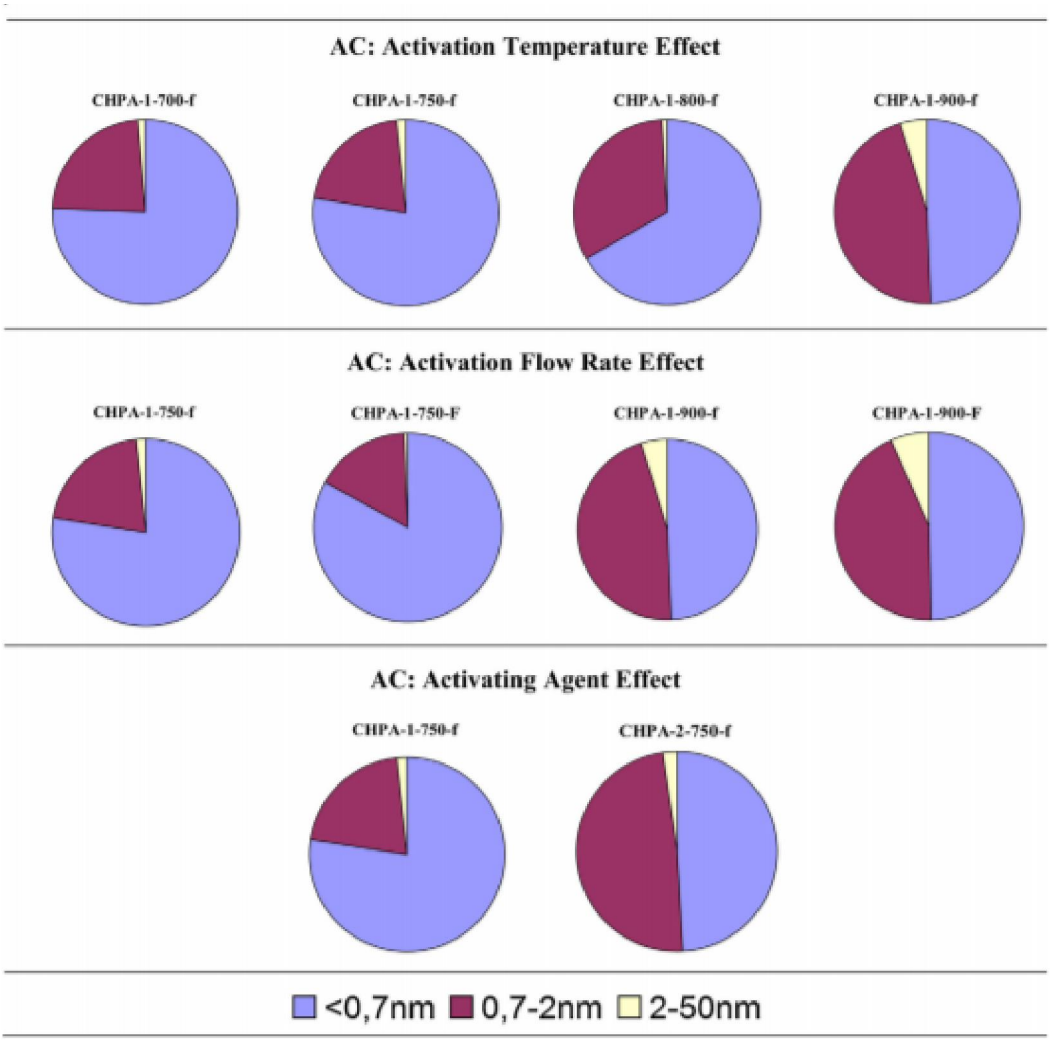

Figure 4.7: Micro-mesoporosity volume distributions (in percentages) within the chestnut shell activated carbons [37].

carbon dioxide emissions [43]. CSS is a three step process:

I) Separation of CO_2 from other emissions

II) CO_2 transportation to the storage site

III) Permanent storage

The transportation and the storage step are already developed technologies. It is the first stage of the CCS that has made difficult its implementation. The separation of the CO_2 accounts for approximately two thirds of the total cost of a CCS [44, 45]. In this sense between the proposed carbon dioxide capture and separation options, post-combustion capture has been appointed as the most feasible to implement in power plants as it can be retrofitted to existing plants without modification of the already existing systems [46]. The process of post-combustion can be done by many separation technologies such as physical adsorption, chemical adsorption, cryogenic separation and membranes. Most of the carbon dioxide capture systems commercially available employ chemical absorption with alkaline amines despite of the method remarkable disadvantages such as high energy requirements, oxidative degradation of the adsorbents, high corrosion and low cost efficiency. Other possible technologies being cryogenic separation and membrane separation, however the cryogenic separation has the disadvantage of using a great quantity of energy that makes it too expensive and the use of membranes is still in a very young developing phase [47]. Adsorption technology involves two steps, on the first step the carbon dioxide adsorption onto a porous adsorbent by the formation of chemical bonds (chemisorption) or by physical interactions such as van der Waals forces (physisorption). The second stage is the regeneration of the adsorption column after equilibration of the system. The regeneration can be done by reducing the pressure (Pressure Swing Adsorption - PSA) or by increasing the temperature (Temperature Swing Adsorption - TSA). The adsorption process using physisorbent materials is considered as the most cost-effective option for carbon dioxide separation due to its low energy requirements, additionally it is a very noble technology that can be easily scale to different plant sizes and used on a wide range of temperatures and pressures. The success of an adsorption separation technology relays on the quality of the employed adsorbent. It has been described that a successful adsorbent for the carbon dioxide capture and storage should satisfy five main requirements [48]:

I) Large CO_2 uptake

II) High sorption rate

III) Good selectivity between CO_2 and other competing gases

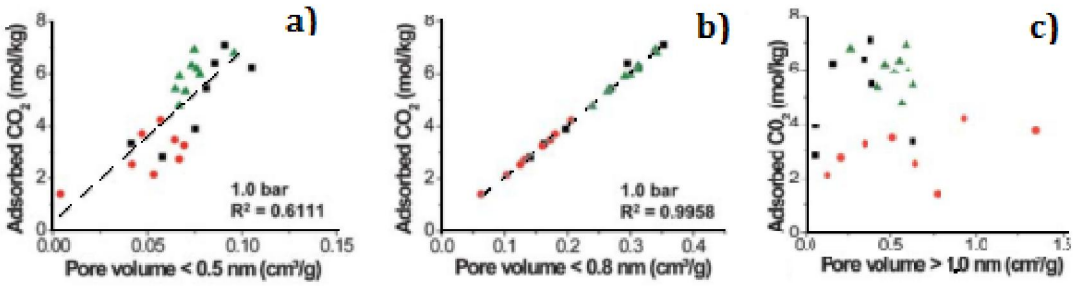

Figure 4.8: CO_2 uptake at 273 K 0.1 MPa for the volume of pores a) Pore Volume < 0.5 nm, b) Pore Volume < 0.8 nm and c) Pore Volume > 1.0 nm [50].

IV) Easy regeneration

V) Low cost and high availability

The search for new adsorbent materials that better fulfill this requirements has become an active field of research. Adsorbents that have been studied for this purposed so far include activated carbons, zeolites, MOFs and polymers. It is important to mention here that development of better adsorbents for the carbon dioxide separation would not be only beneficial to the CCS systems but also for the upgrading of biogas and natural gas. On this contexts, activated carbons (CAs) are considered as a superior material for the CO_2 capture and separation due to their hydrophobic character, lower cost, high thermal stability and low regeneration energy requirements [49]. Similar to the adsorption process of methane, the textural properties of activated carbons play a major role on the adsorption behavior. CO_2 adsorption is enhanced by the presence of micropores of up to 1 nm. By comparing a number of porous carbons, Presser et al. showed that the volume of pores larger than 1 nm is not a major contributor to the CO_2 adsorption (Fig. 8c). In fact, it is the volume of ultramicropores (size smaller than 0.8 nm) that has the higher influence upon CO_2 adsorption as proven by a higher correlation coefficient (R^2 of 0.9958) (Fig. 4.8d). Presser et al. reported that upon very low CO_2 partial pressures such as 0.01 MPa it is the pores with a size smaller than 0.5 nm that are the main contributors [50]. The dependency of the adsorption of carbon dioxide on the ultramicropore volume was also observed by Guojun et al. at 273, 283 and 293 K and pressures between 0.01 MPa and 0.10 MPa [51].

If ultramicropore volume has proven to influence the adsorption capacity of the activated carbons no clear relationship between the BET surface area and the adsorption capacity has been reported for pressures up to 0.1 MPa [50, 51, 52]. The potential theory indicates that CO_2 adsorption happens with micropore filling followed by capillary condensation and liquefaction with increasing pressure, it is expected then that at high pressure the BET surface area and total pore volume gain

influence on the CO_2 adsorption. Drage et al. reported that a pressure of 4.1 MPa a linear relationship between the CO_2 adsorption capacity of activated carbons and the BET surface area can be found [53]. Another important factor to be considered when designing a carbonaceous porous material for carbon dioxide adsorption is the source of the raw material from which it will be produced. One of the main advantage of activated carbons is their versatility, any carbonaceous material can be converted in activate carbon with the main requirements being a high carbon content and low in ash, this arises the possibility of producing environmental friendly activated carbons based on lignocellulosic biomass. On this sense, several efforts have been made to produce CAs from lignocellulosic resources with the aim of CO_2 adsorption (table 4.6).

Table 4.6: Biowaste precursos used to prepare activated carbons along with their activation method, specific surface area and CO_2 storage capacity [34].

Precursors	**Activating Agent**	**Surface Area (m^2 g^{-1})**	**Storage Capacity**
Oil cake/walnut	CO_2	1207	34.72 ml g^{-1}
Coconut shell	CO_2	371	1.8 mmol g^{-1}
Almond-shell	CO_2	862	2.7 mmol g^{-1}
Olive stone	CO_2	1215	3.1 mmol g^{-1}
Coffee residue	CO_2	593	2.4 mmol g^{-1}
Rice husk	$ZnCl_2$	927	1.3 mmol g^{-1}
Peanut shell	KOH	956	4.0 mmol g^{-1}
Sunflower seed	KOH	1790	4.6 mmol g^{-1}
Bamboo	KOH	1846	4.5 mmol g^{-1}
Palm stone	H_3PO_4	924	2.7 mmol g^{-1}

The selection of the raw materials prior to the activated carbon production is of main concern for the gas storage suitability of the adsorbent. Olivares-Marín et al.[54] showed the importance of carefully choosing the precursor, they compared the CO_2 one sample of pre-consumer carpet and two samples of post-consumer sample under the same activation conditions finding that the presence of inorganic binders in the precursor can result in a lower micropore volume lowering then the CO_2 adsorption capacity between the samples from 13.8 wt% to 3.7 wt%. Hao et al. [55] had similar findings when comparing activated carbons obtained from grass cuttings, house manure, organic waste from beer production and bio-sludge from a waste water treatment plant, the activated carbons produced from grass cutting and horse manure showed higher CO_2 adsorption capacities due to a larger volume of ultramicropores. Munusamy et al. [16] showed that using carboxyl methyl cellulose

sodium salt and soluble starch as binders to convert a powdered mango seed shell derived activated carbon into extruded form they could enhance the maximum CO_2 equilibrium adsorption capacity from 14.3 wt.% to 21.3 wt.% at 0.1 MPa and 273 K explained by the formation of surface functionality by the binders on the extruded AC. In addition to the nature of the precursor, the optimal operating conditions of the activation process need to be determined since they can significantly affect the adsorption capacity of the AC. There are two possible activation paths for producing ACs, chemical activation and physical activation. Chemical activation using KOH, H_3PO_4 or $ZnCl_2$ is usually preferred since it results in hierarchical porous structures with high surface areas it also consumes less energy as the chemical activation temperature is between 600 and 800°C versus 800 to 1000°C for physical activation. Chemical activation has the additional advantage that it can be done in one stage where carbonization and impregnation of the precursor are done simultaneously, while physical activation involves a first step of carbonization and a second step where the material is activated in the presence of oxidants such as air, CO_2 and steam [56, 57]. Song et al.[58] compared different activation methods and conditions for corn stalk based ACs. The ACs produced by physical activation at different activation concentrations or activation times presented surface areas lower than 500 m^2 g^{-1} while chemical activation resulted in slightly higher surface areas (up to 639.8 m^2 g^{-1}), additionally the chemical activated carbons also showed higher micropore volumes. This two factors resulted in higher CO_2 uptakes of chemical activated carbons than physical activated ones (Fig. 4.9). Between all the samples a maximum carbon dioxide adsorption capacity of 7.33 wt.% was obtained. Alabadi et al.[59] were able to obtained highly porous activated carbons by chemical activation with KOH of a starch and gelatin 1:1 mix, a CO_2 capture capacity of 3.8 mmol g^{-1} at 298 K and 0.1 MPa was obtained. Using also KOH activation to produce a pine nut-shell-derived activated carbon a high CO_2 uptake of 5.0 mmol g^{-1} at 273 K and 0.1 MPa was determined by Deng et al. [60]. A CO_2 adsorption of 5.22 mmol g^{-1} at 293 K and 0.1 bar, one of the highest reported CO_2 adsorption uptakes for carbonaceous materials, was obtained by KOH chemical activation of Coca-Cola as a source of biomass by Boyjoo et al. [61].

Typical activated carbons show weak affinity towards carbon dioxide with an adsorption capacity of surrounding 5 wt.% at 298 K and a pressure of 0.01 MPa (nearly the CO_2 partial pressure of post-combustion gas) [62]. This value however, can be improved by chemical modification of the AC's surface. One possibility is to introduce Lewis bases onto the activated carbon surface which favors the CO_2 adsorption due to its acidic properties. Nitrogen enrichment has been reported to be an effective way for introducing basic groups on the AC. Meng et al. [63] reported a CO_2 adsorption capacity of up to 17.7% wt. at 298 K and 0.01 MPa when treating an polypyrrole activated carbon with NaOH, they reported that the adsorption

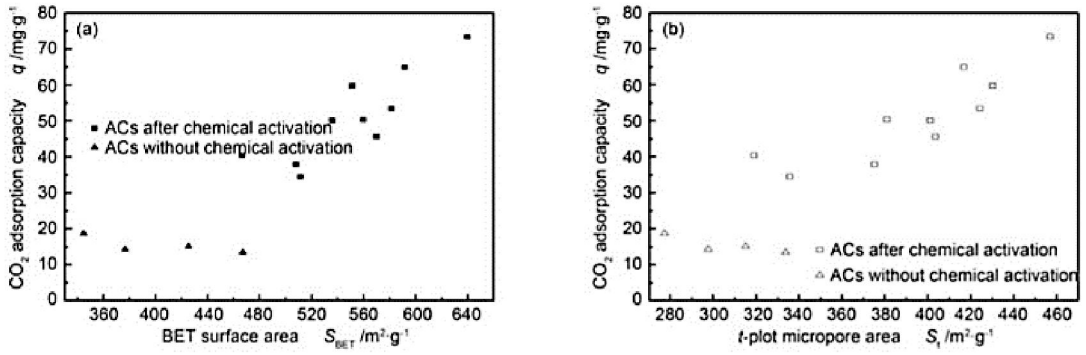

Figure 4.9: Effect of a) BET surface area and b) t-plot micropore area on CO_2 adsorption capacity at 298 K for chemical activated (squares) and physical activated (triangles) activated carbons from corn stalk [58].

capacity was both a function of the nitrogen content and the micropore volume. Other works report the same dependence between the carbon dioxide capacity an both the textural properties and N content [64, 65]. When introducing nitrogen functionalities the presence of oxygen surface groups is desirable, since they will act as anchoring sites for the nitrogen groups. Caglayan et al. [66] studied the effect of different oxidation and heat treatments on the formation of N surface groups. They found that the CO_2 adsorption capacity was enhanced by Na_2CO_3 impregnation of the air oxidized and nitric acid oxidized AC. They reported that sodium atoms (Na) have CO_2 sorption ability and that the oxidation with HNO3 provided anchoring sites for Na atoms. Shafeeyan et al.[67] compared the CO_2 adsorption capacity of a heat-treated under nitrogen AC without pre-oxidation and amination of pre-oxidized AC.The samples that were not pre-oxidized presented a higher BET surface area, pore volume and micropore volume, this due the thermal decomposition of functional groups inside the pores. Furthermore, when the sample is previously oxidized there is a blockage of the micropores entrances by oxygen and also a collapse of some pore walls leading to a decrease of the BET surface area and the micropore volume. However, if the oxidation step is done at high temperature (800 °C) the oxygen surface groups are decomposed and the textural properties are recovered (Fig. 4.10, sample OXA-800). They found a clear relationship between both micropore volumes and nitrogen content with the CO_2 adsorption capacity.

Seema et al. [68] showed that upon Sulphur (S) doping of microporous carbonaceous materials the CO2 adsorption capacity can be increased. They found a correlation between the BET surface area, micropore volume and oxidized Sulphur surface groups with the carbon dioxide adsorption capacity. A maximum adsorption capacity of 4.5 mmol g^{-1} was reached. Xia et al. [69] also reported an increased on the CO_2 adsorption capacity after S-doping of microporous carbons, they obtained a maximum adsorption capacity of 2.46 mmol g^{-1} when a S content of 6.56% was

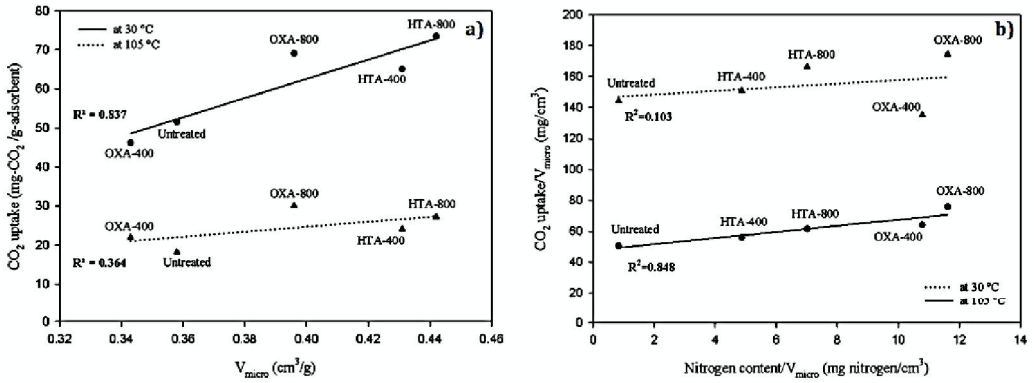

Figure 4.10: Relationship between the CO_2 capture capacity and a) micropore volume, b) nitrogen content (N%). OXA-400 and OXA-800: Pre-oxidazed samples aminated at 400 and 800 °C, HTA-400 and HTA-800: Heat treated samples aminated at 400 and 800 °C without pre-oxidation [67].

present and of 1.69 mmol g^{-1} when there was no Sulphur atoms on the carbonaceous material. It is then that even if the CO_2 adsorption capacity of activated carbons is greatly influenced by the BET surface area and the volume of narrow micropores (¡ 0.8 nm) the surface chemistry can also play an important role in the search of better materails for the CO_2 separation and storage. Different functionalities can be added to the surface of the adsorbent that will participate in the adsorption process trough acid-base interactions and polarizability of the carbon dioxide molecules. In addition to nitrogen and sulphur doping, activated carbons can be treated with metal oxides resulting in chemical reactions between the CO_2 molecules and the metal oxides at elevated temperatures. Published works include impregnation of activated carbons with alkaline metals such as Mg and Ca, and transition metals like Cu, Co, Ni, Fe, Cr and Zn [70, 71, 72]. Son et al. determined the CO_2 adsorption capacity of metal impregnated activated carbons to decrease in the order of Mg>Ca >Co=Cu>Ni (impregnated metal)[72]. Using Zn^{+2} as a promotor (Fig. 4.11), Somy et al. [70] tested the adsorption behavior of activated carbons impregnated by Fe_2O_3 and Cr_2O, finding a 20% increase of the CO_2 adsorption capacity upon Cr_2O impregnation (compared with raw AC); meanwhile Fe_2O_3 impregnation was not effective . Finally, it has been reported that an acidic treatment prior to the metal impregnation can further increase the carbon dioxide adsorption, the acid groups will oxidize the samples and provide oxygen surface groups that can form metal complexes with the metal ions [73].

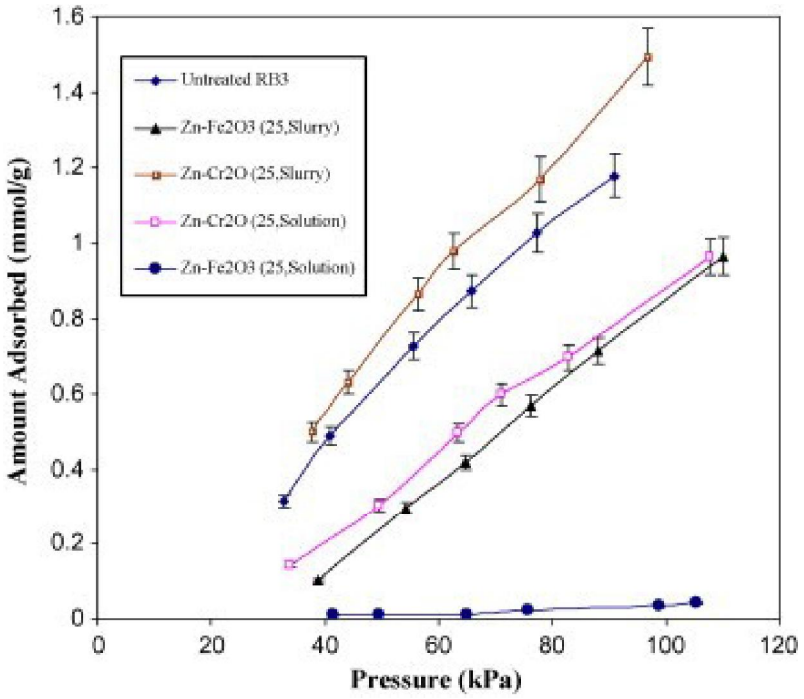

Figure 4.11: CO_2 adsorption isotherms of Zn^{+2}–metal oxide samples prepared by solution and slurry impregnation methods [72].

4.5 Conclusions

From environmental and economic point of value the use of biomass to prepare carbon materials with tunable features is demonstrated in many works. Many sources of biomass or biomass waste were used and optimized activation conditions with physical or chemical agents afford to obtain materials with high specific surface area, high porous volume and tunable pore size characteristics, and various surface chemistries, highly desired for gas storage applications. For the three gases evaluated herein (CH_4 and CO_2), the adsorption capacities on carbon adsorbents shows many similar trends. As demonstrated in many works, the adsorption capacity depends firstly on the available porosity, namely the specific surface area and in particularly microporous volume, the pore size with narrow distributions (0.5 -0.8 nm) being likely more favorable for achieving higher gas adsorption up-takes. In addition to the porosity, the carbon functional groups are also influencing the gas adsorption capacity. The oxygen, nitrogen and sulfur were widely studied and their influence on the gas up-take is not the same for all the gases. For CO_2 adsorption, oxygen seems beneficial to increase the gas up-take while for hydrogen adsorption oxygen proved to be detrimental. Regarding the other heteroatoms (N, S), their impact was found more difficult to precisely demonstrate due to the complexity to design materials with similar texture and oxygen contents, which usually interferes and accounts also in the adsorption process. The impact of the morphology on the gas adsorption is not deeply addressed and deserves further investigations to elucidate its impacts

on the materials density, gas diffusion and volumetric gas capacity. Beside the carbon characteristics that strongly influences the gas adsorption capacity, the analysis condition such as temperature and pressure has significant importance. Due to the week interactions of the gases with the carbon structure, the gas adsorption capacities at room temperature and atmospheric pressure or even high pressure, remain very small.

4.6 Bibliography

[1] Encyclopedia Britannica. Air, Atmospheric Gas, 2018.

[2] Intergovernmental Panel on Climate Change (IPCC). Climate Change 2014 Synthesis Report. Technical report, IPCC, Geneva, Switzerland, 2014.

[3] Amanda Alonso, J. Moral-Vico, Ahmad Abo Markeb, Martí Busquets-Fité, Dimitrios Komilis, Victor Puntes, Antoni Sánchez, and Xavier Font. Critical review of existing nanomaterial adsorbents to capture carbon dioxide and methane. *Science of the Total Environment*, 595:51–62, 2017.

[4] R. Ben-Mansour, M. A. Habib, O. E. Bamidele, M. Basha, N. A.A. Qasem, A. Peedikakkal, T. Laoui, and M. Ali. Carbon capture by physical adsorption: Materials, experimental investigations and numerical modeling and simulations - A review. *Applied Energy*, 161:225–255, 2016.

[5] Shengqian Ma, Daofeng Sun, Jason M. Simmons, Christopher D. Collier, Daqiang Yuan, and Hong Cai Zhou. Metal-organic framework from an anthracene derivative containing nanoscopic cages exhibiting high methane uptake. *Journal of the American Chemical Society*, 130(3):1012–1016, 2008.

[6] Pil-Seon Choi, Ji-Moon Jeong, Yong-Ki Choi, Myung-Seok Kim, Gi-Joo Shin, and Soo-Jin Park. A review: methane capture by nanoporous carbon materials for automobiles. *Carbon letters*, 17(1):18–28, 2016.

[7] Chao Chen and Wha Seung Ahn. CO2 adsorption on LTA zeolites: Effect of mesoporosity. *Applied Surface Science*, 311:107–109, 2014.

[8] Simone Cavenati, Carlos A. Grande, and Alírio E. Rodrigues. Adsorption Equilibrium of Methane, Carbon Dioxide, and Nitrogen on Zeolite 13X at High Pressures. *Journal of Chemical & Engineering Data*, 49(4):1095–1101, 2004.

[9] Mariem Kacem, Mario Pellerano, and Arnaud Delebarre. Pressure swing adsorption for CO_2/N_2 and CO_2/CH_4 separation: Comparison between activated carbons and zeolites performances. *Fuel Processing Technology*, 138:271–283, 2015.

[10] Jae Wook Lee, Hyun Chul Kang, Wang Geun Shim, Chan Kim, and Hee Moon. Methane adsorption on multi-walled carbon nanotube at (303.15, 313.15, and 323.15) K. *Journal of Chemical and Engineering Data*, 51(3):963–967, 2006.

[11] Meei Mei Gui, Yan Xin Yap, Siang Piao Chai, and Abdul Rahman Mohamed. Multi-walled carbon nanotubes modified with (3-aminopropyl)triethoxysilane

for effective carbon dioxide adsorption. *International Journal of Greenhouse Gas Control*, 14:65–73, 2013.

[12] Wei Zhou, Hui Wu, Michael R. Hartman, and Taner Yildirim. Hydrogen and methane adsorption in metal-organic frameworks: A high-pressure volumetric study. *Journal of Physical Chemistry C*, 111(44):16131–16137, 2007.

[13] Philip L Llewellyn, Sandrine Bourrelly, Christian Serre, Alexandre Vimont, Marco Daturi, Lomig Hamon, Guy De Weireld, Jong-san Chang, Do-young Hong, Young Kyu Hwang, and Sung Hwa Jhung. High Uptakes of CO_2 and CH_4 in Mesoporous Metals-Organic Frameworks MIL-100 and MIL-101. *Langmuir*, (18):7245–7250, 2008.

[14] Mirian Elizabeth Casco, Manuel Martínez-Escandell, Enrique Gadea-Ramos, Katsumi Kaneko, Joaquín Silvestre-Albero, and Francisco Rodríguez-Reinoso. High-pressure methane storage in porous materials: Are carbon materials in the pole position? *Chemistry of Materials*, 27(3):959–964, 2015.

[15] Narandalai Byamba-Ochir, Wang Geun Shim, M. S. Balathanigaimani, and Hee Moon. High density Mongolian anthracite based porous carbon monoliths for methane storage by adsorption. *Applied Energy*, 190:257–265, 2017.

[16] Kuppusamy Munusamy, Rajesh S. Somani, and Hari C. Bajaj. Breakthrough adsorption studies of mixed gases on mango (Mangifera indicaL.) seed shell derived activated carbon extrudes. *Journal of Environmental Chemical Engineering*, 3(4):2750–2759, 2015.

[17] E. Buss. Gravimetric measurement of binary gas adsorption equilibria of methane-carbon dioxide mixtures on activated carbon. *Gas Separation and Purification*, 9(3):189–197, 1995.

[18] M. Feroldi, A. C. Neves, C. E. Borba, and H. J. Alves. Methane storage in activated carbon at low pressure under different temperatures and flow rates of charge. *Journal of Cleaner Production*, 172:921–926, 2018.

[19] EEA. *Trends and projections in Europe 2014*. Number 10. 2014.

[20] EPA. Inventory of U.S. Greenhouse Emissions and Sinks. Technical report, 2016.

[21] NaturalGas.org. Natural Gas and the Environment.

[22] National Center for Biotechnology Information. PubChem Compound Database; CID=297.

[23] Tim Burchell and Mike Rogers. Low Pressure Storage of Natural Gas for Vehicular Applications. Technical Report 724, 2000.

[24] DC Energy, U.S. Department of Energy: Washington. MOVE: Methane Oppurtuities for Vehicular Energy. Advanced Research Projects Agency, 2012.

[25] K. Vasanth Kumar, Kathrin Preuss, Maria Magdalena Titirici, and Francisco Rodríguez-Reinoso. Nanoporous Materials for the Onboard Storage of Natural Gas. *Chemical Reviews*, 117(3):1796–1825, 2017.

[26] S. Biloe, V. Goetz, and S. Mauran. Characterization of adsorbent composite blocks for methane storage. *Carbon*, 39(11):1653–1662, 2001.

[27] Roger F. Cracknell, Peter Gordon, and Keith E. Gubbins. Influence of pore geometry on the design of microporous materials for methane storage. *Journal of Physical Chemistry*, 97(2):494–499, 1993.

[28] Myrsini K Antoniou, Evmorfia K Diamanti, Apostolos Enotiadis, Alfonso Policicchio, Konstantinos Dimos, Federica Ciuchi, Enrico Maccallini, Dimitrios Gournis, and Raffaele G Agostino. Methane storage in zeolite-like carbon materials. *Microporous and Mesoporous Materials*, 188:16–22, 2014.

[29] D. Lozano-Castelló, D. Cazorla-Amorós, A. Linares-Solano, and D. F. Quinn. Influence of pore size distribution on methane storage at relatively low pressure: Preparation of activated carbon with optimum pore size. *Carbon*, 40(7):989–1002, 2002.

[30] Andrés A. García Blanco, Andrea F. Vallone, Sophia A. Korili, Antonio Gil, and Karim Sapag. A comparative study of several microporous materials to store methane by adsorption. *Microporous and Mesoporous Materials*, 224:323–331, 2016.

[31] V. C. Menon and S. Komarneni. Porous adsorbents for vehicular natural gas storage: a review. *Journal of Porous Materials*, 5(1):43–58, 1998.

[32] Hoque M. Mozammel, Ota Masahiro, and S. C. Bhattacharya. Activated charcoal from coconut shell using $ZnCl_2$ activation. *Biomass and Bioenergy*, 22(5):397–400, 2002.

[33] Arash Arami-Niya, Wan Mohd Ashri Wan Daud, Farouq S. Mjalli, Faisal Abnisa, and Mohammad Saleh Shafeeyan. Production of microporous palm shell based activated carbon for methane adsorption: Modeling and optimization using response surface methodology. *Chemical Engineering Research and Design*, 90(6):776–784, 2012.

[34] P. González-García. Activated carbon from lignocellulosics precursors: A review of the synthesis methods, characterization techniques and applications. *Renewable and Sustainable Energy Reviews*, 82(August 2017):1393–1414, 2018.

[35] Narges Bagheri and Jalal Abedi. Adsorption of methane on corn cobs based activated carbon. *Chemical Engineering Research and Design*, 89(10):2038–2043, 2011.

[36] Alfonso Policicchio, Enrico MacCallini, Raffaele Giuseppe Agostino, Federica Ciuchi, Alfredo Aloise, and Girolamo Giordano. Higher methane storage at low pressure and room temperature in new easily scalable large-scale production activated carbon for static and vehicular applications. *Fuel*, 104:813–821, 2013.

[37] B. Ruiz, N. Ferrera-Lorenzo, and E. Fuente. Valorisation of lignocellulosic wastes from the candied chestnut industry. Sustainable activated carbons for environmental applications. *Journal of Environmental Chemical Engineering*, 5(2):1504–1515, 2017.

[38] K R Matranga, A L Myers, and E D Glandt. Storage of Natural-Gas By Adsorption on Activated Carbon. *Chemical Engineering Science*, 47(7):1569–1579, 1992.

[39] Akihiro Yamasaki. An Overview of CO_2 Mitigation Options for Global Warming—Emphasizing CO2 Sequestration Options. *Journal of Chemical Engineering of Japan*, 36:361–375, 2003.

[40] NASA. Carbon Dioxide 2018, 2018.

[41] M. G. Plaza, C. Pevida, B. Arias, J. Fermoso, A. Arenillas, F. Rubiera, and J. J. Pis. Application of thermogravimetric analysis to the evaluation of aminated solid sorbents for CO_2 capture. *Journal of Thermal Analysis and Calorimetry*, 92(2):601–606, 2008.

[42] International Energy Agency. CO_2 emissions from fuel combustion. Highlights. Technical report, 2017.

[43] Global CCS Institue. Accelerating the Uptake of CCS: Industrial Use of Captured Carbon Dioxide. Technical Report March, 2011.

[44] Jian Rong Li, Yuguang Ma, M. Colin McCarthy, Julian Sculley, Jiamei Yu, Hae Kwon Jeong, Perla B. Balbuena, and Hong Cai Zhou. Carbon dioxide capture-related gas adsorption and separation in metal-organic frameworks. *Coordination Chemistry Reviews*, 255(15-16):1791–1823, 2011.

[45] Intergovernmental Panel on Climate Change (IPCC). *Carbon Dioxide Capture and Storage*. Number October. 2005.

[46] Zhi Hua Lee, Keat Teong Lee, Subhash Bhatia, and Abdul Rahman Mohamed. Post-combustion carbon dioxide capture: Evolution towards utilization of nanomaterials. *Renewable and Sustainable Energy Reviews*, 16(5):2599–2609, 2012.

[47] Tick Hui Oh. Carbon capture and storage potential in coal-fired plant in Malaysia - A review. *Renewable and Sustainable Energy Reviews*, 14(9):2697–2709, 2010.

[48] Marta Sevilla, Camillo Falco, Maria-Magdalena Titirici, and Antonio B. Fuertes. High-performance CO_2 sorbents from algae. *RSC Advances*, 2(33):12792, 2012.

[49] M. G. Plaza, S. García, F. Rubiera, J. J. Pis, and C. Pevida. Post-combustion CO_2 capture with a commercial activated carbon: Comparison of different regeneration strategies. *Chemical Engineering Journal*, 163(1-2):41–47, 2010.

[50] Volker Presser, John McDonough, Sun-Hwa Yeon, and Yury Gogotsi. Effect of pore size on carbon dioxide sorption by carbide derived carbon. *Energy & Environmental Science*, 4(8):3059, 2011.

[51] Guojun Yin, Zhenyu Liu, Qingya Liu, and Weize Wu. The role of different properties of activated carbon in CO_2 adsorption. *Chemical Engineering Journal*, 230:133–140, 2013.

[52] Jarosław Serafin, Urszula Narkiewicz, Antoni W. Morawski, Rafał J. Wróbel, and Beata Michalkiewicz. Highly microporous activated carbons from biomass for CO_2 capture and effective micropores at different conditions. *Journal of CO2 Utilization*, 18:73–79, 2017.

[53] Trevor C. Drage, James M. Blackman, Cova Pevida, and Colin E. Snape. Evaluation of Activated Carbon Adsorbents for CO_2 Capture in Gasification. *Energy & Fuels*, 23(5):2790–2796, 2009.

[54] M. Olivares-Marín, S. García, C. Pevida, M. S. Wong, and M. Maroto-Valer. The influence of the precursor and synthesis method on the CO_2 capture capacity of carpet waste-based sorbents. *Journal of Environmental Management*, 92(10):2810–2817, 2011.

[55] Wenming Hao, Eva Björkman, Malte Lilliestråle, and Niklas Hedin. Activated carbons prepared from hydrothermally carbonized waste biomass used as adsorbents for CO_2. *Applied Energy*, 112:526–532, 2013.

[56] Gurwinder Singh, Kripal S. Lakhi, In Young Kim, Sungho Kim, Prashant Srivastava, Ravi Naidu, and Ajayan Vinu. Highly Efficient Method for the Synthesis of Activated Mesoporous Biocarbons with Extremely High Surface

Area for High-Pressure CO_2 Adsorption. *ACS Applied Materials & Interfaces*, 9(35):29782–29793, 2017.

[57] Jiacheng Wang and Stefan Kaskel. KOH activation of carbon-based materials for energy storage. *Journal of Materials Chemistry*, 22(45):23710, 2012.

[58] Tao Song, Jing Ming Liao, Jun Xiao, and Lai Hong Shen. Effect of micropore and mesopore structure on CO_2 adsorption by activated carbons from biomass. *Xinxing Tan Cailiao/New Carbon Materials*, 30(2):156–166, 2015.

[59] Akram Alabadi, Shumaila Razzaque, Yuwan Yang, Shi Chen, and Bien Tan. Highly porous activated carbon materials from carbonized biomass with high CO_2 capturing capacity. *Chemical Engineering Journal*, 281:606–612, 2015.

[60] Shubo Deng, Haoran Wei, Tao Chen, Bin Wang, Jun Huang, and Gang Yu. Superior CO_2 adsorption on pine nut shell-derived activated carbons and the effective micropores at different temperatures. *Chemical Engineering Journal*, 253:46–54, 2014.

[61] Yash Boyjoo, Yi Cheng, Hua Zhong, Hao Tian, Jian Pan, Vishnu K. Pareek, San Ping Jiang, Jean François Lamonier, Mietek Jaroniec, and Jian Liu. From waste Coca Cola®to activated carbons with impressive capabilities for CO_2 adsorption and supercapacitors. *Carbon*, 116:490–499, 2017.

[62] Seul Yi Lee and Soo Jin Park. A review on solid adsorbents for carbon dioxide capture. *Journal of Industrial and Engineering Chemistry*, 23:1–11, 2015.

[63] Long Yue Meng and Soo Jin Park. One-pot synthetic method to prepare highly N-doped nanoporous carbons for CO_2 adsorption. *Materials Chemistry and Physics*, 143(3):1158–1163, 2014.

[64] A L Yaumi, M Z Abu Bakar, and B H Hameed. Melamine-nitrogenated mesoporous activated carbon derived from rice husk for carbon dioxide adsorption in fixed-bed. *Energy*, Accepted M, 2018.

[65] Deepak Tiwari, Haripada Bhunia, and Pramod K. Bajpai. Synthesis of nitrogen enriched porous carbons from urea formaldehyde resin and their carbon dioxide adsorption capacity. *Journal of CO2 Utilization*, 21(November 2016):302–313, 2017.

[66] Burcu Selen Caglayan and A. Erhan Aksoylu. CO_2 adsorption on chemically modified activated carbon. *Journal of Hazardous Materials*, 252-253:19–28, 2013.

[67] Mohammad Saleh Shafeeyan, Wan Mohd Ashri Wan Daud, Amirhossein Houshmand, and Arash Arami-Niya. Ammonia modification of activated carbon to enhance carbon dioxide adsorption: Effect of pre-oxidation. *Applied Surface Science*, 257(9):3936–3942, 2011.

[68] Humaira Seema, K. Christian Kemp, Nhien H. Le, Sung Woo Park, Vimlesh Chandra, Jung Woo Lee, and Kwang S. Kim. Highly selective CO_2 capture by S-doped microporous carbon materials. *Carbon*, 66:320–326, 2014.

[69] Yongde Xia, Yanqiu Zhu, and Yi Tang. Preparation of sulfur-doped microporous carbons for the storage of hydrogen and carbon dioxide. *Carbon*, 50(15):5543–5553, 2012.

[70] Afsaneh Somy, Mohammad Reza Mehrnia, Hosein Delavari Amrei, Amin Ghanizadeh, and Mohammadhosein Safari. Adsorption of carbon dioxide using impregnated activated carbon promoted by Zinc. *International Journal of Greenhouse Gas Control*, 3(3):249–254, 2009.

[71] Z O U Yong and Vera G Mata. Adsorption of Carbon Dioxide on Chemically Modified High Surface Area Carbon-Based Adsorbents at High Temperature. *Adsorption*, pages 41–50, 2001.

[72] Seok-Jin Son, Jung-Sik Choi, Ko-Yeon Choo, Sun-Dal Song, Savithri Vijayalakshmi, and Tae-Hwan Kim. Development of carbon dioxide adsorbents using carbon materials prepared from coconut shell. *Korean Journal of Chemical Engineering*, 22(2):291–297, 2005.

[73] Soraya Hosseini, Iman Bayesti, Ehsan Marahel, Farahnaz Eghbali Babadi, Luqman Chuah Abdullah, and Thomas S.Y. Choong. Adsorption of carbon dioxide using activated carbon impregnated with Cu promoted by zinc. *Journal of the Taiwan Institute of Chemical Engineers*, 52:109–117, 2015.


Peredo-Mancilla, D., et al.
Experimental Determination of the CH_4 and CO_2 Pure Gas Adsorption Isotherms on Different Activated Carbons. *J. Chem. Eng. Data*, **2018**, 63, 3027-3034
CHAPTER 5
EXPERIMENTAL DETERMINATION OF THE CH_4 AND CO_2 PURE GAS ADSORPTION ISOTHERMS ON COMMERCIAL ACTIVATED CARBONS
ISBN: 0021-9568
DOI: 10.1021/acs.jced.8b00297
Journal of chemical&engineering data
THERMOPHYSICAL PROPERTIES & PHASE EQUILIBRIA FROM EXPERIMENT & COMPUTATION
ACS Publications

5.1 Chapter Outline

The bibliographic research presented in Chapter 4 indicates that the textural properties of activated carbons have a major role on their gas adsorption properties (see Chapter 4). In this context, the current Chapter is an experimental study aiming to explore the influence of such properties on CH_4 and CO_2 gas adsorption of ACs.

An original set of pure CH_4 and CO_2 adsorption equilibrium data is presented and expressed it in terms of textural properties such as BET surface area, total pore volume and micropore volume. Adsorption isotherms up to 3.5 MPa were performed using a home-made manometric technique at 303.15 K and 323.15 K. The results show a higher adsorption capacity for carbon dioxide than for methane over the whole pressure range for all of the samples. In addition, a contribution to the CO_2 adsorption capacity of the BET surface area and micropore volume is evidenced. The samples showed to have a comparable adsorption capacity to that of conventional adsorbents used for the separation and storage of CO_2.

5.2 Introduction

Treatment and disposal of liquid and solid wastes play an important role in the green house gases (GHG) emissions, with a total contribution of 3.2% of the total GHG, it is the fourth largest contributing sector in the EU, after energy, agriculture and industrial processes [1]. Furthermore, the emission of methane from waste disposal is alone responsible for 2% of the total GHG of the EU[1].

The anaerobic fermentation of the organic fraction of wastes results in a mixture of gases known as *Biogas*. It is composed mainly by carbon dioxide (CO_2) and methane (CH_4) [2]. To prevent the emission of methane into the atmosphere, biogas is collected and flared to transform the CH_4 fraction into CO_2, reducing its global warming potential from 28 kg of CO_2 eq to 1 kg of CO_2 eq. In a minor degree the collected biogas is directly burned to generate electricity with a process efficiency of roughly 38% [3]. However, another possible option that has gained popularity is a process known as '*Upgrading of Biogas*' in which highly pure methane (89 to 96 % purity) is separated from the gas mixture to be later used as an alternative to natural gas or as vehicle fuel [4].

There are several methods available for the upgrading of biogas which include water scrubbing [5, 6], chemical absorption [7, 8], membrane separation [9, 10], pressure swing adsorption [11, 12] and biological treatment [13, 14] . Depending on the implementation site, biogas content, plant scale as well as the final requirements of the produced gas each method presents different advantages and disadvantages. On

this context, Pressure Swing Adsorption (PSA) has a low investment cost, simplicity of operation, low energy requirements, easy to scale plant size (biogas flow-rate from 10 to 10000 m^3/h of biogas), lack of by-products and high efficiency that make it one of the preferred technologies[15, 16].

In a PSA biogas upgrading unit, biogas is put in contact with an adsorbent that selectively adsorbs and desorbs the carbon dioxide fraction. Many types of porous materials are used for the CH_4/CO_2 separation which includes carbon molecular sieves (CMS) [17, 18], zeolites [19, 20], activated carbons [21, 22] and more recently metal organic frameworks (MOFs) [23, 24]. Although zeolites are the typically chosen adsorbent for the PSA biogas upgrading units, the use of activated carbons (AC) presents important advantages such as a high surface area, developed pore volume, hydrophobic character and therefore high resistance to water, lower cost and low energy requirements [25, 26]. Nevertheless, activated carbons usually present low selectivity for carbon dioxide restricting its use[27].

The aim of the present work is to study the methane and carbon dioxide adsorption behavior in different activated carbons. In order to do so, methane (CH_4) and carbon dioxide (CO_2) adsorption isotherms were measured at 303.15 and 323.15 K for an extended range of pressure (0-3.5 MPa) for a set of 5 commercial activated carbons using a $home-made$ manometric device detailed in the literature [28]. A Langmuir two parameters model was used to simulate the adsorption isotherms and to calculate the maximum adsorption capacity of the samples. The effect of the structural properties over the adsorption capacity of the samples was studied.

5.3 Experimental Section

Material Characterization

Several types of activated carbons: CNR-115, RX 1.5, CGran, Rox 0.8 and GAC 1240 (Cabot Corporation, USA) were used for the adsorption studies. The activated carbon morphology was analyze by scanning electron microscopy (SEM) using a FEI Quanta 400 instrument. X-ray powder diffraction (XRD) was used to evaluate the activated carbon structure using a D8 ADVANCE A25-Bruker instrument. This diffractometer works in Bragg-Brentano reflexion geometry $\theta-\theta$ and is equipped with the Lynx Eye XE-T high resolution energy dispersive 1-D detector (Cu K$\alpha_{1,2}$).

Activated textural features were determined by N_2 and CO_2 adsorption performed on a Micromeritics ASAP 2420 device at 77 K and 273 K, respectively. Prior to the porosity analysis, the samples were out-gassed in vacuum at 300 °C for one night before the adsorption analysis. The pore size distributions (PSD) were

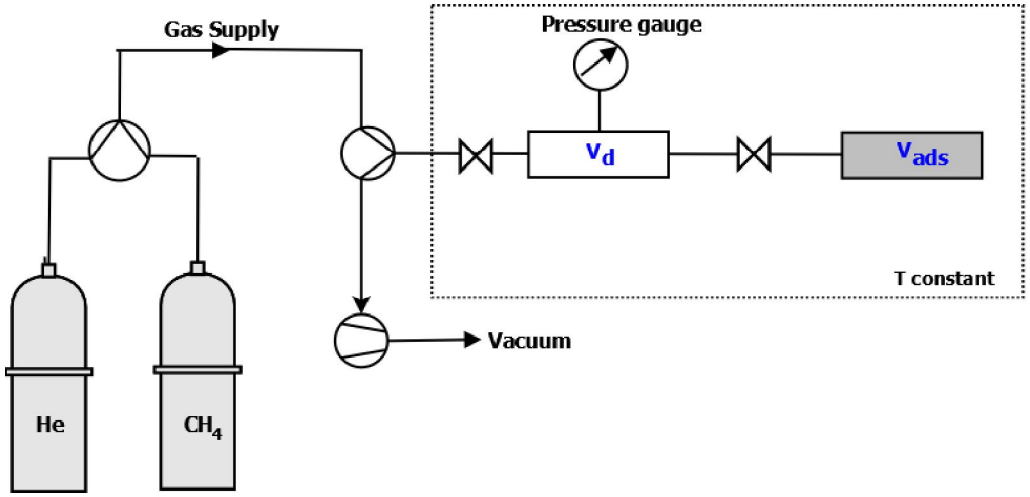

Figure 5.1: Schematic representation of the high pressure manometric device.

determined from the adsorption branch of nitrogen isotherms using the non liquid density functional theory (NLDFT) for carbon slit pores.

The specific surface area (SSA) was calculated from the linear plot in the relative pressure range of 0.01 to 0.05 (Fig. S1 of Supporting Information). Meanwhile, the micropore volume (V_μ) was obtained using the Dubinin-Radushkevich (DR) equation in the relative pressure interval (P/P_0) from 10^{-4} to 10^{-2} and the total pore volume (V_{TOT}) was determined from the amount of nitrogen adsorbed at a relative pressure of 0.95. Subtraction of the micropore volume from total pore volume resulted in the mesopore volume (V_{meso}).

Sample Preparation

5.3.1 Manometric Adsorption Setup

A home-made high-pressure manometric device was developed to obtain the adsorption isotherms of each of the samples, Figure 5.1 shows an schematic view of the apparatus. The main elements of the system are the dosing volume V_d, the adsorption cell V_{ads} and the MKS baratron type 121 A (0.01% uncertainty from vacuum to 3.3 MPa) connected to the dosing volume. A constant temperature in the integrity of the system is ensured by a heating wire controlled by a Eurotherm 3208 PID regulator, with 2 thermocouples fixed in the two cells to verify the isothermic conditions in all the system. The volume of the empty system was calculated by a gravimetric-manometric method consisting of sending a known mass of helium into the V_d recording the resulting pressure and working temperature, thus the volume could be obtained using the ideal gas equation of state. Additionally an expansion of the gas into the adsorption cell was done in order to derive the empty V_{ads} volume.

The uncertainty of the calculations of the empty volumes were inferior to 0.5%. The overall uncertainty of the adsorbed amount (due to the helium volume calibration process and the pressure accuracy) is determined to be lower than 1% over the entire pressure range[29].

Determination of Excess Adsorption

The samples were cleaned directly into the adsorption cell V_{ads} at 100°C under vacuum conditions for 10 h. An additional 5 hours cleaning step (100°C) was performed after void volume determination. In order to have a large enough adsorption area a sample mass of approximately 1 g was chosen.

The accessible volume in the adsorption cell is calculated by successive helium expansions from the V_d to V_{ads} then the all apparatus is evacuated and the temperature for the adsorption isotherm is settled.

To carry out the adsorption isotherm an accumulative process was chosen, with an increase of pressure of approximately 3 bars between each measurement. In this type of procedure successive doses of gas are introduced in the dosing cell and expanded into the adsorption cell, details of the procedure are specified on the literature [30, 31] .

Fitting of Excess Adsorption Isotherms

The adsorption isotherms were correlated by the modified Langmuir model that takes into account the adsorbet phase volume [32]:

$$n_{ads}^{excess} = n_L \frac{p}{p + p_L}\left(1 - \frac{\rho_g(p,T)}{\rho_{ads}}\right) = n_{ads}^{absolute}\left(1 - \frac{\rho_g(p,T)}{\rho_{ads}}\right) \tag{5.1}$$

where n_{ads}^{excess} is the adsorbed amount of gas (mol/kg) at the working pressure p (Mpa),p_L is the Langmuir pressure or the pressure at which half of the adsorption sites are occupied, n_L is the maximum Langmuir capacity (mol/kg), ρ_g and ρ_{ads} represent the gas density and adsorbed phase density at p and T conditions. In this work the adsorbed phase density of CO_2 was fixed to be 1027 kg/m^3[33]. The Langmuir model is limiting for low pressures, thus its application on high-pressure region of the adsorption isotherms is strictly unjustified. However, in many cases it is a reasonable approximation of the excess adsorption isotherms and consequently it can be use as a fitting function [34].

A standard deviation for the fitting process was calculated as:

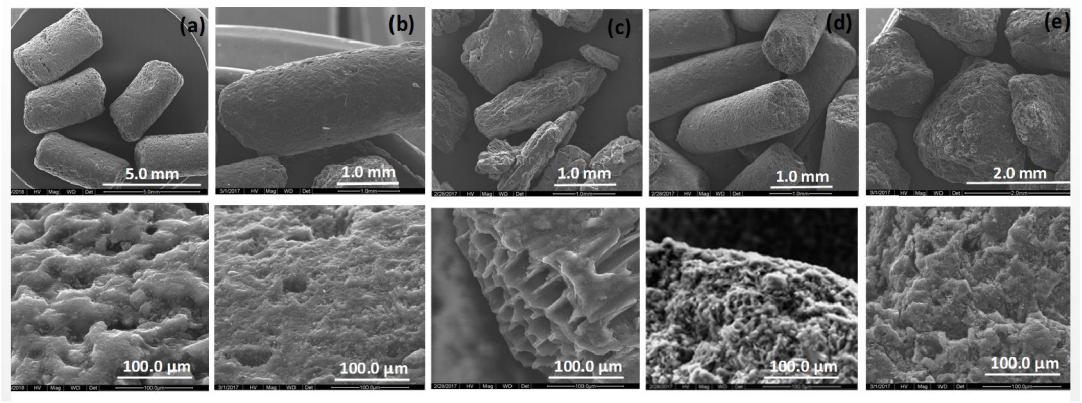

Figure 5.2: SEM images of activated carbons: a) CNR - 115, b) RX 1.5, c) CGran, d) Rox 0.8, e) GAC 1240 at two magnifications (¿1.0 mm and 100 μm)

$$\Delta n = \frac{1}{N} \cdot \sqrt{\sum_{1}^{N} (n_{ads}^{excess} - n_{FIT})^2} \tag{5.2}$$

Where Δn represent the standard deviation between the calculated adsorption values and the experimental ones. N is the number of adsorption values obtained through the experimental measurements, n_{ads}^{excess} is the experimental adsorbed gas amount and n_{FIT} the adsorbed amount calculated with the Langmuir equation.

5.4 Results and Discussion

The activated carbons present either a granular morphology (CNR - 115, RX 1.5 and Rox 0.8, Figure 5.2 a, b, d) or pallet-like morphology (CGran and GAC 1240, Figure 1c, e). Their size varies also with the type of carbon the larger one being observed for CNR - 115 and RX 1.5 while the smallest size is seen for CGran (Fig. 5.2c). At a closer look, most of materials present a rough and porous surface while in the case of CGran big pores in form of channels are noticed.

The XRD diffractogram (Fig. 5.3) show three peaks placed around 24°, 44° and 80° and corresponding to the (002), (100) and (110) diffraction planes of graphite. For all materials, the peaks are very broad indicating highly disordered materials with low degree of graphitization. In the case of RX 1.5, Rox 0.8 and GAC 1240, in addition to the graphite peaks, other peaks are observed. Their intensity is rather low but they have a sharp shape sign of presence of crystalline impurities. The identification revealed the presence of SiO_2 tridymite (PDF 89-3141) for Rox 0.8 and of SiO_2 quartz (PDF 89-1901) and Al silicate (PDF 89-2814) for the GAC 1240 carbon.

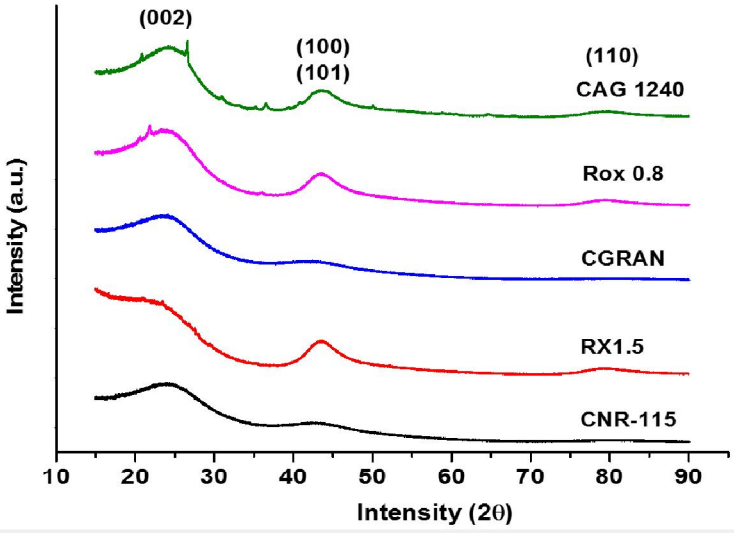

Figure 5.3: XRD patterns of activated carbons: CNR - 115, RX 1.5, CGran, Rox 0.8 and GAC 1240.

Table 5.1: Textural Properties of Carbon Materials

Sample	$\mathbf{S}_{BET}$ ($\mathbf{m^2\ g^{-1}}$)	$\mathbf{V}_{\mu}\ \mathbf{N}_2$ ($\mathbf{cm^3\ g^{-1}}$)	$\mathbf{V}_{TOT}$ ($\mathbf{cm^3\ g^{-1}}$)	$\mathbf{V}_{meso}\ \mathbf{N}_2$ ($\mathbf{cm^3\ g^{-1}}$)
CNR - 115	1714	0.64	0.95	0.31
RX 1.5	1683	0.61	0.81	0.20
CGran	1378	0.45	0.99	0.54
Rox 0.8	1323	0.48	0.64	0.16
GAC 1240	982	0.36	0.56	0.20

The pore size distribution obtained using the DFT model is shown in Figure 7.2. All of the probes are microporous (pores $\leq$ 2 nm) with a minor contribution of mesopores (pores between 2 and 50 nm). A pore size range between 0.5 nm and 2.6 nm was obtained for the activated carbons RX 1.5, CGran, Rox 0.8 and GAC, while CNR - 115 show a slightly wider range (between 0.5 and 3.5 nm).

Table 7.1 gives the textural properties of the activated carbons. The highest microporous volume was found for the samples with highest BET surface area CNR - 115 (S_{BET}=1714 $m^2\ g^{-1}$ and V_{μ}=0.64 $cm^3\ g^{-1}$) and RX 1.5 (S_{BET}=1683 $m^2\ g^{-1}$ and V_{μ}=0.61 $cm^3\ g^{-1}$). Meanwhile, sample CGran had the highest mesopore volume (V_{μ}=0.54 $cm^3\ g^{-1}$).

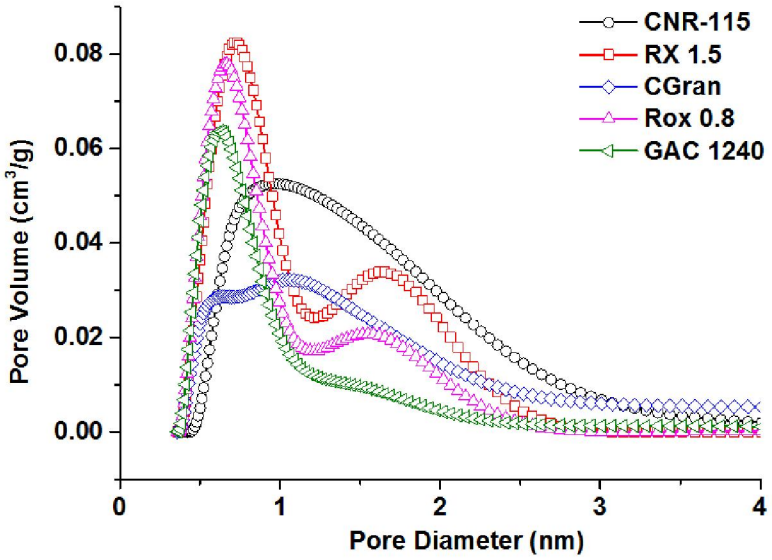

Figure 5.4: NLDFT pore size distribution of activated carbons: CNR - 115, RX 1.5, CGran, Rox 0.8 and GAC 1240

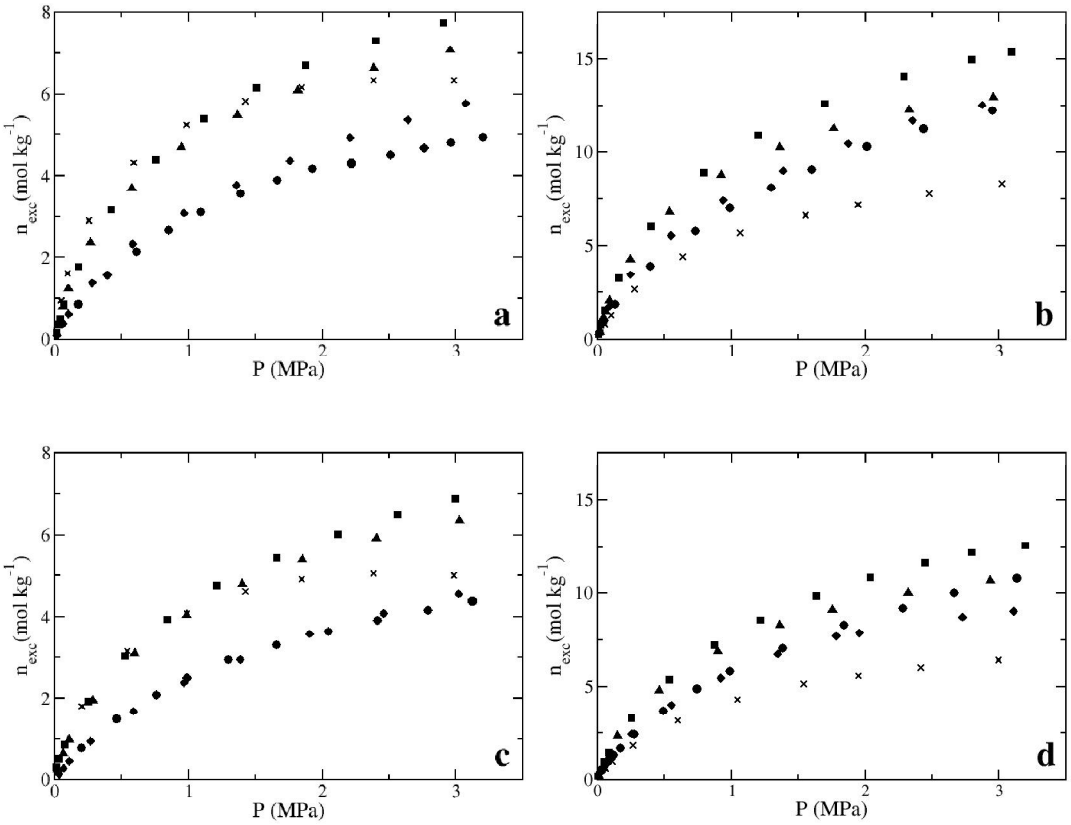

Figure 5.5: Excess adsorption isotherms for samples CNR-115 (cricle), RX 1.5 (square), CGran (diamond), Rox 0.8 (triangle), GAC 1240 (crosses). a) CH_4 adsorption at 303.15 K b) CO_2 adsorption at 303.15 K c) CH_4 adsorption at 323.15 K d) CO_2 adsorption at 323.15 K.

The CH_4 and CO_2 adsorption isotherms were obtained at 303.15 and 323.15 K for the 5 samples of activated carbons up to 3.5 MPa with a reproducibility superior to 99% (average absolute deviation of less than 1%). The experimental data is listed on Table 5.4-5.8 of the Chapter's Appendix. Figures 5.5a and 5.5c show the methane adsorption isotherms at both working temperatures, while Figures 5.5b and 5.5d display the carbon dioxide adsorption isotherms. It can also been seen that all the studied samples present a significant higher adsorption of CO_2 than that of CH_4 at both temperatures, agreeing with the general behavior of activated carbons for the critical temperature and pressure of methane (190.55 K and 4.59 MPa) are much lower than those of carbon dioxide (304.45 K and 7.38 MPa) resulting in the CO_2 molecules acting as condensable vapor and CH_4 as supercritical gas [35]. Another possible explanation for the higher adsorption of carbon dioxide is that contrary to methane, it presents a quadrupole moment resulting in higher adsorbate-adsorbate interactions within the adsorbed phase. For the methane molecules, since no dipole or quadrupole moments are present the interactions between adsorbate molecules are smaller [36].

Figure 5.5 also shows a decrease in the adsorption capacity with increasing temperature which can be explained by the exothermic nature of a physical adsorption process. It can be seen from Figures 5.5b and 5.5d that the sample that presents the higher CO_2 values throughout the pressure range is the RX 1.5 activated carbon (square), this sample also presents the higher methane adsorption (Figure 5.5a and Figure 5.5c).

The CO_2 adsorption isotherms were fitted using the Langmuir 2 parameters model (Table 5.2), the obtaining fitting parameter values are representative of a good fitting process of the data. There is a clear correlation between the maximum Langmuir capacity and the BET surface area as shown in Figure 5.6, a higher BET surface area results in a higher CO_2 maximum adsorption capacity, this behavior is to be expected since the BET surface area is a measurement of the available physisorption sites.

To further study the relationship between the structural properties and the carbon dioxide adsorption capacity, the $n_L(CO_2)$ was plotted against the total pore volume (Fig. 5.7), the micropore volume (Fig. 5.8) and the mesopore volume(Fig. 5.9). The total pore volume did not show a significant influence in the adsorption capacity, however, a linear correlation between the micropore volume and the maximum Langmuir capacity can be depicted throughout the studied samples. This relationship between the adsorption capacity and the micropore volume has been previously reported in the literature[37, 38].

The measured carbon dioxide adsorbed amounts at 0.1 MPa (CO_2 ads.) as

Table 5.2: Langmuir Fitting Parameters

303.15 K			
sample	n_L **(mol kg^{-1})**	ρ_L **(MPa)**	Δn
CNR - 115	19.26	1.679	0.073
RX 1.5	20.46	0.986	0.068
CGran	17.78	1.22	0.101
Rox 0.8	16.34	0.751	0.052
GAC 1240	10.79	0.91	0.037
323.15 K			
sample	n_L **(mol kg^{-1})**	ρ_L **(MPa)**	Δn
CNR - 115	17.02	1.816	0.054
RX 1.5	17.62	1.224	0.043
CGran	14.478	1.456	0.067
Rox 0.8	14.02	0.898	0.051
GAC 1240	8.67	1.03	0.019

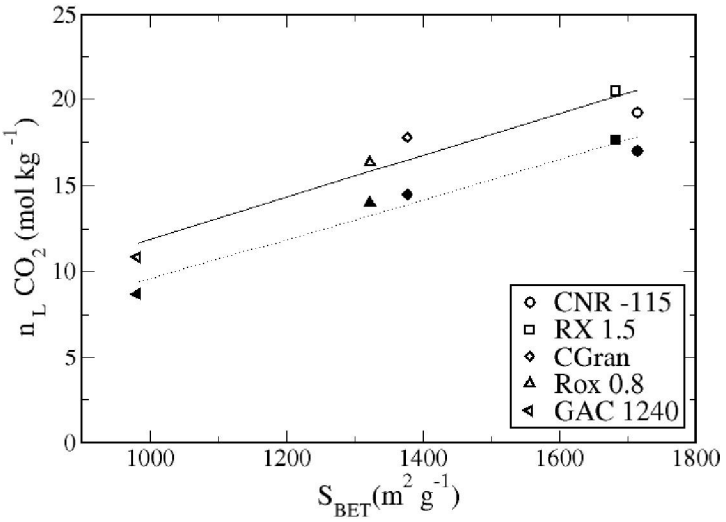

Figure 5.6: Maximum Langmuir adsorption capacity at 303.15 K (open symbols) and 323.15 K (filled symbols) as a function of the BET surface area. The correlation between the data is shown by linear regression, continued line for 303.15 K (r^2=0.959) and dotted line for 323.15 K (r^2=0.991).

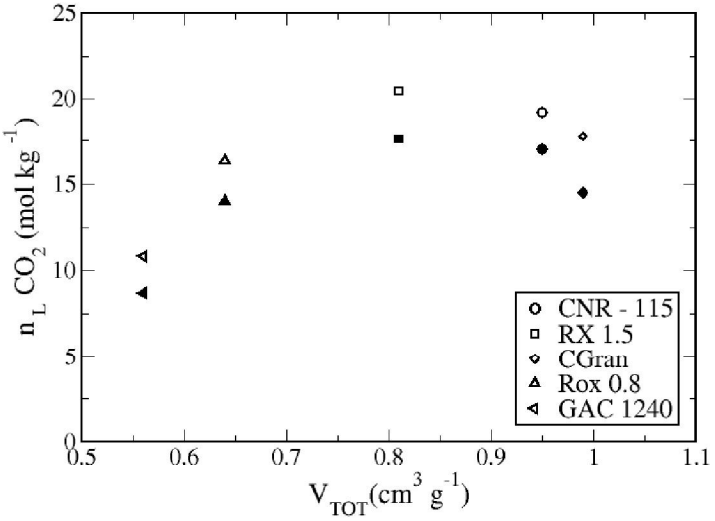

Figure 5.7: Maximim Langmuir adsorption capacity at 303.15 K (open symbols) and 323.15 K (filled symbols) as a function of the total pore volume.

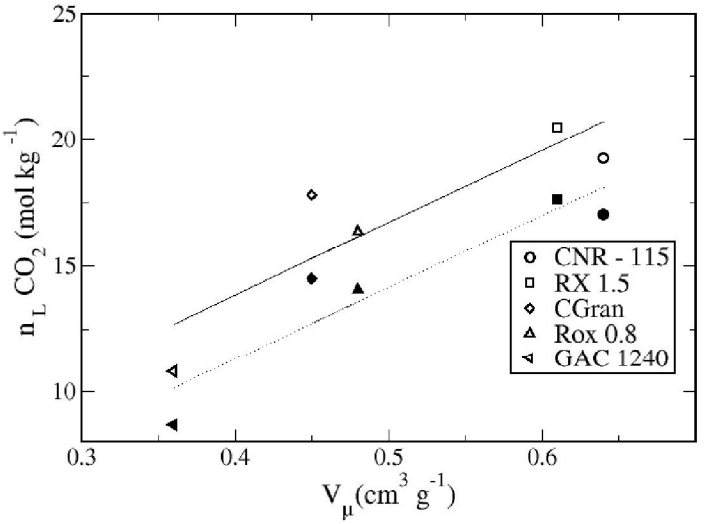

Figure 5.8: Maximim Langmuir adsorption capacity at 303.15 K (open symbols) and 323.15 K (filled symbols) as a function of the micropore volume. The correlation between the data is shown by linear regression, continued line for 303.15 K (r^2=0.883) and dotted line for 323.15 K (r^2=0.929).

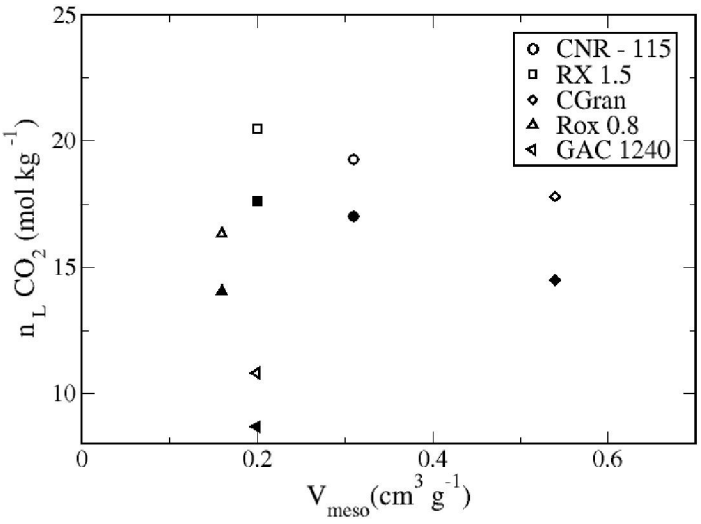

Figure 5.9: Maximim Langmuir adsorption capacity at 303.15 K (open symbols) and 323.15 K (filled symbols) as a function of the mesopore volume.

well as the obtained maximum adsorption capacity (CO_2 Max.) are compared on Table 5.3 with conventional adsorbents used for the CH_4/CO_2 separation. The CO_2 adsorption values at 0.1 MPa of the studied samples are in agreement with the reported values of the Norit R1 and WV1050 activated carbons but significantly lower than that of zeolites. This behavior is in agreement with the literature, since it has been reported that zeolites tend to reach a maximum adsorption value at low pressures (P=0.1 MPa), while activated carbons adsorption capacities increase constantly for a bigger pressure range having then low adsorption at low pressure and high adsorption at high pressure[39]. The maximum adsorption capacity of the studied activated carbons presents itself promising for the adsorption of carbon dioxide.

5.5 Conclusion

The adsorption isotherms of pure CH_4 and CO_2 were obtained for a series of 5 microporous activated carbons at two working temperatures (303.15 and 323.15 K). The data were well fitted to a Langmuir two parameters model. All of the studied samples showed a higher adsorption of carbon dioxide than of methane. A decrease in the adsorption capacity of both gases with increasing temperature was obtained for all of the activated carbons, this behavior is characteristic of physical adsorption processes. The samples showed an adsorption capacity comparable to that of conventional adsorbents used on CH_4/CO_2 separation processes with the highest maximum Langmuir capacity being 20.46 mol kg^{-1} for sample RX 1.5 at

Table 5.3: Comparison of CO_2 Adsorption with Different Adsorbents

Sample	**S_{BET} (m^2 g^{-1})**	**T (K)**	**CO_2 ads. (0.1 MPa) (mmol g^{-1})**	**CO_2 Max. adsorption (mmol g^{-1})**
AC Norit R1 [40]	3000	293	2.23	9.221
WV1050 [41]	1615	293	1.69	17.396
Zeolite NaX [42]	534	303	4.20	5.9774
Zeolite 13X [43, 44]	584	308	4.05[a]	17.901
		305	4.9	
CNR - 115	1714	303	1.08	18.949
RX 1.5	1683	303	1.89	20.177
CGran	1378	303	1.35	17.532
Rox 0.8	1323	303	1.41	16.154
GAC 1240	982	303	1.07	10.652

[a] P=0.095 MPa

273.15 K. The adsorption capacity was found to be related with the BET surface area and the micropore volume. Meanwhile, the total pore volume and the mesopore volume did not seem to influence the adsorption process.

5.6 Bibliography

[1] European Environment Agency. Annual European Union greenhouse gas inventory 1990-2015 and inventory report. Technical Report May, 2017.

[2] Raúl Muñoz, Leslie Meier, Israel Diaz, and David Jeison. A review on the state-of-the-art of physical/chemical and biological technologies for biogas upgrading. *Rev. Environ. Sci. Bio.*, 14(4):727–759, 2015.

[3] Katherine Starr, Gara Villalba, and Xavier Gabarrell. Upgraded biogas from municipal solid waste for natural gas substitution and CO_2 reduction - A case study of Austria, Italy, and Spain. *Waste Manage.*, 38(1):105–116, 2015.

[4] Adele Brunetti, Yu Sun, Alessio Caravella, Enrico Drioli, and Giuseppe Barbieri. Process intensification for greenhouse gas separation from biogas: More efficient process schemes based on membrane-integrated systems. *Int. J. Greenh. Gas Con.*, 35:18–29, 2015.

[5] Andreas Lemmer, Yuling Chen, Anna Maria Wonneberger, Frank Graf, and Rainer Reimert. Integration of a water scrubbing technique and two-stage pressurized anaerobic digestion in one process. *Energies*, 8(3):2048–2065, 2015.

[6] Rimika Kapoor, P. M.V. Subbarao, Virendra Kumar Vijay, Goldy Shah, Shivali Sahota, Dhruv Singh, and Mahesh Verma. Factors affecting methane loss from a water scrubbing based biogas upgrading system. *Appl. Energy*, 208(April):1379–1388, 2017.

[7] Fouad R.H. Abdeen, Maizirwan Mel, Mohammed Saedi Jami, Sany Izan Ihsan, and Ahmad Faris Ismail. A review of chemical absorption of carbon dioxide for biogas upgrading. *Chin. J. Chem. Eng.*, 24(6):693–702, 2016.

[8] S. Sutanto, J. W. Dijkstra, J. A.Z. Pieterse, J. Boon, P. Hauwert, and D. W.F. Brilman. CO_2 removal from biogas with supported amine sorbents: First technical evaluation based on experimental data. *Sep. Purif. Technol.*, 184:12–25, 2017.

[9] Qingyao He, Ge Yu, Shuiping Yan, Ludovic F. Dumée, Yanlin Zhang, Vladimir Strezov, and Shuaifei Zhao. Renewable CO_2 absorbent for carbon capture and biogas upgrading by membrane contactor. *Sep. Purif. Technol.*, 194(1):207–215, 2018.

[10] Bouchra Belaissaoui and Eric Favre. Novel dense skin hollow fiber membrane contactor based process for CO_2 removal from raw biogas using water as absorbent. *Sep. Purif. Technol.*, 193(October 2017):112–126, 2018.

[11] Noelia Álvarez-Gutiérrez, Susana García, María Victoria Gil, Fernando Rubiera, and Covadonga Pevida. Dynamic Performance of Biomass-Based Carbons for CO_2/CH_4 Separation. Approximation to a Pressure Swing Adsorption Process for Biogas Upgrading. *Energy Fuels*, 30(6):5005–5015, 2016.

[12] Mónica P. S. Santos, Carlos A Grande, and Alírio E. Rodrigues. Dynamic Study of the Pressure Swing Adsorption Process for Biogas Upgrading and Its Responses to Feed Disturbances. *Ind. Eng. Chem. Res.*, 52(15):5445–5454, 2013.

[13] Melanie Bahr, Ignacio Díaz, Antonio Dominguez, Armando González Sánchez, and Raul Muñoz. Microalgal-biotechnology as a platform for an integral biogas upgrading and nutrient removal from anaerobic effluents. *Environ. Sci. Technol.*, 48(1):573–581, 2014.

[14] Martin Karlsson and Patrik Nygren. ENZYMATIC UPGRADING OF BIOGAS. Technical report, 2015.

[15] Rosaria Augelletti, Maria Conti, and Maria Cristina Annesini. Pressure swing adsorption for biogas upgrading. A new process configuration for the separation of biomethane and carbon dioxide. *J. Clean Prod.*, 140:1390–1398, 2016.

[16] Muhammad Farooq, Alexandra H. Bell, M.N. Almustapha, and John M. Andresen. Bio-methane from an-aerobic digestion using activated carbon adsorption. *Anaerobe*, 46:33–40, 2017.

[17] Simone Cavenati, Carlos A. Grande, and Alírio E. Rodrigues. Upgrade of Methane from Landfill Gas by Pressure Swing Adsorption. *Energy Fuels*, 19(6):2545–2555, 2005.

[18] Dong June Seo, Zhichao Gou, Hirotaka Fujita, Takao Fujii, and Akiyoshi Sakoda. Simple fabrication of molecular sieving carbon for biogas upgrading via a temperature controlled carbonization of Phyllostachys pubescens. *Renew. Energy*, 86:693–702, 2016.

[19] Zoltán Bacsik, Ocean Cheung, Petr Vasiliev, and Niklas Hedin. Selective separation of CO_2 and CH_4 for biogas upgrading on zeolite NaKA and SAPO-56. *Appl. Energ.*, 162:613–621, 2016.

[20] A. Alonso-Vicario, José R. Ochoa-Gómez, S. Gil-Río, O. Gómez-Jiménez-Aberasturi, C. A. Ramírez-López, J. Torrecilla-Soria, and A. Domínguez. Purification and upgrading of biogas by pressure swing adsorption on synthetic and natural zeolites. *Microporous Mesoporous Mater.*, 134(1-3):100–107, 2010.

[21] N. Álvarez-Gutiérrez, M. V. Gil, F. Rubiera, and C. Pevida. Adsorption performance indicators for the CO_2/CH_4 separation: Application to biomass-based activated carbons. *Fuel Process. Technol.*, 142:361–369, 2016.

[22] Dipendu Saha, Karl Nelson, Jihua Chen, Yuan Lu, and Soydan Ozcan. Adsorption of CO_2 , CH_4 , and N_2 in Micro-Mesoporous Nanographene: A Comparative Study. *J. Chem. Eng. Data*, 60(9):2636–2645, 2015.

[23] F. A. Kloutse, A. Hourri, S. Natarajan, P. Benard, and R. Chahine. Experimental benchmark data of CH_4, CO_2 and N_2 binary and ternary mixtures adsorption on MOF-5. *Sep. Purif. Technol.*, 197(January):228–236, 2018.

[24] Renju Zacharia, Luis Fernando Gomez, Richard Chahine, Daniel Cossement, and Pierre Benard. Thermodynamics and kinetics of CH_4/CO_2 binary mixture separation by metal-organic frameworks from isotope exchange and adsorption break-through. *Microporous and Mesoporous Mater.*, 263(December 2017):165–172, 2018.

[25] Jose F. Vivo-Vilches, Agustin F. Pérez-Cadenas, Francisco J. Maldonado-Hódar, Francisco Carrasco-Marín, Rui P V Faria, Ana M. Ribeiro, Alexandre F P Ferreira, and Alirio E. Rodrigues. Biogas upgrading by selective adsorption onto CO_2 activated carbon from wood pellets. *Journal Environ Chem Eng*, 5(2):1386–1393, 2017.

[26] Shanshan Wang, Linghong Lu, Di Wu, Xiaohua Lu, Wei Cao, Tingting Yang, and Yudan Zhu. Molecular Simulation Study of the Adsorption and Diffusion of a Mixture of CO_2/CH_4 in Activated Carbon: Effect of Textural Properties and Surface Chemistry. *J. Chem. Eng. Data*, 61(12):4139–4147, 2016.

[27] Marta Sevilla, Camillo Falco, Maria-Magdalena Titirici, and Antonio B. Fuertes. High-performance CO_2 sorbents from algae. *RSC Adv.*, 2(33):12792, 2012.

[28] Olga Patricia Ortiz Cancino, Deneb Peredo Mancilla, Manuel Pozo, Edgar Pérez, and David Bessieres. Effect of Organic Matter and Thermal Maturity on Methane Adsorption Capacity on Shales from the Middle Magdalena Valley Basin in Colombia. *Energy Fuels*, 31(11):11698–11709, 2017.

[29] David Pino and David Bessieres. CH_4/CO_2 Mixture Adsorption on a Characterized Activated Carbon. *J. Chem. Eng. Data*, 62(4):1475–1480, 2017.

[30] D. Bessières, Th Lafitte, J. L. Daridon, and S. L. Randzio. High pressure thermal expansion of gases: Measurements and calibration. *Thermochim. Acta*, 428(1-2):25–30, 2005.

[31] Adil Mouahid, David Bessieres, Frédéric Plantier, and Gilles Pijaudier-Cabot. A thermostated coupled apparatus for the simultaneous determination of adsorption isotherms and differential enthalpies of adsorption at high pressure and high temperature. *J. Therm. Anal. Calorim.*, 109(2):1077–1087, 2012.

[32] M. Gasparik, A. Ghanizadeh, P. Bertier, Y. Gensterblum, S. Bouw, and Bernhard M. Krooss. High-pressure methane sorption isotherms of black shales from the Netherlands. *Energy Fuels*, 26(8):4995–5004, 2012.

[33] Olga Patricia Ortiz Cancino, David Pino Pérez, Manuel Pozo, and David Bessieres. Adsorption of pure CO_2 and a CO_2/CH_4mixture on a black shale sample: Manometry and microcalorimetry measurements. *J. Petrol. Sci. Eng.*, 159(August):307–313, 2017.

[34] Manuel Pozo, David Pino, and David Bessieres. Effect of thermal events on maturation and methane adsorption of Silurian black shales (Checa, Spain). *Appl. Clay Sci.*, 136:208–218, 2017.

[35] Melina C. Castrillon, Karine Oliveira Moura, Caiua Araujo Alves, Moises Bastos-Neto, Diana C. S. Azevedo, Jorg Hofmann, Jens Möllmer, Wolf-Dietrich Einicke, and Roger Glaser. CO_2 and H_2S removal from CH_4-rich streams by Adsorption on Activated Carbons Modified with K_2CO_3, NaOH or Fe_2O_3. *Energy Fuels*, pages 9596–9604, 2016.

[36] F. Rodriguez-Reinoso, M. Molina-Sabio, and M. A. Muñecas. Effect of microporosity and oxygen surface groups of activated carbon in the adsorption of molecules of different polarity. *J. Phys. Chem.*, 96(6):2707–2713, 1992.

[37] Jarosław Serafin, Urszula Narkiewicz, Antoni W. Morawski, Rafał J. Wróbel, and Beata Michalkiewicz. Highly microporous activated carbons from biomass for CO_2 capture and effective micropores at different conditions. *J. CO2 Util.*, 18:73–79, 2017.

[38] Shubo Deng, Haoran Wei, Tao Chen, Bin Wang, Jun Huang, and Gang Yu. Superior CO_2 adsorption on pine nut shell-derived activated carbons and the effective micropores at different temperatures. *Chem. Eng. J.*, 253:46–54, 2014.

[39] Mariem Kacem, Mario Pellerano, and Arnaud Delebarre. Pressure swing adsorption for CO_2/N_2 and CO_2/CH_4 separation: Comparison between activated carbons and zeolites performances. *Fuel Process. Technol.*, 138:271–283, 2015.

[40] F. Dreisbach, R. Staudt, and J. U. Keller. High pressure adsorption data of methane, nitrogen, carbon dioxide and their binary and ternary mixtures on activated carbon. *Adsorption*, 5(3):215–227, 1999.

[41] R. B. Rios, F. M. Stragliotto, H. R. Peixoto, A. E. B. Torres, M. Bastos-Neto, D. C. S. Azevedo, and C. L. Cavalcante Jr. Studies on the adsorption behavior of CO_2/CH_4 mixtures using activated carbon. *Braz. J. Chem. Eng.*, 30(4):939–951, 2013.

[42] Yundong Li, Honghong Yi, Xiaolong Tang, Fenrong Li, and Qin Yuan. Adsorption separation of CO_2/CH_4 gas mixture on the commercial zeolites at atmospheric pressure. *Chem. Eng. J.*, 229:50–56, 2013.

[43] Simone Cavenati, Carlos A. Grande, and Alírio E. Rodrigues. Adsorption Equilibrium of Methane, Carbon Dioxide, and Nitrogen on Zeolite 13X at High Pressures. *J. Chem. Eng. Data*, 49(4):1095–1101, 2004.

[44] Aroon Kongnoo, Supak Tontisirin, Patcharin Worathanakul, and Chantaraporn Phalakornkule. Surface characteristics and CO_2 adsorption capacities of acid-activated zeolite 13X prepared from palm oil mill fly ash. *Fuel*, 193:385–394, 2017.

Appendix

Table 5.4: GAC 1240 Adsorption

CH_4				**CO_2**			
303.15 K		**323.15 K**		**303.15 K**		**323.15 K**	
P (MPa)	**n_{exc} (mol kg^{-1})**	**P (MPa)**	**n_{exc} (mol kg^{-1})**	**P (MPa)**	**n_{exc} (mol kg^{-1})**	**P (MPa)**	**n_{exc} (mol kg^{-1})**
0.019	0.398	0.203	1.798	0.024	0.382	0.025	0.239
0.048	0.941	0.545	3.144	0.058	0.810	0.063	0.597
0.099	1.600	0.989	4.071	0.102	1.276	0.111	0.963
0.258	2.884	1.428	4.605	0.277	2.633	0.266	1.824
0.592	4.320	1.847	4.910	0.637	4.390	0.601	3.147
0.986	5.230	2.386	5.048	1.068	5.659	1.048	4.289
1.428	5.821	2.986	4.999	1.555	6.613	1.543	5.129
1.847	6.165			1.948	7.161	1.951	5.570
2.386	6.333			2.481	7.748	2.417	5.988
2.985	6.338			3.023	8.327	2.998	6.406

Uncertainties: ΔT=0.2 K, ΔP=0.01 MPa, $\Delta n/n$=1%

Table 5.5: RX 1.5 Adsorption

CH_4				**CO_2**			
303.15 K		**323.15 K**		**303.15 K**		**323.15 K**	
P (MPa)	**n_{exc} (mol kg^{-1})**	**P (MPa)**	**n_{exc} (mol kg^{-1})**	**P (MPa)**	**n_{exc} (mol kg^{-1})**	**P (MPa)**	**n_{exc} (mol kg^{-1})**
0.015	0.159	0.013	0.308	0.009	0.270	0.008	0.191
0.039	0.484	0.035	0.514	0.026	0.789	0.024	0.514
0.071	0.846	0.075	0.836	0.059	1.532	0.049	0.934
0.180	1.766	0.254	1.906	0.159	3.223	0.084	1.437
0.424	3.150	0.528	3.020	0.401	6.015	0.255	3.261
0.754	4.385	0.840	3.929	0.796	8.920	0.536	5.361
1.117	5.379	1.211	4.739	1.201	10.894	0.877	7.186
1.512	6.151	1.662	5.413	1.701	12.606	1.220	8.564
1.877	6.707	2.117	6.018	2.291	14.055	1.637	9.851
2.404	7.297	2.562	6.492	2.796	14.953	2.039	10.825
2.908	7.733	2.996	6.879	3.093	15.361	2.449	11.606
						2.798	12.157
						3.200	12.533

Uncertainties: ΔT=0.2 K, ΔP=0.01 MPa, $\Delta n/n$=1%

Table 5.6: CGran Adsorption

CH_4				**CO_2**			
303.15 K		**323.15 K**		**303.15 K**		**323.15 K**	
P (MPa)	**n_{exc} (mol kg^{-1})**	**P (MPa)**	**n_{exc} (mol kg^{-1})**	**P (MPa)**	**n_{exc} (mol kg^{-1})**	**P (MPa)**	**n_{exc} (mol kg^{-1})**
0.018	0.100	0.032	0.131	0.016	0.422	0.022	0.397
0.064	0.384	0.067	0.272	0.046	1.059	0.056	0.821
0.106	0.606	0.112	0.443	0.089	1.732	0.095	1.223
0.282	1.363	0.271	0.934	0.247	3.420	0.255	2.437
0.587	2.317	0.590	1.671	0.551	5.523	0.554	4.007
0.968	3.074	0.969	2.369	0.939	7.389	0.924	5.440
1.361	3.762	1.389	2.934	1.390	9.009	1.348	6.717
1.761	4.357	1.907	3.556	1.875	10.447	1.785	7.677
2.209	4.917	2.462	4.076	2.355	11.684	1.958	7.852
2.641	5.360	3.022	4.548	2.877	12.516	2.729	8.722
3.074	5.768					3.109	9.033

Uncertainties: ΔT=0.2 K, ΔP=0.01 MPa, Δn/n=1%

Table 5.7: Rox 0.8 Adsorption

CH_4				**CO_2**			
303.15 K		**323.15 K**		**303.15 K**		**323.15 K**	
P (MPa)	**n_{exc} (mol kg^{-1})**	**P (MPa)**	**n_{exc} (mol kg^{-1})**	**P (MPa)**	**n_{exc} (mol kg^{-1})**	**P (MPa)**	**n_{exc} (mol kg^{-1})**
0.026	0.336	0.022	0.242	0.018	0.414	0.152	2.311
0.064	0.790	0.064	0.626	0.047	1.124	0.461	4.783
0.103	1.220	0.110	0.974	0.091	2.053	0.901	6.859
0.270	2.343	0.287	1.941	0.246	4.239	1.364	8.270
0.578	3.670	0.599	3.074	0.540	6.759	1.757	9.116
0.949	4.683	0.989	4.034	0.926	8.780	2.323	9.995
1.367	5.474	1.403	4.783	1.364	10.263	2.936	10.65
1.819	6.083	1.851	5.380	1.765	11.249		
2.387	6.635	2.406	5.924	2.330	12.233		
2.957	7.065	3.027	6.351	2.960	12.960		

Uncertainties: ΔT=0.2 K, ΔP=0.01 MPa, Δn/n=1%

Table 5.8: CNR - 115 Adsorption

CH_4				**CO_2**			
303.15 K		**323.15 K**		**303.15 K**		**323.15 K**	
P (MPa)	**n_{exc} (mol kg^{-1})**	**P (MPa)**	**n_{exc} (mol kg^{-1})**	**P (MPa)**	**n_{exc} (mol kg^{-1})**	**P (MPa)**	**n_{exc} (mol kg^{-1})**
0.177	0.851	0.197	0.779	0.131	1.862	0.035	0.569
0.392	1.569	0.463	1.478	0.393	3.916	0.080	1.005
0.609	2.146	0.758	2.091	0.728	5.787	0.119	1.319
0.849	2.671	0.989	2.503	0.986	7.015	0.171	1.697
1.091	3.112	1.294	2.950	1.296	8.119	0.274	2.440
1.387	3.554	1.656	3.306	1.600	9.091	0.488	3.689
1.660	3.904	2.046	3.635	2.012	10.301	0.743	4.872
1.923	4.179	2.409	3.914	2.436	11.253	0.986	5.825
2.220	4.299	2.789	4.164	2.947	12.227	1.380	7.046
2.509	4.513	3.124	4.373			1.839	8.319
2.760	4.682					2.281	9.224
2.960	4.809					2.663	10.035
3.200	4.940					3.135	10.805

Uncertainties: ΔT=0.2 K, ΔP=0.01 MPa, $\Delta n/n$=1%

Peredo-Mancilla, D., et al. CO2 and CH4 Adsorption Behavior of Biomass-Based Activated Carbons. *Energies*, **2018**, 11, 3136.

CHAPTER 6

EXPERIMENTAL OF THE CH_4 AND CO_2 PURE GAS ADSORPTION ISOTHERMS ON BIOMASS BASED ACTIVATED CARBONS

ISBN: 19961073
DOI: 10.3390/en111131367

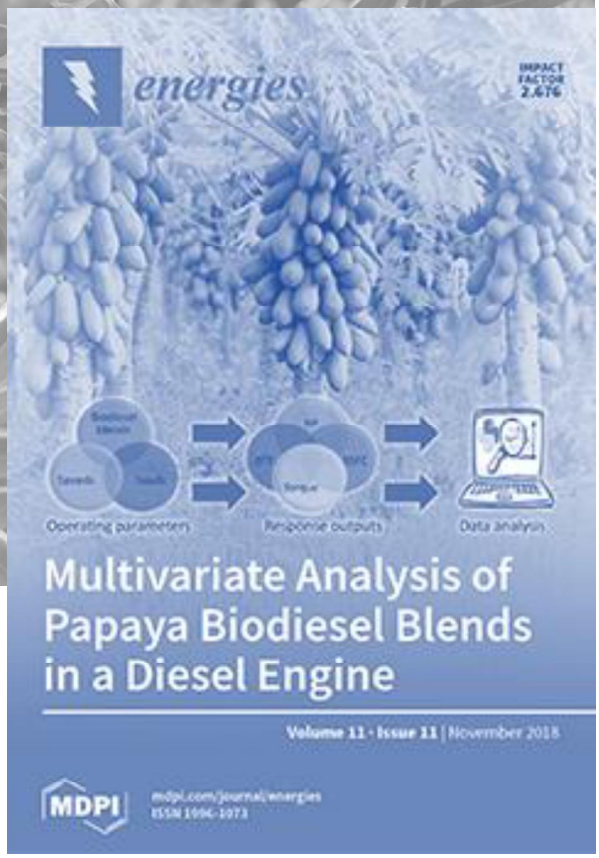

6.1 Chapter Outline

Chapters 4 and 5 demonstrated the key role of textural properties of activated carbons on the gas adsorption process. A high surface area translates into a higher existence of sorption sites, thus translating into an increase of the maximum adsorption capacity of the adsorbents. In addition, the presence of micropores with a size close to 0.8 nm is beneficial for both carbon dioxide and methane adsorption.

One of the main advantages of using activated carbons as gas adsorbent materials is that both their chemical and textural properties are tunable with ease. Through the shifting of the preparation method (i.e. activation temperature, activation time, activation agent) it is possible to obtain samples presenting different pore sizes and pore distribution as well as particular acid/basic surface properties.

The influence of the activation method on the CO_2 and CH_4 adsorption uptake is analyzed on this Chapter. For this purpose, the adsorption isotherms of three biomass-based activated carbons obtained by different activation methods (H_3PO_4 chemical activation and H_2O and CO_2physical activation) are reported. Methane and carbon dioxide pure gas adsorption experiments were carried out at two working temperatures (303.15 and 323.15 K).

The results show that for the three adsorbents the CO_2 adsorption was more important than that of CH_4. In addition, chemical activation results in the higher specific surface area and micropore volume leading to a higher adsorption capacity of both CO_2 and CH_4. For methane adsorption, the presence of mesopores facilitated the diffusion of the gas molecules into the micropores. In the case of carbon dioxide adsorption, the presence of more oxygen groups on the water vapor activated carbon enhanced its adsorption capacity.

6.2 Introduction

As part of the efforts being made to fight climate change, governments of 195 countries signed the Paris Agreement, in which they agreed to keep the increase of the global average temperature well below 2 °C from the preindustrial temperatures [1]. In order to meet this target, the EU set a 20-20-20 goal: 20% increase of energy efficiency, 20% reduction of greenhouse gas (GHG) emissions and 20% of EU energy from renewables by 2020. Furthermore, 10% of transportation fuels have to come from renewable sources such as biofuels [2].

Biogas is a gaseous mixture produced when organic matter is degraded by microorganisms under anaerobic conditions in a process known as anaerobic digestion

(AD); its main components are methane (CH_4) in a concentration of 50–70 vol% and carbon dioxide (CO_2) ranging from 30–45 vol% Collected biogas can be directly burned to produce electricity with an efficiency of roughly 38% [3]. Alternatively, the energy density of biogas can be increased by an upgrading process in which the non-combustible gas (CO_2) and other impurities are separated to produce biomethane, a highly-purified methane stream (around 98% purity), which can function as a vehicle fuel or can also be injected into the natural gas grid.

The use of biogas and biomethane as alternative energy sources has gained attention, because it results in the reduction of greenhouse gases from both the burning of fossil fuels and from the landfill of organic wastes, which accounts for 3.2% of the total GHG emissions of the EU. Consequently, in Europe, more than 90% of the produced biogas is already being used for electricity generation, and the upgrading of biogas is being promoted more and more [4]. EU energy production from biomethane rose from 752 GWh in 2011 to 17.264 GWh in 2016 (+16.512 GWh). Moreover, in 2016, biomethane production in Europe increased by 4.971 GWh (+40%), proving an accelerated development in the sector [5].

Adsorption-based processes have been widely explored for the upgrading of biogas. They present several advantages such as relatively low energy requirements and low capital investment costs, flexibility of design, safety and simplicity of operation, as well as a high separation efficiency [6]. In this type of separation technology, the components of a gas mixture are separated by their molecular characteristics and affinity to an adsorbent material. For this purpose, a variety of materials have been studied including zeolites [7, 8, 9], carbon molecular sieves (CMS) [10, 11, 12], metal organic frameworks (MOFs) [13, 14, 15] and activated carbons (ACs) [16, 17, 18]. Among these materials, activated carbons present advantages in terms of: (i) hydrophobicity; thus, there is no need for a drying step before upgrading; (ii) low heat of adsorption, therefore a low energy of regeneration; (iii) the possibility of heteroatoms' functionalization to modify their adsorption behavior; and (iv) high CO_2 adsorption capacity at ambient pressure [19]. Furthermore, activated carbons can be produced with a lower cost than other adsorbents, with a wide range of available precursor materials. In fact, any carbonaceous material can be used as a precursor for activated carbon production as long as it has a low ash content and a high proportion of carbon [20]. In this sense, the use of agro-industrial wastes as an alternative to coal and wood as precursors for activated carbon production has been widely studied [21, 22, 23]. This waste-valorization process reduces the environmental and economic costs associated with the precursors while eliminating the need for disposal or incineration of unwanted agricultural by-products [24]. Materials such as corn cobs, palm shells, starch, coconut shells, durian shell, olive stones and bamboo have already been studied for activated carbon production [25, 26, 27, 19, 28, 29, 30, 31, 32].

In particular, olive stones are seen as suitable precursors, giving activated carbon with high adsorption capacities, important mechanical strength and low ash content [33, 29]. A complete review of precursors, activation methods and applications of biomass-based activated carbons is available elsewhere [34].

Depending on the activation conditions, ACs can present surface areas as high as 3000 m^2 g^{-1}. Activated carbons can be produced in two ways: physical activation and chemical activation. Physical activation is a two-step process that begins with the carbonization of the precursor at high temperatures (up to 1073 K), a process in which the volatile compounds present in the precursor are removed under an inert atmosphere (i.e., nitrogen atmosphere) producing a carbon-rich material. Carbonization is followed by the activation step: the material is exposed to an oxidizing gas current (such as air, CO_2 and water vapor) at a temperature between 1073 and 1273 K. On the other hand, chemical activation consists of the immersion of the raw material into a dehydrating agent followed by a heat treatment step. Examples of dehydrating agents are sodium and potassium hydroxide (KOH and NaOH), zinc chloride ($ZnCl_2$) and phosphoric acid (H_3PO_4). Chemical activation with KOH results in activated carbons with a high micropore volume, a key factor for CH_4 and CO_2 adsorption; nevertheless, this activation agent presents the disadvantage of low production yields due to the presence of potassium atoms on the resulting structure, which lowers the activated carbon yield; thus, the carbon content of the obtained activated carbon is lower than that of the precursor material. The use of ZnCl as the activation agent has environmental disadvantages due to zinc chloride's high corrosivity. Therefore, H_3PO_4 has become the most used impregnation agent for AC production [35].

Different activation methods and activation conditions (i.e., temperature and time of activation) result in differences in the textural properties such as surface area, pore size distribution and micropore volume, as well as in the chemical properties of the obtained activated carbons. The textural properties are the most determining factor of the adsorption behavior in a physical adsorption process. However, specific interactions between the adsorbed gas and the adsorbent may also play a role in the adsorption process, and they are unique for each adsorbent/adsorbate pair [36]. Therefore, it is necessary to establish the best activation method for each particular adsorption process.

Several studies have been published on the CH_4 and CO_2 adsorption capacity of CO_2 physically-activated carbon, as well as KOH chemically-activated carbons, but a less important number of works report H_3PO_4 activation [19, 25, 37, 38, 39, 35, 31, 40, 41, 42]. The literature review shows that the use of olive stones as precursor materials for activated carbon production is a promising alternative for biogas upgrading with the additional advantage of waste valorization. In this

context, the present work provides a novel systematic analysis of the influence of both the textural properties and surface chemistry of olive stone activated carbons on the methane and carbon dioxide adsorption. The effect of the activation method (physical versus chemical activation) on the properties of the obtained activated carbons is also discussed. To this end, the adsorption capacity of both methane and carbon dioxide is determined for three activated carbons produced from olive stones by different activation methods: CO_2 physical activation, H_2O physical activation and H_3PO_4 chemical activation. The factors influencing the gas adsorption capacity are discussed in terms of the effect of the activation method on both the textural and chemical properties of the obtained activated carbon.

6.3 Materials

6.3.1 Sample Preparation

Three activated carbons were prepared using olive stones provided by an olive oil factory located in Zarzis (Tunisia); two of them were obtained by physical activation and the other one by chemical activation. Prior to the activation procedures, the raw materials, were thoroughly washed with hot distilled water, dried under ambient conditions for 24 h and crushed to form particles with a diameter between 1 and 3 mm. The activated carbon preparation methods are summarized in this section. A detailed description of the selection procedure of the optimal activation conditions and sample characterization can be found in [43, 44, 45].

Physical Activation

Two physical activation methods were carried out: activation with water vapor and activation with carbon dioxide. Both methods followed a two-step scheme in which the first step was the carbonization of the precursor under a continuous flow of purified nitrogen with a flow rate of 10 NL/h. Using a heating velocity of 5 K/min, the precursor was heated from room temperature to a temperature of 873 K and kept at this final temperature for 60 min. Nitrogen flow was used in order to evacuate the residual oxygen from the system. The second step was the activation of the samples consisting of placing the sample under a gas flow of the activation agent at a flow velocity of 10 Nl/h and a temperature of 1023 K for 360 min (temperature ramp of 15 K/min). For the water vapor activated carbon (AC-H_2O), the activation agent was water 70 vol. % in N_2. Meanwhile, for CO_2 activation, a flow of pure carbon dioxide was employed.

Chemical Activation

The olive stones were immersed in an orthophosphoric acid aqueous solution (50% w/w) at a weight ratio of 1:3. The mixture was kept under stirring for 9 h at 383 K. Consecutively, the solution was filtrated, dried and flushed by a stream of nitrogen at a temperature of 443 K for 30 min and an extra 150 min at 683 K. The heating velocity during this whole procedure was 5 K/min. The sample, referred to as AC-H_3PO_4, had a chemical activation yield of 33 wt%.

6.3.2 Samples Properties

The characterization of the activated carbons was done by means of textural properties (such as surface area and pore volume) and surface chemistry. The specific surface area was calculated by means of the Brunauer–Emmett–Teller (BET) method [46] from the linear plot of the nitrogen adsorption isotherm at 77 K in the relative pressure range of 0.05–0.15 (Figure 6.5a of the Appendix). Total pore volume was determined by the amount of nitrogen adsorbed by each material at a relative pressure $P/P^\circ = 0.99$. The t-plot method was used for the calculation of the micropore volume. The mesopore volume was defined as the difference between the total pore volume and the micropore volume. Finally, the pore size distribution (PSD) (Figure 6.5b of the Chapter Appendix) was obtained by non-local density functional theory (NLDFT) using a model for slit carbon pores. The textural properties of the three activated carbons are summarized in Table 6.1 and can also be found in the literature [43]. The three activated carbons are mainly microporous. The water vapor activated carbon has a higher total pore volume V_{TOT} due to the presence of an important volume of mesopores $V_{meso} = 0.30$ cm^3 g^{-1}). The presence of mesopores on water vapor-activated carbons due to a higher gasification of the carbon source of the precursor has been previously reported [43, 47]. On the other hand, the chemically-activated carbon AC-H_3PO_4 has significantly higher specific surface area (SSA) and micropore volume V_μ than the physically-activated ones, in agreement with the literature [48].

Table 6.1: Textural Properties of Carbon Materials.

Sample	**SSA** (**m**^{2} **g**$^{-1}$)	**V**$_\mu$ (**cm**^{3} **g**$^{-1}$)	**V**$_{TOT}$ (**cm**^{3} **g**$^{-1}$)	**V**$_{meso}$ (**cm**^{3} **g**$^{-1}$)
AC-H_3PO_4	1178	0.45	0.49	0.04
AC-CO_2	757	0.30	0.32	0.02
AC-H_2O	754	0.28	0.58	0.30

The surface chemistry of the adsorbent can be of great importance for the adsorption process; for this reason, the type and quantity of surface oxygenated groups were determined by means of a home-made temperature programmed desorption device coupled with a mass spectrometer (TPD-MS). In the TPD-MS experiments, a sample weighting 10 mg of each activated carbon was placed in a quartz tube that was introduced to an oven. The temperature of the oven was then increased at a rate of 5 K per minute under vacuum conditions. The surface properties of the sample were analyzed in the temperature range 298–1173 K. During the heating process, the quantitative evolution of gases was analyzed by mass spectrometry. The total amount of emitted CO and CO_2 during the TPD-MS analysis was obtained by integration of the desorption peaks (see Table 6.2). With the increase of temperature, oxygenated groups decomposed into CO_2 and CO. The desorption temperature gives information about the nature of oxygenated groups present on the carbon surface. Furthermore, by correlation between diffuse reflectance infrared Fourier transform spectroscopy (DRIFTS) spectra of different activated carbons and their TPD-MS profiles, it has been established that the emission of carbon dioxide results from the decomposition of lactones, carboxylic acids and anhydrides, while carbon monoxide is emitted by the decomposition of groups such as phenols, ethers and quinones [49].

Table 6.2: Cumulated Amounts of the Emmited CO and CO_2 During the TPD-MS Analysis of Carbon Materials.

Sample	**CO (mmol g^{-1})**	**CO_2 (mmol g^{-1})**
AC-H_3PO_4	3.43	0.72
AC-CO_2	1.06	0.38
AC-H_2O	1.25	0.39

In this context, the chemically-activated carbon (AC-H_3PO_4) presented higher amounts of oxygenated groups, mainly carboxylic acids, quinones and anhydrides. Among the physically-activated carbons, the water vapor activation resulted in more surface oxygen in the form of phenol and carboxylic acids. Meanwhile, carbon dioxide activation resulted in the formation of quinones, lactones and carboxylic acids on the activated carbon surface [43].

6.4 Experimental Methodology

6.4.1 High Pressure Manometric Adsorption Setup

The instrument used in the present study was a high pressure (HP) manometric device. A schematic view of this "homemade" apparatus is provided in Figure 6.1. The fundamental elements of this apparatus are the dosing cell (V_{dos}) and the adsorption cell (V_{ads}). The pressure was measured by a MKS pressure transducer Baratron Type 121 A (MKS Instruments, München, Deutschland). (0.01% uncertainty in the full scale from vacuum to 3.3 MPa) connected to the dosing cell. The two cells were isolated by spherical valves, thus limiting the "dead space" volume. During the adsorption experiments, the isothermal condition of the system was ensured by a heating wire controlled by a Eurotherm 3208 PID. (Schneider Electric, Worthing, United Kingdom). Thermocouples located at several points of the instrument allowed verifying the non-appearance of temperature gradients within the system. This setup was designed to operate over wide a range of pressure (0–3.3 MPa) and temperature up to 373.15 K [50, 51].

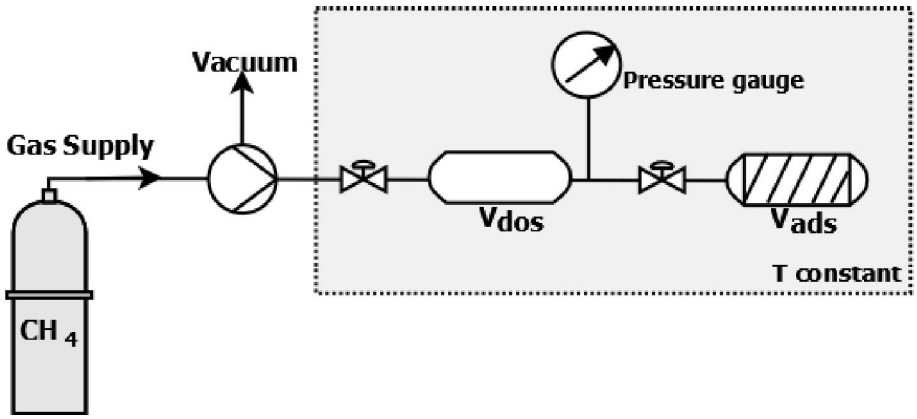

Figure 6.1: Schematic diagram of the HP/HT manometric adsorption set-up.

6.4.2 Determination of Excess Adsorption

Prior to the adsorption experiments, both the dossing cell volume and adsorption cell volume need to be calculated. The volume of the dosing cell was measured by a gravimetric scheme in which the pressure change at a given temperature due to a known quantity of carbon dioxide (CO_2) was recorded, using the NIST isothermal properties of carbon dioxide the corresponding volume was calculated [52]. The adsorption cell accessible volume, also known as void volume, in the presence of the sample of activated carbon was calculated by helium (He) expansions from the dossing cell to the adsorption cell (helium is considered as a non-sorbing gas). The experimental methodology applied for the adsorption isotherms measurement is based on a mass

balance principle. The uncertainty on the calculations of the void and adsorption cell volume was always inferior to 0.5%. In all the cases an outgassing process consisting of keeping the sample under vacuum conditions at 473 K for 10 h was performed before any experiment. The adsorption isotherms were obtained by an accumulative process: successive doses (≈3 bar) of the adsorbate (CH_4 or CO_2) were introduced in the dosing cell and expanded into the adsorption cell. The stability of the pressure was the chosen indicator of equilibrium conditions. The reproducibility of the experiment was tested by repeating one of the adsorption isotherm 3 times, the absolute standard deviation was found to be less than 1%.

6.4.3 Parametrization of Excess Adsorption Isotherms

The excess adsorption isotherms were fitted to a modified Langmuir model:

$$n_{exc} = n_L \frac{p}{p + p_L} \left(1 - \frac{\rho_g(p,T)}{\rho_{ads}} \right) \tag{6.1}$$

On this expression n_{exc} represents the adsorbed amount of gas (mol kg^{-1}) at a pressure p (MPa); p_L is the pressure at which half of the adsorption sites are occupied (monolayer), also known as the Langmuir pressure, n_L is the maximum Langmuir capacity which corresponds to the adsorbed amount in which the monolayer is filled, ρ_g is the gas density (kg m^{-3}) at pressure p and temperature T. Meanwhile ρ_{ads} (kg m^{-3}) stands for the adsorbed phase density, on this work it was fixed to the inverse of the van der Waals volume of each gas (373 kg m^{-3} for methane and 1027 kg m^{-3} for carbon dioxide) [53]. The Langmuir model has the advantage of taking into account the volume of the adsorbed phase. It has a theoretical basis whilst other models such as Toth (1995) [54] and Sips (1948) [55] are empirical. This model was initially developed for the low pressure region, nevertheless it provides a reasonable estimation of the excess adsorption isotherms at higher pressures [17].

The best fit of the Langmuir model for each adsorption isotherm was obtained by minimizing the root mean square error ($RMSE$) provided by Equation (6.2) [7]:

$$RMSE = \frac{1}{k} \cdot \sqrt{\sum_{1}^{k} (n_{exp} - n_{calc})^2} \tag{6.2}$$

where n_{exp} and n_{calc} are the experimental and calculated adsorption amounts in mol kg^{-1} at a pressure p for a number k of data points in the adsorption isotherm.

6.5 Results

CH_4 and CO_2 adsorption isotherms were obtained for a set of the three olive-stones based activated carbons (Figures 6.2 and 6.3) up to a pressure of 3.2 MPa at two working temperatures: 303.15 and 323.15 K with a reproducibility superior to 99% (average absolute deviation of less than 1%). All the isotherms were fitted by the Langmuir two parameters model (see Equation (6.1)), the obtained fitting parameters and root mean square error ($RMSE$) are presented in Table 6.3 (CH_4 adsorption) and Table 6.4 (CO_2 adsorption). The goodness of the fitting process is depicted by the RMSE values, values under 0.09 were obtained for the fitting of all the isotherms.

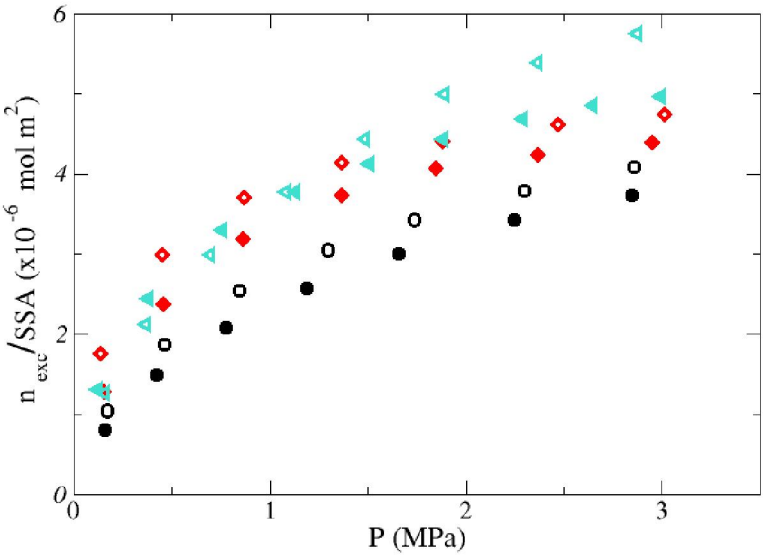

Figure 6.2: CH_4 Adsorption isotherms for three olive-stones based activated carbons: AC-H_3PO_4 (black circles), AC-CO_2 (red diamonds) and AC-H_2O (turquoise triangles). Open symbols represent the adsorption data at 303.15 K while the data at 323.15 is shown by the filled symbols. Uncertainties: $\Delta p = 0.01$ MPa, $\Delta T = 0.2$ K. The obtained Langmuir fitting isotherms are shown by the solid lines.

A higher adsorption of carbon dioxide than methane can be noticed for the three ACs (Figures 6.2 and 6.3). It is a typical behavior of activated carbons adsorption that can be explained by the presence of a quadrupole moment on the molecule of carbon dioxide that leads to stronger adsorptive/adsorbent interactions. Another possible explanation can be given in terms of the critical point of the gases, the critical temperature (190 K) and critical pressure (4.59 MPa) of methane are much lower than those of carbon dioxide (304.45 K and 7.38 MPa) which means that carbon dioxide is in the form of a condensable vapor while methane acts as supercritical gas at the adsorption conditions. A lower adsorption and lower maximum Langmuir capacity (n_L) upon an increase on the adsorption temperature are evidenced

on Figures 6.2 and 6.3) and Tables 6.3 and 6.4, indicating a physical adsorption process. Furthermore, for both adsorptives, the chemically activated carbon AC-H_3PO_4 showed the higher adsorption capacity, the adsorption tendency vary in the following order: AC-H_3PO_4 ¿ AC-H_2O ¿ AC-CO_2.

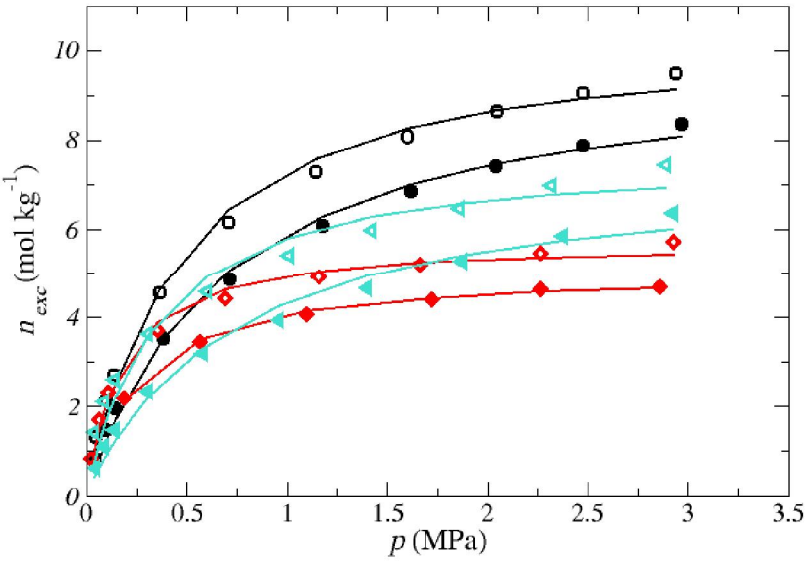

Figure 6.3: CO_2 Adsorption isotherms for three olive-stones based activated carbons: AC-H_3PO_4 (black circles), AC-CO_2 (red diamonds) and AC-H_2O (turquoise triangles). Open symbols represent the adsorption data at 303.15 K while the data at 323.15 is shown by the filled symbols.Uncertainties: $\Delta p = 0.01$ MPa, $\Delta T = 0.2$ K. The obtained Langmuir fitting isotherms are shown by the solid lines.

Table 6.3: Langmuir Fitting Parameters for the CH_4 Adsorption Isotherms.

CH_4 Adsorption				
Sample	**Temperature (K)**	**n_L (mol kg^{-1})**	**ρ_L (MPa)**	***RMSE***
AC-H_3PO_4	303.15	6.518	0.932	0.042
	323.15	6.369	1.182	0.037
AC-CO_2	303.15	3.913	0.273	0.043
	323.15	3.830	0.076	0.031
AC-H_2O	303.15	5.417	0.714	0.067
	323.15	5.301	1.011	0.056

The superior adsorption of AC-H_3PO_4 can be explained in regards of the textural properties of the samples (see Table 6.1), the chemically activated carbon has the highest specific surface area and micropore volume, both adsorption enhancing factors. A higher surface area means more physisorption available sites, while a linear relationship between the micropore volume and the adsorption of both methane and carbon dioxide has been reported [21, 56]. Concerning the difference in the methane adsorption capacity of the two physically activated carbons, the presence of mesoporosity on the structure of the water vapor activated carbon AC-H_2O is thought to be the determining factor. Both physically activated carbons have similar SSA and micropore volume, with the only difference being the mesopore volume. In fact, it has been shown that activated carbons that combine both micropores and mesopores can adsorb a significantly higher amount of CH_4 than their totally microporous counterparts [57].

Table 6.4: Langmuir Fitting Parameters for the CO_2 Adsorption Isotherms.

CO_2 Adsorption				
Sample	**Temperature (K)**	n_L **(mol kg^{-1})**	ρ_L **(MPa)**	***RMSE***
AC-H_3PO_4	303.15	10.873	0.488	0.080
	323.15	10.254	0.733	0.065
AC-CO_2	303.15	5.878	0.181	0.059
	323.15	5.191	0.273	0.020
AC-H_2O	303.15	7.968	0.371	0.073
	323.15	7.721	0.772	0.087

While methane adsorption by activated carbons is only influenced by the textural properties of the adsorbent, the carbon dioxide adsorption is also thought to be related to the surface chemistry. On the present work, the influence of the surface chemistry is depicted by normalizing the CO_2 adsorption isotherms by the surface area (Figure 6.4). One could expect that by doing this the adsorption of the chemical activated carbon would still be the most important due to a higher micropore volume. In reality, the AC-H_2O shows the higher adsorption. Chemical activation with phosphoric acid (H_3PO_4) is reported to produce acid activated carbon surfaces [58], which seems to reduce the interactions between the basic surface groups and the carbon dioxide molecules explaining its lower adsorption when the textural effect is eliminated by normalizing the adsorption isotherms by the specific surface area. However, the negative influence of acid surface groups on the AC-H_3PO_4 is small compared to the effect of its higher surface area, thus showing a higher adsorption

capacity when no normalization of the isotherms is made (Table 6.4).

Among the two physical activated carbons AC-H_2O has the highest quantity of oxygenated surface groups (Table 6.2), which explains its dominant adsorption when SSA normalized. An increase on the CO_2 adsorption capacity upon the presence of oxygen-containing surface functionalities by means of acid-base interactions and hydrogen bonds formation between the adsorbate and the activated carbons surface [59, 60]. The high electronic density of oxygen on the oxygenated surface groups, due to electron gain from the carbon surface atoms, allows them to act as electron-donors in which case the CO_2 adsorbate molecules behave as basic groups.

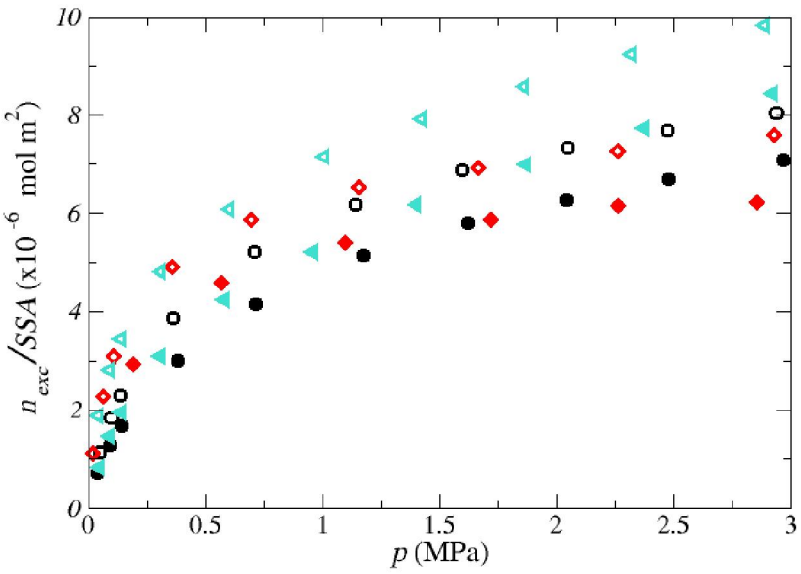

Figure 6.4: SSA normalized CO_2 Adsorption isotherms of the activated carbons: AC-H_3PO_4 (black circles), AC-CO_2 (red diamonds) and AC-H_2O (turquoise triangles). Open symbols represent the adsorption data at 303.15 K while the data at 323.15 is shown by the filled symbols 323.15 K.

Table 6.5 shows the comparison of the methane and carbon dioxide adsorption capacities ($\boldsymbol{n_{CH4}}$ and $\boldsymbol{n_{CO2}}$) of the activated carbons studied on this work with other biomass-based activated carbons of the literature at similar adsorption temperature (T) . It can be seen that the adsorption values are well in the range reported on the literature for both carbon dioxide and methane. Their competitive adsorption capacities and higher carbon dioxide adsorption capacity over methane make the olive stones activated carbons suitable materials for further studies on the CH_4 and CO_2 storage and separation.

Table 6.5: Adsorption capacities of different biomass-bassed adsorbents.

Sample	**Precursor**	**Activation Agent**	**T (K)**	n_{CH4} (mol kg^{-1})	n_{CO2} (mol kg^{-1})
AC-H_3PO_4 *	Olive stones	H_3PO_4	303.15	6.518	10.873
AC-CO_2 *	Olive stones	CO_2	303.15	3.913	5.878
AC-H_2O *	Olive stones	H_2O	303.15	5.417	7.968
BC [19]	Babassu coconut	CO_2	293	5.343	10.49
CS [19]	Coconut shell	CO_2	293	7.259	14.67
Pinpel20 [61]	Wood pellets	CO_2	303	3.36	6.66
MSS-AC [62]	Mango Seeds	H_3PO_4	303	0.858	8.788
CS-H_2O [39]	Cherry stones	H_2O	303	8.36	14.45

* This work.

6.6 Conclusions

On this work, the effects of the textural and chemical properties of three activated carbons on the adsorption behavior of carbon dioxide and methane were studied. For this purpose, three activated carbons produced from olive stones by CO_2 physical activation, H_2O physical activation and H_3PO_4 chemical activation were employed. The activated carbons were mainly microporous. The activated carbon obtained by chemical activation with phosphoric acid of the precursor material presents higher surface area, total pore volume and micropore volume which lead to a higher adsorption capacity for both methane and carbon dioxide. Even though that the two physically activated carbons have similar surface areas and micropore volume, the water vapor activated carbon has also an important volume of mesopores that facilitated the diffusion of the methane molecules into the micropores, thus its methane adsorption capacity was higher. In the case of carbon dioxide, adsorption specific interactions between the adsorptive and adsorbent were also found to participate in the adsorption process. Amongst the two physically activated carbons, H_2O activated carbon had the highest content of oxygen surface group and therefore a higher CO_2 adsorption capacity. Nevertheless, even if the surface chemistry of the adsorbents can influence the adsorption of carbon dioxide, textural properties are still the main governing parameters. Finally, the three activated carbons from olive stones had a higher adsorption of carbon dioxide than to methane, meaning a higher selectivity towards carbon dioxide than methane. Furthermore, their carbon dioxide and methane adsorption capacities were found to be in the range of other biomass-based activated carbons reported in the literature making them suitable candidates for the

upgrading of biogas.

6.7 Bibliography

[1] European Comission. Paris Agreement.

[2] European Comission. Renewable Energy. Moving towards a low carbon economy.

[3] Katherine Starr, Gara Villalba, and Xavier Gabarrell. Upgraded biogas from municipal solid waste for natural gas substitution and CO_2 reduction - A case study of Austria, Italy, and Spain. *Waste Manage.*, 38(1):105–116, 2015.

[4] Shivali Sahota, Goldy Shah, Pooja Ghosh, Rimika Kapoor, Subhanjan Sengupta, Priyanka Singh, Vandit Vijay, Arunaditya Sahay, Virendra Kumar Vijay, and Indu Shekhar Thakur. Review of trends in biogas upgradation technologies and future perspectives. *Bioresour. Technol. Rep.*, 1:79–88, 2018.

[5] EBA European Biogas Association. EBA statictical report 2017 published soon.

[6] Irini Angelidaki, Laura Treu, Panagiotis Tsapekos, Gang Luo, Stefano Campanaro, Henrik Wenzel, and Panagiotis G. Kougias. Biogas upgrading and utilization: Current status and perspectives. *Biotechnol. Adv.*, 36(2):452–466, 2018.

[7] Yangyang Jiang, Jianghua Ling, Penny Xiao, Yingdian He, Qinghu Zhao, Zheng Chu, Yingshu Liu, Ziyi Li, and Paul A. Webley. Simultaneous biogas purification and CO_2 capture by vacuum swing adsorption using zeolite NaUSY. *Chem. Eng. J.*, 334(November 2017):2593–2602, 2018.

[8] Heqing Gong, Siew Siang Lee, and Tae Hyun Bae. Mixed-matrix membranes containing inorganically surface-modified 5A zeolite for enhanced CO_2/CH_4 separation. *Micropor. Mesopor. Mater.*, 237:82–89, 2017.

[9] D. A. Kennedy and F. H. Tezel. Cation exchange modification of clinoptilolite – Screening analysis for potential equilibrium and kinetic adsorption separations involving methane, nitrogen, and carbon dioxide. *Micropor. Mesopor. Mater.*, 262(July 2017):235–250, 2018.

[10] Seok-Jin Son, Jung-Sik Choi, Ko-Yeon Choo, Sun-Dal Song, Savithri Vijayalakshmi, and Tae-Hwan Kim. Development of carbon dioxide adsorbents using carbon materials prepared from coconut shell. *Korean J. Chem. Eng.*, 22(2):291–297, 2005.

[11] Luis A.M. Rocha, Kari Anne Andreassen, and Carlos A. Grande. Separation of CO_2/CH_4 using carbon molecular sieve (CMS) at low and high pressure. *Chem. Eng. Sci.*, 164:148–157, 2017.

[12] Aarti Arya, Swapnil Divekar, Ruchika Rawat, Pushpa Gupta, Madhukar O. Garg, Soumen Dasgupta, Anshu Nanoti, Ranjeet Singh, Penny Xiao, and Paul A. Webley. Upgrading biogas at low pressure by vacuum swing adsorption. *Ind. Eng. Chem. Res.*, 54(1):404–413, 2015.

[13] S. A.S.C. Samarasinghe, Chong Yang Chuah, Yanqin Yang, and Tae Hyun Bae. Tailoring CO_2/CH_4 separation properties of mixed-matrix membranes via combined use of two- and three-dimensional metal-organic frameworks. *J. Membr. Sci.*, 557(January):30–37, 2018.

[14] Renju Zacharia, Luis Fernando Gomez, Richard Chahine, Daniel Cossement, and Pierre Benard. Thermodynamics and kinetics of CH_4/CO_2 binary mixture separation by metal-organic frameworks from isotope exchange and adsorption break-through. *Micropor. Mesopor. Mater.*, 263(November 2017):165–172, 2018.

[15] Youdong Cheng, Xuerui Wang, Chuankun Jia, Yuxiang Wang, Linzhi Zhai, Qing Wang, and Dan Zhao. Ultrathin mixed matrix membranes containing two-dimensional metal-organic framework nanosheets for efficient CO_2/CH_4 separation. *J. Membr. Sci.*, 539(June):213–223, 2017.

[16] Ke Xin Yao, Yanli Chen, Yue Lu, Yunfeng Zhao, and Yi Ding. Ultramicroporous carbon with extremely narrow pore distribution and very high nitrogen doping for efficient methane mixture gases upgrading. *Carbon*, 122:258–265, 2017.

[17] Sirichai Koonaphapdeelert, James Moran, Pruk Aggarangsi, and Asira Bunkham. Low pressure biomethane gas adsorption by activated carbon. *Energy Sustain. Dev.*, 43:196–202, 2018.

[18] Dipendu Saha, Karl Nelson, Jihua Chen, Yuan Lu, and Soydan Ozcan. Adsorption of CO_2 ,CH_4 , and N_2 in Micro-Mesoporous Nanographene: A Comparative Study. *J. Chem. Eng. Data*, 60(9):2636–2645, 2015.

[19] Priscila Costa Vilella, Jéssyca Alves Lira, Diana C.S. Azevedo, Moisés Bastos-Neto, and Ronaldo Stefanutti. Preparation of biomass-based activated carbons and their evaluation for biogas upgrading purposes. *Ind. Crops Prod.*, 109(August):134–140, 2017.

[20] Nor Adilla Rashidi and Suzana Yusup. An overview of activated carbons utilization for the post-combustion carbon dioxide capture. *J. CO2 Util.*, 13:1–16, 2016.

[21] Jarosław Serafin, Urszula Narkiewicz, Antoni W. Morawski, Rafał J. Wróbel, and Beata Michalkiewicz. Highly microporous activated carbons from biomass for CO_2 capture and effective micropores at different conditions. *J. CO2 Util.*, 18:73–79, 2017.

[22] Gayatri Yadavalli, Hanwu Lei, Yi Wei, Lei Zhu, Xuesong Zhang, Yupeng Liu, and Di Yan. Carbon dioxide capture using ammonium sulfate surface modified activated biomass carbon. *Biomass Bioenergy*, 98:53–60, 2017.

[23] Wenming Hao, Eva Björkman, Malte Lilliestråle, and Niklas Hedin. Activated carbons prepared from hydrothermally carbonized waste biomass used as adsorbents for CO_2. *Appl. Energy*, 112:526–532, 2013.

[24] R. R. Gil, B. Ruiz, M. S. Lozano, and E. Fuente. Influence of the pyrolysis step and the tanning process on KOH-activated carbons from biocollagenic wastes. Prospects as adsorbent for CO_2 capture. *J. Anal. Appl. Pyrolysis*, 110(1):194–204, 2014.

[25] Narges Bagheri and Jalal Abedi. Adsorption of methane on corn cobs based activated carbon. *Chem. Eng. Res. Des.*, 89(10):2038–2043, 2011.

[26] Arash Arami-Niya, Wan Mohd Ashri Wan Daud, and Farouq S. Mjalli. Comparative study of the textural characteristics of oil palm shell activated carbon produced by chemical and physical activation for methane adsorption. *Chem. Eng. Res. Des.*, 89(6):657–664, 2011.

[27] Akram Alabadi, Shumaila Razzaque, Yuwan Yang, Shi Chen, and Bien Tan. Highly porous activated carbon materials from carbonized biomass with high CO_2 capturing capacity. *Chem. Eng. J.*, 281:606–612, 2015.

[28] Yong Chen, Liu-jiang Zhou, Yu-zhen Hong, Feng Cao, Ling Li, and Jian-bao Li. Preparation of high-surface-area activated carbon from coconut shell fibers. *Carbon*, 48(10):3005, 2010.

[29] Margaret Iley, H Marsh, and F. Rodriguez-Reinoso. The Adsorptive Properties of Carbonised Olive Stones. *Carbon*, 11:633–636, 1973.

[30] G. Zhao, G. Zou, H. Hou, P. Ge, X. Cao, and X. Ji. Sulfur-doped carbon employing biomass-activated carbon as a carrier with enhanced sodium storage behavior. *J. Mater. Chem. A*, 5:24353–24360, 2017.

[31] S. M. Yakout and G. Sharaf El-Deen. Characterization of activated carbon prepared by phosphoric acid activation of olive stones. *Arab. J. Chem.*, 9:S1155–S1162, 2016.

[32] Haoran Wei, Shubo Deng, Bingyin Hu, Zhenhe Chen, Bin Wang, Jun Huang, and Gang Yu. Granular Bamboo-Derived Activated Carbon for High CO 2 Adsorption: The Dominant Role of Narrow Micropores. *ChemSusChem*, 5(12):2354–2360, 2012.

[33] N. Álvarez-Gutiérrez, S. García, M. V. Gil, F. Rubiera, and C. Pevida. Towards bio-upgrading of biogas: Biomass waste-based adsorbents. *Energy Procedia*, 63:6527–6533, 2014.

[34] P. González-García. Activated carbon from lignocellulosics precursors: A review of the synthesis methods, characterization techniques and applications. *Renew. Sust. Energ. Rev.*, 82(August 2017):1393–1414, 2018.

[35] M. V. Gil, M. Martínez, S. García, F. Rubiera, J. J. Pis, and C. Pevida. Response surface methodology as an efficient tool for optimizing carbon adsorbents for CO_2 capture. *Fuel Process. Technol.*, 106:55–61, 2013.

[36] W. Djeridi, N. Ben Mansour, A. Ouederni, P. L. Llewellyn, and L. El Mir. Influence of the raw material and nickel oxide on the CH_4 capture capacity behaviors of microporous carbon. *Int. J. Hydrogen Energy*, 40(39):13690–13701, 2015.

[37] N Soudani, S Najar-Souissi, V Abderkader-Fernandez, and Abdelmottaleb Ouederni. Effects of nitrogen plasma treatment on the surface characteristics of olive stone-based activated carbon. *Environ. Technol.*, 38:956–966, 2017.

[38] M Balsamo, B Tsyntsarski, Alessandro Erto, T Budinova, B Petrova, N Petrov, and Amedeo Lancia. Dynamic studies on carbon dioxide capture using lignocellulosic based activated carbons. *Adsorption*, pages 633–643, 2015.

[39] Noelia Álvarez-Gutiérrez, Susana García, María Victoria Gil, Fernando Rubiera, and Covadonga Pevida. Dynamic Performance of Biomass-Based Carbons for CO_2 /CH_4 Separation. Approximation to a Pressure Swing Adsorption Process for Biogas Upgrading. *Energy Fuels*, 30(6):5005–5015, 2016.

[40] Alessandro Erto, B Tsyntsarski, M Balsamo, T Budinova, Amedeo Lancia, B Petrova, and N Petrov. Synthesis of Activated Carbons by Thermal Treatments of Agricultural Wastes for CO_2 Capture from Flue Gas. *Combust. Sci. Technol.*, 188:581–593, 2016.

[41] Meriem Moussa, Najoua Bader, Nausika Querejeta, Inés Durán, Covadonga Pevida, and Abdelmottaleb Ouederni. Toward sustainable hydrogen storage and carbon dioxide capture in post-combustion conditions. *J. Environ. Chem. Eng.*, 5(2):1628–1637, 2017.

[42] Marco Balsamo, Ana Silvestre-Albero, Joaquín Silvestre-Albero, Alessandro Erto, Francisco Rodríguez-Reinoso, and Amedeo Lancia. Assessment of CO2adsorption capacity on activated carbons by a combination of batch and dynamic tests. *Langmuir*, 30(20):5840–5848, 2014.

[43] Imen Ghouma, Mejdi Jeguirim, Uta Sager, Lionel Limousy, Simona Bennici, Eckhard Däuber, Christof Asbach, Roman Ligotski, Frank Schmidt, and Abdelmottaleb Ouederni. The potential of activated carbon made of agro-industrial residues in NOx immissions abatement. *Energies*, 10(12), 2017.

[44] Imen Ghouma, Mejdi Jeguirim, Sophie Dorge, Lionel Limousy, Camélia Matei Ghimbeu, and Abdelmottaleb Ouederni. Activated carbon prepared by physical activation of olive stones for the removal of NO_2 at ambient temperature. *C. R. Chim.*, 18(1):63–74, 2015.

[45] Lionel Limousy, Imen Ghouma, Abdelmottaleb Ouederni, and Mejdi Jeguirim. Amoxicillin removal from aqueous solution using activated carbon prepared by chemical activation of olive stone. *Environ. Sci. Pollut. R.*, 24:9993–10004, 2017.

[46] Stephen Brunauer, P. H. Emmett, and Edward Teller. Adsorption of Gases in Multimolecular Layers. *J. Am. Chem. Soc.*, 60(2):309–319, 1938.

[47] Silvia Román, Beatriz Ledesma, Andrés Álvarez-Murillo, Awf Al-Kassir, and Talal Yusaf. Dependence of the microporosity of activated carbons on the lignocellulosic composition of the precursors. *Energies*, 10(4), 2017.

[48] Tao Song, Jing Ming Liao, Jun Xiao, and Lai Hong Shen. Effect of micropore and mesopore structure on CO_2 adsorption by activated carbons from biomass. *Xinxing Tan Cailiao/New Carbon Mater.*, 30(2):156–166, 2015.

[49] J.L Figueiredo, M.F.R Pereira, M.M.A Freitas, and J.J.M Órfão. Modification of the surface chemistry of activated carbons. *Carbon*, 37(9):1379–1389, 1999.

[50] Olga Patricia Ortiz Cancino, Deneb Peredo Mancilla, Manuel Pozo, Edgar Pérez, and David Bessieres. Effect of Organic Matter and Thermal Maturity on Methane Adsorption Capacity on Shales from the Middle Magdalena Valley Basin in Colombia. *Energy Fuels*, 31(11):11698–11709, 2017.

[51] Deneb Peredo-Mancilla, Cecile Hort, Mejdi Jeguirim, Camelia Matei Ghimbeu, Lionel Limousy, and David Bessieres. Experimental Determination of the CH_4 and CO_2 Pure Gas Adsorption Isotherms on Different Activated Carbons. *J. Chem. Eng. Data*, page acs.jced.8b00297, 2018.

[52] U.S. Secretary of Commerce. Isothermal Properties for Carbon Dioxide, 2017.

[53] Yves Gensterblum, Alexej Merkel, Andreas Busch, and Bernhard M. Krooss. High-pressure CH_4 and CO_2 sorption isotherms as a function of coal maturity and the influence of moisture. *Int. J. Coal Geol.*, 118:45–57, 2013.

[54] József Tóth. Uniform interpretation of gas/solid adsorption. *Adv. Colloid Interface Sci.*, 55:1–239, 1995.

[55] Robert Sips. On the Structure of a Catalyst Surface. *J. Chem. Phys.*, 16:490–495, 1948.

[56] D. Lozano-Castelló, D. Cazorla-Amorós, A. Linares-Solano, and D. F. Quinn. Influence of pore size distribution on methane storage at relatively low pressure: Preparation of activated carbon with optimum pore size. *Carbon*, 40(7):989–1002, 2002.

[57] Mirian Elizabeth Casco, Manuel Martínez-Escandell, Enrique Gadea-Ramos, Katsumi Kaneko, Joaquín Silvestre-Albero, and Francisco Rodríguez-Reinoso. High-pressure methane storage in porous materials: Are carbon materials in the pole position? *Chem. Mater.*, 27(3):959–964, 2015.

[58] Piotr Nowicki, Helena Wachowska, and Robert Pietrzak. Active carbons prepared by chemical activation of plum stones and their application in removal of NO_2. *J. Hazard. Mater.*, 181(1-3):1088–1094, 2010.

[59] Yangyang Liu and Jennifer Wilcox. Molecular Simulation Studies of CO_2 Adsorption by Carbon Model Compounds for Carbon Capture and Sequestration Applications. *Environ. Sci. Technol.*, 47(1):95–101, 2013.

[60] Wei Xing, Chao Liu, Ziyan Zhou, Jin Zhou, Guiqiang Wang, Shuping Zhuo, Qingzhong Xue, Linhua Song, and Zifeng Yan. Oxygen-containing functional group-facilitated CO_2 capture by carbide-derived carbons. *Nanoscale Res. Lett.*, 9(1):1–8, 2014.

[61] Jose F. Vivo-Vilches, Agustin F. Pérez-Cadenas, Francisco J. Maldonado-Hódar, Francisco Carrasco-Marín, Rui P V Faria, Ana M. Ribeiro, Alexandre F P Ferreira, and Alirio E. Rodrigues. Biogas upgrading by selective adsorption onto CO_2 activated carbon from wood pellets. *J. Environ. Chem. Eng.*, 5(2):1386–1393, 2017.

[62] Kuppusamy Munusamy, Rajesh S. Somani, and Hari C. Bajaj. Breakthrough adsorption studies of mixed gases on mango (Mangifera indicaL.) seed shell derived activated carbon extrudes. *J. Environ. Chem. Eng.*, 3(4):2750–2759, 2015.

Appendix

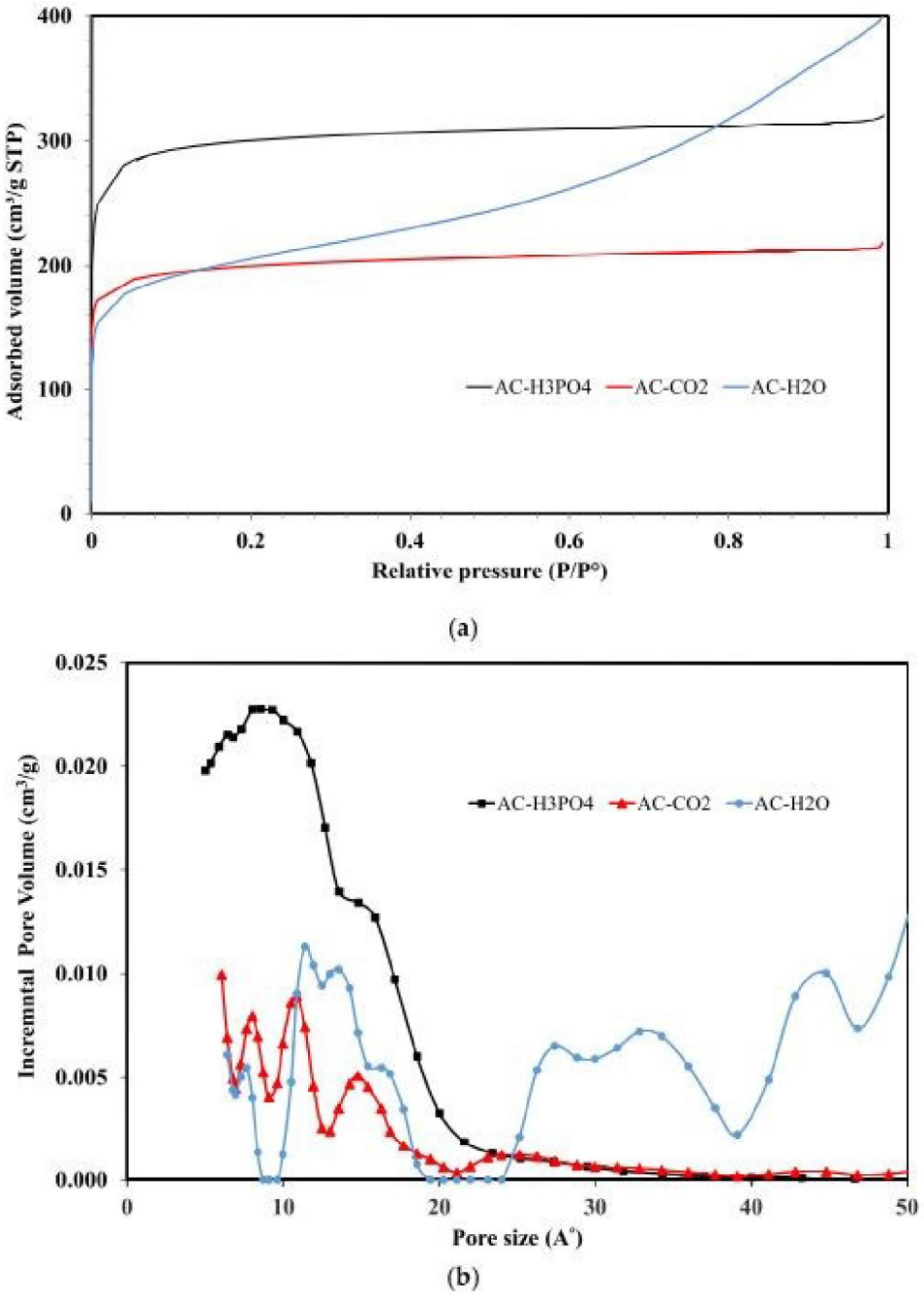

Figure 6.5: a) Adsorption and desorption of Nitrogen (N2) at 77 K on the Olive stones activated carbons, b) Pore size distribution (PSD) of the olive stones activated carbons obtained by means of density functional theory (DFT).

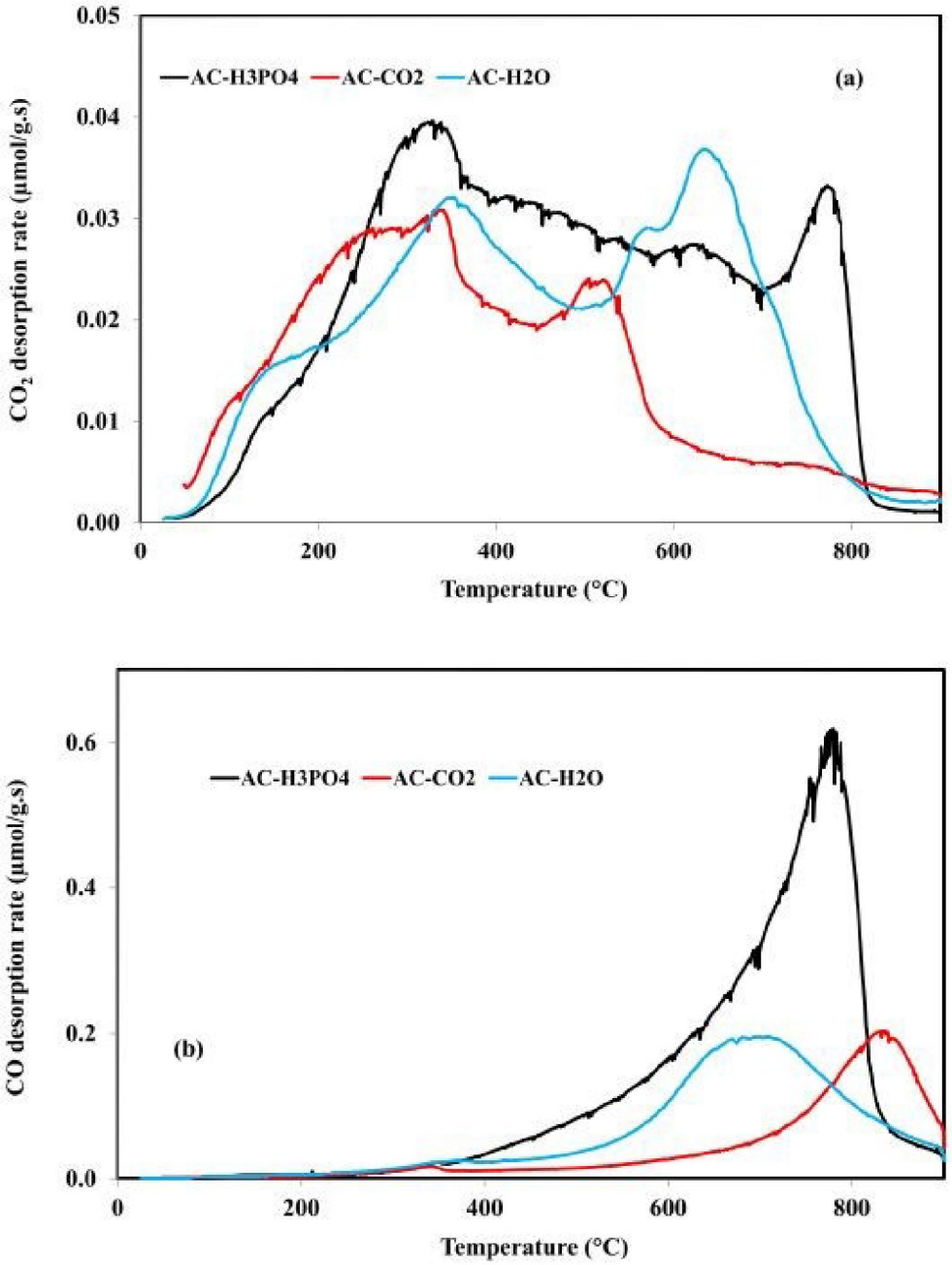

Figure 6.6: a) Emmited CO_2 during temperature programmed desorption-mass spectroscopy (TPD-MS) of the olive stones activated carbons, b) Emmited CO during temperature programmed desorption-mass spectroscopy (TPD-MS) of the olive stones activated carbons .

Peredo-Mancilla, D., et al. Comparative study of the CH_4/CO_2 Adsorption Selectivity of Activated Carbons for Biogas Upgrading. *J. Environ. Chem. Eng.* 2019, Accepted Manuscript

DOI: 10.1016/j.jece.2019.103368

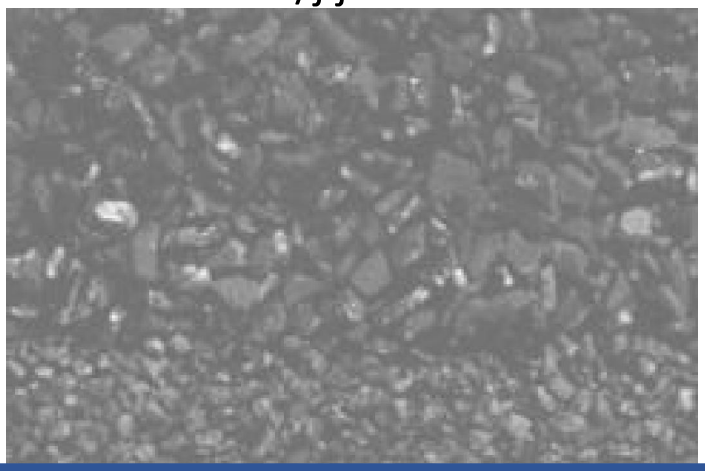

CHAPTER 7

EXPERIMENTAL DTERMINATION OF THE CH_4/CO_2 SELECTIVITY OF COMMERCIAL ACTIVATED CARBONS

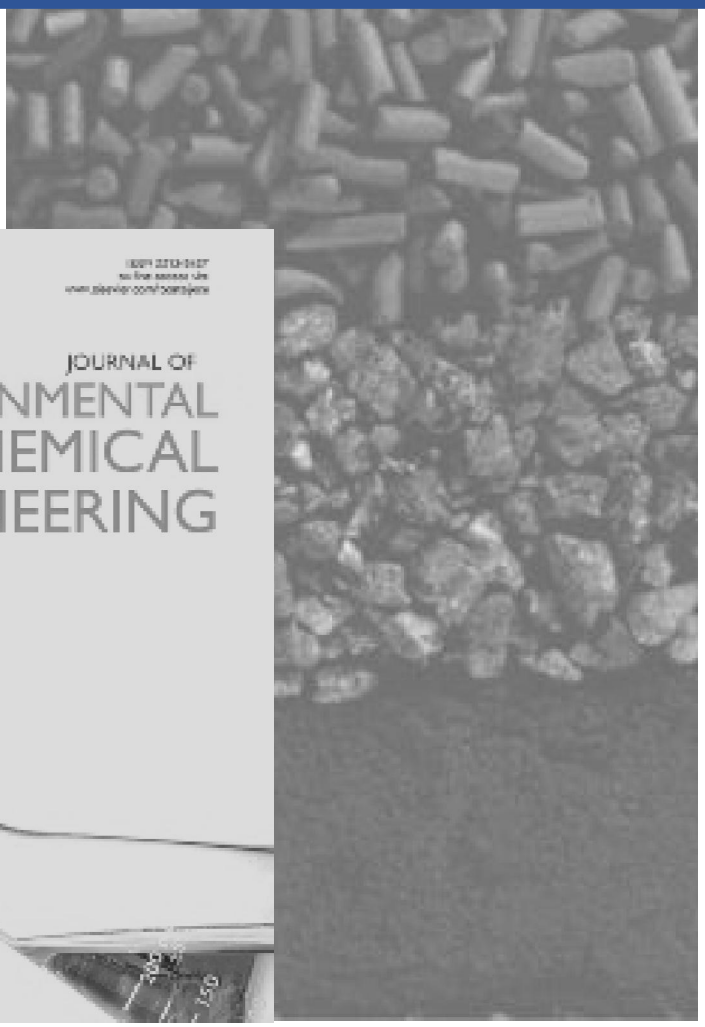

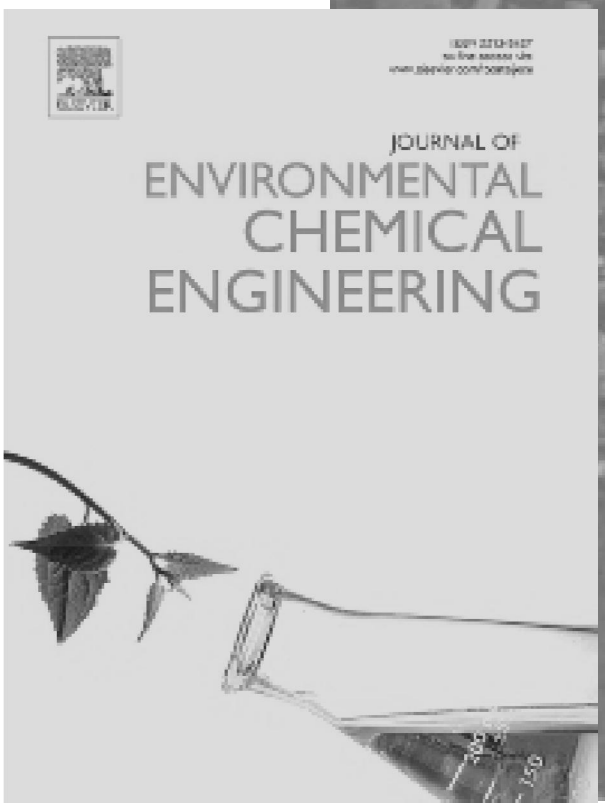

7.1 Chapter Outlook

Thanks to Chapters 5 and 6, the effect of both textural and chemical properties on the pure gas adsorption has been established. The present Chapter follows with the calculation of the second performance indicator for biogas upgrading by activated carbons: the CH_4/CO_2 selectivity.

The selectivity of an adsorbent material denotes its capacity to predominantly adsorb one gas over other(s) when a mixture of gases is present. For biogas upgrading application, the adsorbent most retain the majority of carbon dioxide into its matrix with the methane fraction remaining in the gas bulk, in other words it most have a high CH_4/CO_2 selectivity. The present Chapter explores the influencing factors of the selectivity of activated carbons. To this end, the CH_4/CO_2 equimolar mixture adsorption isotherms of the 5 commercial activated carbons introduced in Chapter5 are here presented.

The adsorption measurements were carried out under isothermal conditions at a temperature of 303 K on the pressure range of 0 to 3 MPa. The obtained results indicate that a higher BET surface area in addition to a narrow pore size distribution centered at a pore size of 0.8 nm results in higher CH_4/CO_2 total adsorption capacity. Furthermore, whilst the presence of basic functionalities on the surface of the adsorbents seems to enhanced the adsorption of carbon dioxide, the adsorption selectivity is influenced by both textural and chemical properties of the samples. The selectivity is detpicted higher for activated carbon ROx 0.8 (selectivity factor up to 4.7), a microporous steam activated carbon with a mild surface area (1323 $m^2 g^{-1}$), narrow pore size distribution with an average pore size of 0.84 nm. Higher BET surface areas and average pore sizes appear detrimental of the selectivity. Finally, the presence of sulfur surface groups is reported to increase the selectivity factor.

7.2 Introduction

The constant increment of global energy demand and the fight against climate change have created the need of turning our energy production systems towards renewable energies [1]. One key alternative to the burning of fossil fuels is the use of biofuels. Derived from biomass, the use of biofuels has environmental benefits such as a decrease in the emissions of CO_2, SO_x and hydrocarbons [2].

Biomethane production via upgrading of biogas is a sustainable source of advanced transport biofuel [3]. The conversion of biogas to biomethane, involves the separation of the methane fraction (53 to 70%) from the carbon dioxide portion

(30 to 40%) to obtain a highly purified methane stream (≈95%) that meets the domestic gas pipeline requirements [4, 5]. Compared to other upgrading techniques, the separation of biogas by physical adsorption has the advantages of low investment and operation costs, high efficiency, null production of chemical wastes and no watter requirement [6, 7]. It consists in the selective partitioning of carbon dioxide from biogas into an adsorbent material also known as the adsorbent [8]. Adsoprbent materials are ussually highly porous solids with high specific surface area and developped porosity [9].

Activated carbons (ACs) are commonly used as adsorbents due to their high surface area, developed microporosity, thermal stability, ease of regeneration and low production cost [10, 11]. They are recognized for their adsorption performance on a variety of separation processes including removal of heavy metals from water [12, 13] and [14], pharmaceutical and organic pollutants removal [15, 16, 17], treatment of flue gas [18, 19], purification of natural gas [20, 21] and upgrading of biogas [22]; [23]. Pure CO_2 gas adsorption has been reported to be influenced by the textural properties of the adsorbents, mainly the narrow micropore volume ($<$0.7 nm) [24, 25, 26, 27]. Nevertheless, the surface chemistry of the adsorbent is also thought to play a role on the adsorption process ([28, 29]). Liu et al. [30] studied the effect of surface heterogenity on the adsorption process, they results showed an ehacement of CO_2 adsorption when oxygen surface groups such as -OH and -COOH were present, these oxygen functionalities are highly electronegative which allows them to act as basic adsorption sites. Karimi et al. [31] reported an increase on CO_2 adsorption capacity upon removal of surface acidic groups. In fact, due to the acidic properties of carbon dioxide, surface chemistry modification of activated carbons consisting in the addition of basic functionalities is a well studied strategy for the preparation of carbon capture adsorbents [32, 33, 34].

When CO_2 separation of CH_4/CO_2 mixture is concerned, the ideal adsorbent should have a high selectivity provided by different adsorption behavior for the two gases, or in other words it must preferentially adsorb carbon dioxide with the vast majority of methane molecules remaining in the gaseous phase [35]. The two molecules have similar kinetic diameters, 0.330 nm for CO_2 and 0.382 nm for CH_4 which make it very complicated to design kinteic-based adsorbents [36]. However, the two molecules have an important difference of polarity, CO_2 has a quadrupolar moment of 13.4×10^{-40} cm^2, while CH_4 is a non polar molecule [37]. The presence of polar surface functionalities results in an increased selectivity towards carbon dioxide by means of stronger adsorbate-adsorbant interactions as it was demostrated by Park et al [38]. They found that a high content of sulfur and potassium on 3 biomass-based activated carbons privileged the adsorption of CO_2. Upon functionalization with NaOH, Fe_2CO_3 of a commercial activated carbon, Castrillon et al.

found that the stronger basicity as well as developed microporosity of the NaOH modified carbon resulted in the highest selectivity [39]. Using molecular dynamics simulations, Wang et al. demonstrated that a low pressure the selectivity is highly influenced by the surface chemistry, whilst at the high pressure region the pore size distribution is the major contributing factor [40].

Although the kind of studies briefly reviewed here are of great importance for the development of new and more efficient biogas upgrading techniques, the bibliography comprising the CO_2 separation from CH_4 by activated carbons remains to this day very limited. The present work explores the role of textural and chemical properties of activated carbons on the CH_4/CO_2 selectivity, by means of the equimolar binary mixture adsorption isotherms for a set of 5 well characterized commercial activated carbons. To the best of our knowledge, this is the first experimental work dealing with the comparison of selectivity values of activated carbons in terms of their textural and surface properties.

7.3 Materials and Methods

The adsorption selectivity studies were performed on five activated carbons produced by Cabot Corporation (USA). The activated carbons named CNR-115 and CGran are chemically activated with phosphoric acid while GAC 1240, RX 1.5 and Rox 0.8 are physically activated with steam.

7.3.1 Characterization of the samples

Textural characterization

The textural properties of the activated carbons were obtained by means of nitrogen (N_2) adsorption at 77 K carried out on a Micrometrics ASAP 2000 automatic apparatus with a preparatory step consisting of placing the samples under vacuum for 12 h at 573 K. The BET surface area was obtained from the linear plot in the low pressure region (P/P_0=0.01-0.05) [41]. The total pore volume was calculated from the amount of adsorbed nitrogen at a relative pressure of 0.95. The Dubinin-Radushkevich (DR) equation was used on the relative pressure range of 10^{-4} to 10^{-2} for obtaining the micropore volume [42], the mesopore volume is calculated as the difference between the total pore volume and the micropore volume. This properties can also be found on a previous work of the authors [43].

The pore size distribution was obtained applying the non liquid density functional theory (NLDFT) with the carbon slit pores model to the N_2 adsorption data.

Surface Chemistry characterization

To evaluate the surface chemistry of the activated carbons the temperature programmed desorption TPD profiles were obtained using a "home made" apparatus coupled with mass spectrometry. The temperature of a quartz tube containing 10 g of the sample was increased from 298 to 1223 K at a rate of 2 K per minute, the evolution of carbon monoxide (CO) and carbon dioxide (CO_2) was followed quantitatively using the mass spectrometer (INFINCON Transpector).

In addition, the acid/basic character of the activated carbons was studied by the measurement of the zero charge point pH ($\boldsymbol{pH_{PZC}}$). For each AC, a quantity of 0.1 g was put in contact with a set of 5 solutions with pH values ranging from 4 to 10 prepared by additions of NaOH 0.1 N or HCl 0.1 N in distillate water. The AC containing solutions were kept under string for 72 h and the pH of the solution was determined by a Denever Instrument model 215 pH meter. The five solutions containing one of the activated carbons had similar final pH values that correspond to the $\boldsymbol{pH_{PZC}}$. The $\boldsymbol{pH_{PZC}}$ value was refined by following the same protocol using three solutions of pH close to the final values of the first set for each activated carbon.

The presence of acidic and basic oxygen surface groups was studied by the method of Boehm [44]. To calculate the quantity of acidic groups an indirect titration method as described by Schonherr et al. was followed [45]: 200 mg of AC was added to 50 mL of 0.01 N solution of NaOH. The activated carbons solutions were kept under stirring for 72 h. The supernatant carbons were separated from the solutions by centrifugation followed by decantation. Then, three 10 mL aliquots were taken and 20 mL of 0.01 N hydrochloric acid were added to each sample. Finally, the sodium carbonate Na_2CO_3 0.01 N titration curves were obtained. For each activated carbon-NaOH solution a reference sample containing 50 mL of the NaOH solution was subjected to the same protocol from stirring to titration.

The amount of surface basic functionalities was measured by titration of HCl with Na_2CO_3. The samples containing 50 mL of HCl 0.01 N and 0.200 mg of AC followed the same separation method and treatment time described for basic functionalities. On this case however, direct titration of the 10 mL aliquots by Na_2CO_3 was carried out. The error of the followed Boehm titration protocol is reported to be $\sim$0.15% of the aliquot volume (10 mL) [45].

7.3.2 CH_4/CO_2 Adsorption experiments

A high pressure manometric device coupled with gas chromatography CG was designed for the calculation of the equimolar CH_4/CO_2 mixture adsorption isotherms, an schematic view of this apparatus can be seen in Figure 7.1. Its main components are the dossing and asorption cells ($\boldsymbol{V_{dos}}$ and $\boldsymbol{V_{ads}}$) (Top Industries, volume: 20.5 cm^3), a recirculation pump (GK-M 24/02, max. flow: 2.8 l/min and max. system pressure: 15 MPa), a manometer (MKS baratron type 121 A, 0.01% uncertainty from vacuum to 3.3 MPa), FID gas chromatograph (Agilent Technologies 7890 A). Isothermal conditions are achieved by a heating wire controlled by a PID regulator (Eurotherm 3208) and monitored throughout the experiments by two thermocouples placed on each of the cells.

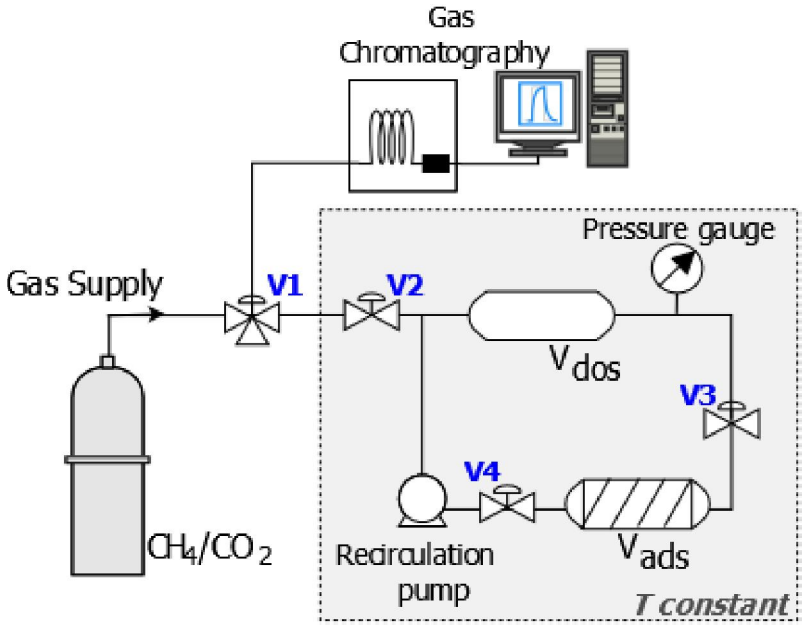

Figure 7.1: Schematic representation of the HP adsorption manometric device coupled with gas chromatography.

The procedure starts with the calculation of the accessible volume in the presence of the adsorbent, otherwise known as dead-space volume. To this end, an amount of sample with an adsorption area of at least $\sim$30 m^2 is placed inside the adsorption volume $\boldsymbol{V_{ads}}$ and cleaned by an 8 h out-gassing process at 373 K under vacuum pressure ($\leq 10^{-2}$ Pa). The dead space volume is obtained by successive helium expansions from the dossing cell $\boldsymbol{V_{dos}}$ to the adsorption cell $\boldsymbol{V_{ads}}$ [46]. Between the dead-space volume calibration and the adsorption measurements, the system is put under vacuum for an additional 4 hours in order to remove any traces of helium.

The protocol for determination of the gas mixture adsorption isotherm follows a mass balance principle. An amount of the CH_4/CO_2 is introduce into the dossing cell

and the pressure is recorded once the thermal equilibrium is reached (i.e. constant pressure). The gas is then expanded into the adsorption cell by opening the valves 3 and 4, homogeneity of the gas during the adsorption process is attained through recirculation of the gas by the recirculation pump, equilibrium is once more achieved and pressure recorded. Valves 3 and 4 are closed isolating the adsorption cell and a discrete dose of the gas isolated in the dossing section of the system is sent to be analyzed by the gas chromatograph.

The total adsorbed amount ($\boldsymbol{n_{ads}}$) can be then calculated from the difference between the quantity of moles introduced on the dossing cell ($\boldsymbol{n_{dos}}$) and the amount of moles in the gas phase after adsorption ($\boldsymbol{n_g}$) (eq. 7.1).

$$\boldsymbol{n_{ads} = n_{dos} - n_g} \tag{7.1}$$

From the total adsorbed amount a fraction corresponds to methane and the rest carbon dioxide. Thus, the molar fraction of each gas remaining on the gas phase after the adsorption ($\boldsymbol{y_{CH_4}}$ and $\boldsymbol{y_{CO_2}}$) needs to be calculated from the integration of the CG peaks. The methane mole fraction in the gas phase is obtained by equation 7.2.

$$\boldsymbol{y_{CH_4} = \frac{n_{CH_4,g}}{n_{CH_4,g} + n_{CO_2,g}}} \tag{7.2}$$

The ratio of moles of methane in the adsorbed phase $\boldsymbol{x_{CH_4}}$ can be express also express in the form of a mole fraction (eq. 7.3)

$$\boldsymbol{x_{CH_4} = \frac{n_{CH_4,ads}}{n_{CH_4,ads} + n_{CO_2,ads}}} \tag{7.3}$$

Therefore, the quantity of adsorbed moles of methane for the first step of the isotherm is given by multiplication of $\boldsymbol{x_{CH_4}}$ times the total number of adsorbed moles ($\boldsymbol{n_{ads}}$) as shown by equation 7.4.

$$\boldsymbol{n_{CH_4,ads} = x_{CH_4} \times n_{ads}} \tag{7.4}$$

In a similar way, the number of moles of carbon dioxide in the adsorbed phase ($\boldsymbol{n_{CO_2,ads}}$) is expressed by equation 7.5

$$\boldsymbol{n_{CO_2,ads} = x_{CO_2} \times n_{ads}} \tag{7.5}$$

For the following steps, the gas in the dossing section of the system is evacuated

by the vacuum pump and a new dose of the 50-50% mixture is added to the dossing cell, the pressure is recorded and valves 3 and 4 are opened. The gas molecules that were introduced in the system enter in contact with the gas that was isolated in the adsorption cell on the previous step, recirculation of the gas takes place and a new equilibrium is reached. Therefore, the adsorbed quantity of each gas at a given ($\boldsymbol{i}$) step of the isotherm can be calculated by equations 7.6 and 7.7:

$$\boldsymbol{n^i_{CH_4,ads}} = (\frac{\mathbf{1}}{\mathbf{2}}\boldsymbol{n_{dos}} + \boldsymbol{n_g^{i-1}}) - (\boldsymbol{n^i_{CH_4,ads}}\boldsymbol{y^1_{CH_4}}) \tag{7.6}$$

$$\boldsymbol{n^i_{CO_2,ads}} = (\frac{\mathbf{1}}{\mathbf{2}}\boldsymbol{n_{dos}} + \boldsymbol{n_g^{i-1}}) - (\boldsymbol{n^i_{CO_2,ads}}\boldsymbol{y^1_{CO_2}}) \tag{7.7}$$

The total adsorbed amount of each gas is calculated by addition of the adsorbed amount on the present step to that of the precedent ones:

$$\boldsymbol{n_{CH_4,ads}} = \sum_{\boldsymbol{i}} \boldsymbol{n_{CH_4,ads}} \tag{7.8}$$

and

$$\boldsymbol{n_{CO_2,ads}} = \sum_{\boldsymbol{i}} \boldsymbol{n_{CO_2,ads}} \tag{7.9}$$

7.4 Results

7.4.1 Activated Carbons Characterization

Figure 7.2 b) shows the pore size distribution profiles (PSD) for the five activated carbons. A predominance of peaks of under 2 nm can be depicted on this figure, characteristic of microporous materials. Nevertheless, a contribution of mesopores (pores from 2 to 50 nm) is also present.

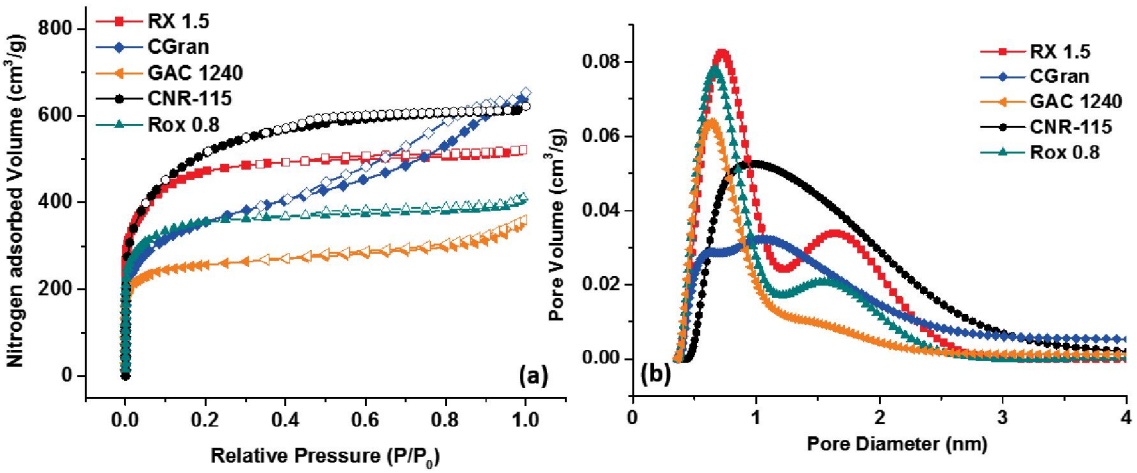

Figure 7.2: a) Nitrogen adsorption isotherms at 77 K and b) NLDFT pore size distribution of activated carbons RX 1.5, CGran, GAC 1240, CNR-115 and ROx 0.8.

The nitrogen adsorption isotherms on Fig. 7.2 a) show type I behavior for activated carbons RX 1.5, GAC 1240, CNR-115 and Rox 0.8 indication of microporous materials. CGran shows a type IV isotherm depicting the presence of an important volume of mesopores. Table 7.1 shows ACs surface areas (S_{BET}) ranging from 982 (GAC 1240) up to 1714 (CNR-115) in accordance with typical values for carbonaceous materials [47]. The obtained values of micropore volume (V_{micro}) confirm a developed microporosity of the samples. Furthermore, the activated carbons with higher BET surface area, RX 1.5 and CNR-115, also display bigger micropore volumes (0.61 and 0.64 respectively). The presence of an important volume of mesopores (V_{meso}) on CGran resulted in the biggest total pore volume V_{tot}, closely followed by CNR-115. Finally, the average pore size (L0) of each sample was calculated using the NLDFT-PSD profiles. The values of L0 ranged from 0.76 (GAC 1240) to 1.10 (CNR-115).

Table 7.1: Textural Characterization of Activated Carbons

Sample	$\mathbf{S_{BET}}$ $\mathbf{(m^2\ g^{-1})}$	$\mathbf{V_{micro}}$ $\mathbf{(cm^3\ g^{-1})}$	$\mathbf{V_{meso}}$ $\mathbf{(cm^3\ g^{-1})}$	$\mathbf{V_{tot}}$ $\mathbf{(cm^3\ g^{-1})}$	**L0** **(nm)**
RX 1.5	1683	0.61	0.20	0.81	0.93
CGran	1378	0.45	0.54	0.99	1.00
GAC 1240	982	0.36	0.20	0.56	0.76
CNR-115	1714	0.64	0.31	0.95	1.10
Rox 0.8	1323	0.48	0.16	0.64	0.84

The acid-base properties of the activated carbons were studied by means of

their the zero charge point pH ($\boldsymbol{pH_{PZC}}$) which corresponds to the pH at which the positive and negative surface charges cancel each other. Table 7.2 displays the obtained values for the aqueous solutions of the activated carbons. A wide range of $\boldsymbol{pH_{PZC}}$ values can be noticed between the activated carbons following the tendency from more to less acidic of CGran > CNR-115 > Gac 1240 > ROx 0.8 > RX 1.5, this trend is closely linked to the activation method used for the preparation of the carbon, with those activated chemically (CGran and CNR-115) showing the highest acidity.

Table 7.2: Acid-Base character of Activated Carbons

Sample	$\boldsymbol{pH_{PZC}}$	**Total Acid (mmol g^{-1})**	**Total Basic (mmol g^{-1})**
RX 1.5	9.75	0.18	0.73
CGRAN	3.86	1.74	0.01
GAC 1240	8.13	0.18	0.49
CNR-115	6.14	0.49	0.61
ROx 0.8	8.74	0.21	0.61

Moreover, the basic $\boldsymbol{pH_{PZC}}$ values of RX 1.5, ROx 0.8 and GAC 1240 indicates the presence of oxygen functionalities from the families of carbonyles and ethers since they have been reported to create $\boldsymbol{\pi}$-electrons rich zones that make the surface acts as a Lewis base [48]. By contrast, activated carbons surface acidity is thought to be related to the presence of carboxylic acids, lactones and phenols that increase the surface polarity, in the present case a part of acidity may come also from phosforic groups created due to the H_3PO_4 activation agent used [49]. Boehm titration method results (Table 7.2) confirm the presence of an superior quantity of such functional groups in the acidic $\boldsymbol{pH_{PZC}}$ carbon CGran than on the other activated carbons. Furthermore, activated carbons showing a higher $\boldsymbol{pH_{PZC}}$ presented a bigger quantity of basic oxygen functionalities.

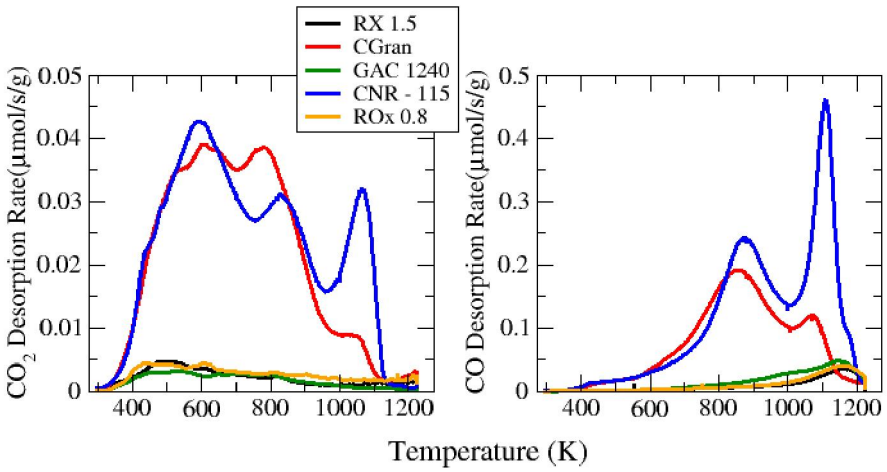

Figure 7.3: CO_2 and CO TPD desorption profiles for activated carbons RX 1.5, CGran, GAC 1240, CNR-115 and ROx 0.8.

To further investigate the types and quantities of surface groups the TPD-MS profiles were obtained for all of the samples (see Figures 7.3 and 7.4). Moreover, the CO and CO_2 TPD-MS profiles show the desorption rates of oxygen surface functionalities upon increasing of the temperature. A considerably bigger amount of oxygen surface groups on activated carbons CGran and CNR-115 can be observed in agreement with the results obtained by the $\boldsymbol{pH_{PZC}}$. The carbon dioxide desorption profiles of these two activated carbons, indicate the occuring of surface carboxylic groups and lactones functionalities demostrated by the presence of desorption peaks at a temperature below 673 and 923 K respectively. In addition, the peak at 1100 for CNR-115 indicates the presence of thermally stable functionalities such as carbonates. On the other side, the CO desorption profiles of these activated carbons show two peaks, the first one at 900 K corresponds to phenol groups, whilst the second one arises from the presence of very thermally stable functionalities such as quinones, ethers, and anhydrides. The remaining activated carbons display a low concentration of oxygen functionalities where the presence of carboxylic acids, ethers and quinones can be depicted. Overall the surface acidic groups quantified by the emission of CO_2 groups are significantly in lower quantities than the basic groups decomposed as CO groups (see Fig. 7.4). This result is in rather good agreement with the amount of basic and acidic groups determined by bohem titration (Table 7.2).

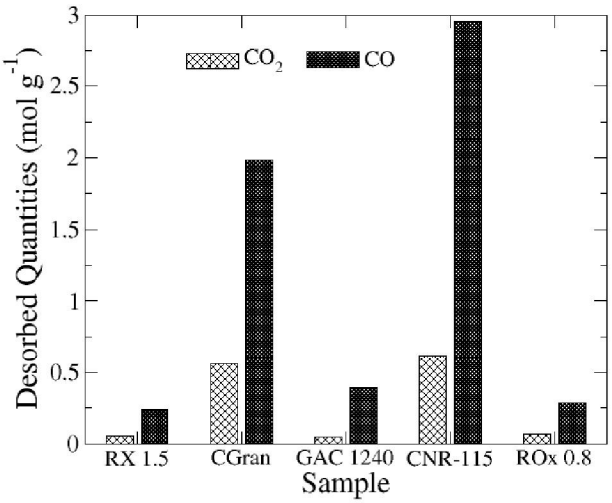

Figure 7.4: CO_2 and CO_2 TPD total emitted quantities for activated carbons RX 1.5, CGran, GAC 1240, CNR-115 and ROx 0.8 obtained by integration of the desorption peaks.

7.4.2 CH_4/CO_2 Adsorption experiments

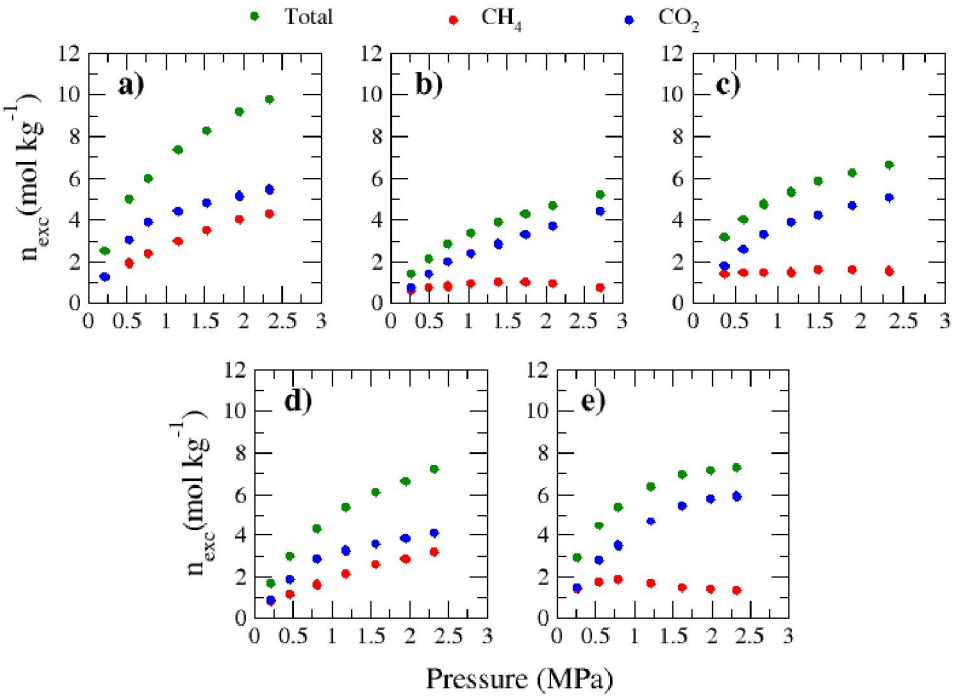

Figure 7.5: CH_4/CO_2 mixture and individual components in the mixture adsorption at 303 K for activated carbons a) RX 1.5, b) CGran, c) GAC 1240, d) CNR-115 and e) ROx 0.8. (*green: Total, red: CH_4 and blue: CO_2*).

The CH_4/CO_2 equimolar mixture adsorption isotherms were obtained for the studied activated carbons at a temperature of 303 K (see Fig. 7.5, Tables 7.3-7.7). The results show a superior carbon dioxide adsorption (blue) compared to that of methane (red) for the five activated carbons. The explanation lays on the difference in polarity of the two probe molecules, while the molecule of carbon monoxide has a high quadrupole moment, methane is a non-polar molecule. Thus, the higher polarizability of CO_2, leads to stronger interactions between the adsorbate and the surface groups of the activated carbons [50]. In addition, an increase of the total adsorbed quantity upon pressure augmentation can also be observed in consistency with typical adsorption behavior on activated carbons.

Carbon dioxide pure gas adsorption on the studied activated carbons was previously found to be directly related to their BET surface area and micropore volume [43]. Here, activated carbons CNR-115 and RX 1.5 present higher adsorption capacities than the rest of activated carbons (see Figure 7.5) which could indicate influential effect of the BET surface area on the adsorption capacity in agreement

with the literature [51, 52]. The calculation of the BET surface area provides an estimation of available physisorption sites, thus explaining the higher adsorption of this carbons. Nonetheless, it can be seen that even though the adsorption capacity of carbon dioxide is favored, their methane adsorption is also important, an unwanted behavior for the separation of these two gases. Furthermore, when adsorption competition between the two gases is present, other factors seem to play an important role as evidenced upon comparison of the adsorption isotherms of CGran and ROx 0.8 (Fig 7.5 b) and e)). The two samples have very similar surface areas (1378 and 1323 $m^2\ g^{-1}$) and micropore volume (0.45 and 0.48 $cm^3\ g\ -1$) but nevertheless the CO_2 and CH_4/CO_2 total adsorption are significantly more important on ROx 0.8. One possible explanation for the difference in adsorption capacity of these 2 activated carbons relays on tn their pore size distribution, ROx presents a more narrow pore distribution with a typical pore size close to 0.7 nm, meanwhile CGran present a wider pore distribution centered at $\approx$ 1 nm. In fact, a narrow pore distribution with an average pore size between 0.7 and 0.8 nm has been reported to be optimal for adsorption of both methane and carbon dioxide [53, 26]. Another explanation lays on the surface chemistry of the samples. Xue et al. [54] found that the surface chemistry of the adsorbent also affects the total adsorbed quantity and individual components adsorption of gas mixtures. As aforementioned CGran has the lowest $pHPZC$ and the highest quantity of acidic surface functionalities, with CO_2 behaving as a lewis acid, the result is the decrease on the adsorbed amount of the equimolar mixture. This is also a valid explanation for the significant decrease on the CNR-115 adsorption compared to RX 1.5.

In addition to the adsorbed quantity, the adsorbent preference for carbon dioxide over methane is a very important indicator of the performance on the CH_4/CO_2 separation. The selectivity factor is then defined by equation 7.10,

$$S_{ij} = \frac{y_i/y_j}{x_i/x_j} \tag{7.10}$$

Where $S_{i/j}$ is the selctivity factor for the i/j separation. On this equation, i stands for CH_4 and j for CO_2, the CH_4 and CO_2 bulk phase mole fractions are represented by y_i and y_j and the adsorbed mole fractions by x_i and x_j.

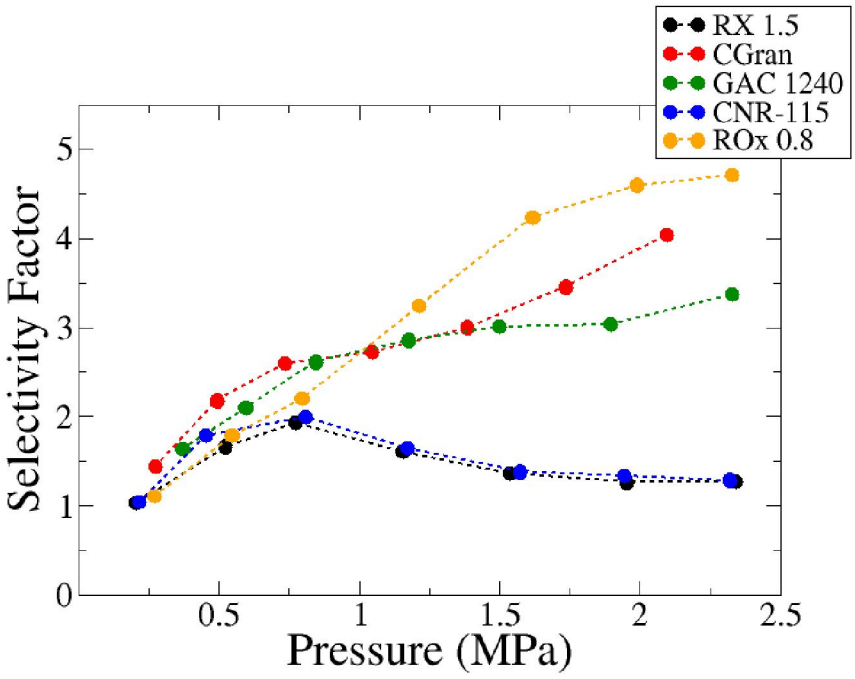

Figure 7.6: CH_4/CO_2 selectivity factor at 303 K for activated carbons: RX 1.5 (black), CGran (red), GAC 1240 (green), CNR-115 (blue) and ROx 0.8 (yellow). Dashed lines are added for visualization purposes.

Figure 7.6 presents the selectivity factor obtained for the activated carbons over the studied pressure range. On this figure, an enhancement of the selectivity of the activated carbons with increasing of the gas pressure can be observed for GAC 1240, CGran and ROx 0.8, explained by the shape of the adsorption isotherms, the adsorbed gas quantity grows steeper for carbon dioxide than for methane for these ACs. The rise in selectivity with pressure is also reported to be related to intermolecular cooperative (energetic) effects [55]. At small pressures the interaction of the gas molecules with the adsorbent is predominant, thus the CO_2 molecules are preferentially adsorbed on the pores surface due to stronger adsorbent-adsorbate interactions. Activated carbons RX 1.5 and CNR-115 present a more developed microporosity with pores under 1 nm (Fig. 7.2), at low pressure the flat and smaller carbon dioxide molecules can easily diffuse in the micropores, at higher pressures, methane molecules are compressed resulting in an increase of their concentration on the adsorbed phase and consequently in a lower selectivity factor. In addition, their high surface area also lowers their selectivity by a weakening of the influence of the adsorbent-adsorbate interaction strength upon the overall adsorption process [40]. The highest selectivity factor at high pressure was found for the activated carbon ROx 0.8 an activated carbon with a mild surface area (1323 $m^2\ g^{-1}$) and the lowest mesopore volume (0.16 cm^3) between the activated carbons. In contrast with the other samples, this carbon showed an important presence of sulfur surface groups during the TPD-MS analysis (SO_2 total desorbed quantity: 0.24 mol g^{-1}), the

existence of S-based surface groups has been found to increase the surface basicity thus resulting in higher CO_2 adsorption and CH_4/CO_2 selectivity [56, 57].

Finally, the surface chemistry of the activated carbons have been reported to have an effect on the selectivity [40, 58], in particular, the presence of basic functionalities is reported to increase selectivity on the low pressure range. In this work, no direct relationship between the presence of such groups and the selectivity was found, instead, the selectivity of the studied activated carbons seems to be given by a mixture of factors including micropore volume, pore size, surface area and surface chemistry. With selectivity been enhanced by small surface area, narrow pore size distribution at an optimal average pore size of 0.8 nm and the presence of basic surface functionalities.

7.5 Conclusions

The present work provides a comprehensive analysis of the mayor factors influencing the adsorption capacity and selectivity of the carbon dioxide and methane mixture onto activated carbons. To this end, the equimolar CH_4/CO_2 binary mixture adsorption isotherms were obtained for a set of five activated carbons on the pressure range of 0 to 3 MPa. The presence of basic functionalities had a possitive effect on the carbon dioxide adsorption capacity. In addition, higher surface area resulted in increased mixture adsorption capacity, however, it's effect was detrimental for the gas separation process, i.e. the adsorption capacity of methane was also increased reducing the adsorbent selectivity. Overall, a mix of textural and chemical properties was found to be responsible the selectivity of an adsorbent.

7.6 Bibliography

[1] Na Yang and Rui Wang. Sustainable technologies for the reclamation of greenhouse gas CO_2. *J. Clean. Prod.*, 103:784–792, 2015.

[2] Eyasu Shumbulo Shuba and Demeke Kifle. Microalgae to biofuels: 'Promising' alternative and renewable energy, review. *Renew. Sust. Energ. Rev.*, 81(May 2017):743–755, 2018.

[3] Muhammad Rizwan Tabassum, Ao Xia, and Jerry D. Murphy. Biomethane production from various segments of brown seaweed. *Energ. Convers. Manage.*, 174(July):855–862, 2018.

[4] Laura Annamaria Pellegrini, Giorgia De Guido, and Stefano Langé. Biogas to liquefied biomethane via cryogenic upgrading technologies. *Renew. Energy*, 124:75–83, 2018.

[5] Rosaria Augelletti, Maria Conti, and Maria Cristina Annesini. Pressure swing adsorption for biogas upgrading. A new process configuration for the separation of biomethane and carbon dioxide. *J. Clean. Prod.*, 140:1390–1398, 2016.

[6] Renju Zacharia, Luis Fernando Gomez, Richard Chahine, Daniel Cossement, and Pierre Benard. Thermodynamics and kinetics of CH_4/CO_2 binary mixture separation by metal-organic frameworks from isotope exchange and adsorption break-through. *Micropor. Mesopor. Mat.*, 263(December 2017):165–172, 2018.

[7] Irini Angelidaki, Laura Treu, Panagiotis Tsapekos, Gang Luo, Stefano Campanaro, Henrik Wenzel, and Panagiotis G. Kougias. Biogas upgrading and utilization: Current status and perspectives. *Biotechnol. Adv.*, 36(2):452–466, 2018.

[8] N. Álvarez-Gutiérrez, M. V. Gil, F. Rubiera, and C. Pevida. Simplistic approach for preliminary screening of potential carbon adsorbents for CO_2 separation from biogas. *J. CO2 Util.*, 28(September):207–215, 2018.

[9] Martin Miltner, Alexander Makaruk, and Michael Harasek. Review on available biogas upgrading technologies and innovations towards advanced solutions. *J. Clean. Prod.*, 161(2017):1329–1337, 2017.

[10] Yuannan Zheng, Qingzhao Li, Chuangchuang Yuan, Qinglin Tao, Yang Zhao, Guiyun Zhang, and Junfeng Liu. Influence of temperature on adsorption selectivity: Coal-based activated carbon for CH 4 enrichment from coal mine methane. *Powder Technol.*, 347:42–49, 2019.

[11] M. Feroldi, A. C. Neves, C. E. Borba, and H. J. Alves. Methane storage in activated carbon at low pressure under different temperatures and flow rates of charge. *J. Clean. Prod.*, 172:921–926, 2018.

[12] J. Valentín-Reyes, R. B. García-Reyes, A. García-González, E. Soto-Regalado, and F. Cerino-Córdova. Adsorption mechanisms of hexavalent chromium from aqueous solutions on modified activated carbons. *J. Environ. Manage.*, 236(July 2016):815–822, 2019.

[13] Surachai Karnjanakom and Panya Maneechakr. Adsorption behaviors and capacities of Cr(VI) onto environmentally activated carbon modified by cationic (HDTMA and DDAB) surfactants. *J. Mol. Struct.*, 1186:80–90, 2019.

[14] George Z. Kyzas, George Bomis, Ramonna I. Kosheleva, Eleni K. Efthimiadou, Evangelos P. Favvas, Margaritis Kostoglou, and Athanasios C. Mitropoulos. Nanobubbles effect on heavy metal ions adsorption by activated carbon. *Chem. Eng. J.*, 356(September 2018):91–97, 2019.

[15] Nasly Delgado, Alberto Capparelli, Agustín Navarro, and Damián Marino. Pharmaceutical emerging pollutants removal from water using powdered activated carbon: Study of kinetics and adsorption equilibrium. *J. Environ. Manage.*, 236(February):301–308, 2019.

[16] Ndagijimana Pamphile, Liu Xuejiao, Yu Guangwei, and Wang Yin. Synthesis of a novel core-shell-structure activated carbon material and its application in sulfamethoxazole adsorption. *J. Hazard. Mater.*, 368(October 2018):602–612, 2019.

[17] G. Durán-Jiménez, V. Hernández-Montoya, M. A. Montes-Morán, A. Bonilla-Petriciolet, and N. A. Rangel-Vázquez. Adsorption of dyes with different molecular properties on activated carbons prepared from lignocellulosic wastes by Taguchi method. *Micropor. Mesopor. Mat.*, 199:99–107, 2014.

[18] M. A. Lopez-Anton, M. Rumayor, M. Díaz-Somoano, and M. R. Martínez-Tarazona. Influence of a CO_2-enriched flue gas on mercury capture by activated carbons. *Chem. Eng. J.*, 262:1237–1243, 2015.

[19] Dariusz Wawrzyńczak, Izabela Majchrzak-Kucęba, Kamil Srokosz, Mateusz Kozak, Wojciech Nowak, Janusz Zdeb, Wojciech Smółka, and Artur Zajchowski. The pilot dual-reflux vacuum pressure swing adsorption unit for CO_2 capture from flue gas. *Sep. Purif. Technol.*, 209(March 2018):560–570, 2019.

[20] Melise F.De Aguiar and Gerson L.V. Coelho. Adsorption of sulfur compounds from natural gas by different adsorbents and desorption using supercritical CO_2. *J. Environ. Chem. Eng.*, 5(5):4353–4364, 2017.

[21] Saeed Ghanbari and Catherine H. Niu. Characteristics of oat hull based biosorbent for natural gas dehydration in a PSA process. *J. Nat. Gas Sci. Eng.*, 61(November 2018):320–332, 2019.

[22] Jose F. Vivo-Vilches, Agustín F. Pérez-Cadenas, Francisco J. Maldonado-Hódar, Francisco Carrasco-Marín, Rui P.V. Faria, Ana M. Ribeiro, Alexandre F.P. Ferreira, and Alirio E. Rodrigues. Biogas upgrading by selective adsorption onto CO_2 activated carbon from wood pellets. *J. Environ. Chem. Eng.*, 5(2):1386–1393, 2017.

[23] Muhammad Rashed Al Mamun, Mohammad Razaul Karim, Mohammed M. Rahman, Abdullah M. Asiri, and Shuichi Torii. Methane enrichment of biogas

by carbon dioxide fixation with calcium hydroxide and activated carbon. *J. Taiwan Inst. Chem. E.*, 58:476–481, 2016.

[24] Fabio Montagnaro, Ana Silvestre-Albero, Joaquín Silvestre-Albero, Francisco Rodríguez-Reinoso, Alessandro Erto, Amedeo Lancia, and Marco Balsamo. Post-combustion CO_2 adsorption on activated carbons with different textural properties. *Micropor. Mesopor. Mat.*, 209:157–164, 2015.

[25] Jarosław Serafin, Urszula Narkiewicz, Antoni W. Morawski, Rafał J. Wróbel, and Beata Michalkiewicz. Highly microporous activated carbons from biomass for CO2capture and effective micropores at different conditions. *J. CO2 Util.*, 18:73–79, 2017.

[26] Volker Presser, John McDonough, Sun-Hwa Yeon, and Yury Gogotsi. Effect of pore size on carbon dioxide sorption by carbide derived carbon. *Energy Environ. Sci.*, 4(8):3059, 2011.

[27] Guojun Yin, Zhenyu Liu, Qingya Liu, and Weize Wu. The role of different properties of activated carbon in CO2adsorption. *Chem. Eng. J.*, 230:133–140, 2013.

[28] Deneb Peredo-Mancilla, Imen Ghouma, Cecile Hort, David Bessieres, and Camélia Matei Ghimbeu. Gas storage. In *Char and Carbon Materials Derived from Biomass*, pages 341–382. Elsevier Inc., Amsterdam, 2019.

[29] Ravikrishna Chatti, Amit K. Bansiwal, Jayashri A. Thote, Vivek Kumar, Pravin Jadhav, Satish K. Lokhande, Rajesh B. Biniwale, Nitin K. Labhsetwar, and Sadhana S. Rayalu. Amine loaded zeolites for carbon dioxide capture: Amine loading and adsorption studies. *Micropor. Mesopor. Mat.*, 121(1-3):84–89, 2009.

[30] Yangyang Liu and Jennifer Wilcox. Effects of surface heterogeneity on the adsorption of CO_2 in microporous carbons. *Environ. Sci. Technol.*, 46(3):1940–1947, 2012.

[31] Mohsen Karimi, José A.C. Silva, Carmem N.D.P. Gonçalves, Jose L. Diaz De Tuesta, Alírio E. Rodrigues, and Helder T. Gomes. CO_2 Capture in Chemically and Thermally Modified Activated Carbons Using Breakthrough Measurements: Experimental and Modeling Study. *Ind. Eng. Chem. Res.*, 57(32):11154–11166, 2018.

[32] Long Yue Meng and Soo Jin Park. One-pot synthetic method to prepare highly N-doped nanoporous carbons for CO_2 adsorption. *Mater. Chem. Phys.*, 143(3):1158–1163, 2014.

[33] Gayatri Yadavalli, Hanwu Lei, Yi Wei, Lei Zhu, Xuesong Zhang, Yupeng Liu, and Di Yan. Carbon dioxide capture using ammonium sulfate surface modified activated biomass carbon. *Biomass Bioenergy*, 98:53–60, 2017.

[34] Burcu Selen Caglayan and A. Erhan Aksoylu. CO_2 adsorption on chemically modified activated carbon. *J. Hazard. Mater.*, 252-253:19–28, 2013.

[35] Yunfeng Zhao, Xin Liu, and Yu Han. Microporous carbonaceous adsorbents for CO_2 separation via selective adsorption. *RSC Adv.*, 5(38):30310–30330, 2015.

[36] D. A. Kennedy and F. H. Tezel. Cation exchange modification of clinoptilolite – Screening analysis for potential equilibrium and kinetic adsorption separations involving methane, nitrogen, and carbon dioxide. *Micropor. Mesopor. Mat.*, 262(July 2017):235–250, 2018.

[37] Deanna M. D'Alessandro, Berend Smit, and Jeffrey R. Long. Carbon dioxide capture: Prospects for new materials. *Angew. Chem. Int. Ed. Engl.*, 49(35):6058–6082, 2010.

[38] Jaewoo Park, Nour F. Attia, Minji Jung, Myoung Eun Lee, Kiyoung Lee, Jaewoo Chung, and Hyunchul Oh. Sustainable nanoporous carbon for CO_2, CH_4, N_2, H_2 adsorption and CO2/CH4 and CO2/N2 separation. *Energy*, 158:9–16, 2018.

[39] Melina C. Castrillon, Karine O. Moura, Caiuã A. Alves, Moises Bastos-Neto, Diana C.S. Azevedo, Jörg Hofmann, Jens Möllmer, Wolf Dietrich Einicke, and Roger Gläser. CO_2 and H_2S Removal from CH_4-Rich Streams by Adsorption on Activated Carbons Modified with K_2CO_3, NaOH, or Fe_2O_3. *Energ. Fuels*, 30(11):9596–9604, 2016.

[40] Shanshan Wang, Linghong Lu, Di Wu, Xiaohua Lu, Wei Cao, Tingting Yang, and Yudan Zhu. Molecular Simulation Study of the Adsorption and Diffusion of a Mixture of CO2/CH4 in Activated Carbon: Effect of Textural Properties and Surface Chemistry. *J. Chem. Eng. Data*, 61(12):4139–4147, 2016.

[41] Stephen Brunauer, P. H. Emmett, and Edward Teller. Adsorption of Gases in Multimolecular Layers. *J. Am. Chem. Soc.*, 60(2):309–319, 1938.

[42] Mikhail Mikhailovich Dubinin and L.V. Radushkevich. *Doklady akademii nauk SSSR*, 55:331, 1947.

[43] Deneb Peredo-Mancilla, Cecile Hort, Mejdi Jeguirim, Camelia Matei Ghimbeu, Lionel Limousy, and David Bessieres. Experimental Determination of the CH_4 and CO_2 Pure Gas Adsorption Isotherms on Different Activated Carbons. *J. Chem. Eng. Data*, 63:3027–3034, 2018.

[44] H. P. Boehm. Some aspects of the surface chemistry of carbon blacks and other carbons. *Carbon*, 32(5):759–769, 1994.

[45] Jan Schönherr, Johannes R. Buchheim, Peter Scholz, and Philipp Adelhelm. Boehm Titration Revisited (Part I): Practical Aspects for Achieving a High Precision in Quantifying Oxygen-Containing Surface Groups on Carbon Materials. *C*, 4(2):21, 2018.

[46] D. Bessières, Th Lafitte, J. L. Daridon, and S. L. Randzio. High pressure thermal expansion of gases: Measurements and calibration. *Thermochim. Acta*, 428(1-2):25–30, 2005.

[47] Yong Chen, Liu-jiang Zhou, Yu-zhen Hong, Feng Cao, Ling Li, and Jian-bao Li. Preparation of high-surface-area activated carbon from coconut shell fibers. *Carbon*, 48(10):3005, 2010.

[48] Carlos Moreno-Castilla. Adsorption of organic molecules from aqueous solutions on carbon materials. *Carbon*, 42(1):83–94, 2004.

[49] Camelia Matei Ghimbeu, Roger Gadiou, Joseph Dentzer, Dominique Schwartz, and Cathie Vix-Guterl. Influence of surface chemistry on the adsorption of oxygenated hydrocarbons on activated carbons. *Langmuir*, 26(24):18824–18833, 2010.

[50] Noelia Álvarez-Gutiérrez, Susana García, María Victoria Gil, Fernando Rubiera, and Covadonga Pevida. Dynamic Performance of Biomass-Based Carbons for CO_2/CH_4 Separation. Approximation to a Pressure Swing Adsorption Process for Biogas Upgrading. *Energ. Fuels*, 30(6):5005–5015, 2016.

[51] Mohammad Boshir Ahmed, Md Abu Hasan Johir, John L Zhou, Huu Hao Ngo, Long Duc Nghiem, Christopher Richardson, Mohammad Ali Moni, and Macguire R Bryant. Activated carbon preparation from biomass feedstock: Clean production and carbon dioxide adsorption. *J. Clean. Prod.*, 225:405–413, 2019.

[52] Jasminder Singh, Soumen Basu, and Haripada Bhunia. Dynamic CO_2 adsorption on activated carbon adsorbents synthesized from polyacrylonitrile (PAN): Kinetic and isotherm studies. *Micropor. Mesopor. Mat.*, 280(November 2018):357–366, 2019.

[53] D. Lozano-Castelló, D. Cazorla-Amorós, A. Linares-Solano, and D. F. Quinn. Influence of pore size distribution on methane storage at relatively low pressure: Preparation of activated carbon with optimum pore size. *Carbon*, 40(7):989–1002, 2002.

[54] Cai Long Xue, Wen Ping Cheng, Wen Ming Hao, Ma Hong, and Rui Feng Li. CH4/N2 Adsorptive Separation on Zeolite X/AC Composites. *J. Chem. (Hindawi, Online)*, 2019:13–14, 2019.

[55] Roger F. Cracknell, David Nicholson, Stephen R. Tennison, and Jill Bromhead. Adsorption and selectivity of carbon dioxide with methane and nitrogen in slit-shaped carbonaceous micropores: Simulation and experiment. *Adsorption*, 2(3):193–203, 1996.

[56] Yongde Xia, Yanqiu Zhu, and Yi Tang. Preparation of sulfur-doped microporous carbons for the storage of hydrogen and carbon dioxide. *Carbon*, 50(15):5543–5553, 2012.

[57] Humaira Seema, K. Christian Kemp, Nhien H. Le, Sung Woo Park, Vimlesh Chandra, Jung Woo Lee, and Kwang S. Kim. Highly selective CO_2 capture by S-doped microporous carbon materials. *Carbon*, 66:320–326, 2014.

[58] Shohreh Fatemi, Masoud Vesali-Naseh, Mona Cyrus, and Jalal Hashemi. Improving CO_2/CH_4 adsorptive selectivity of carbon nanotubes by functionalization with nitrogen-containing groups. *Chem. Eng. Res. Des.*, 89(9):1669–1675, 2011.

Appendix

Table 7.3: RX 1.5 Adsorption data for each component of the CH_4/CO_2 equimolar mixture at 303 K

RX 1.5								
P (MPa)	**n_{exc} CH_4 (mol kg^{-1})**	**n_{exc} CO_2 (mol kg^{-1})**	**n_{exc} TOT (mol kg^{-1})**	y_{CH4}	y_{CO2}	x_{CH4}	x_{CO2}	F.S.
0,2052	1,2441	1,2622	2,5063	0,5036	0,4964	0,4964	0,5036	1,02
0,5234	1,9505	3,0525	5,0030	0,5155	0,4845	0,3899	0,6101	1,66
0,7737	2,3566	3,8819	5,9741	0,5389	0,4611	0,3777	0,6223	1,92
1,1546	2,9535	4,3765	7,3301	0,5205	0,4795	0,4029	0,5971	1,60
1,5371	3,5132	4,7739	8,2871	0,5008	0,4992	0,4239	0,5761	1,36
1,9547	3,9957	5,1547	9,1503	0,4956	0,5044	0,4367	0,5633	1,26
2,3429	4,2973	5,4857	9,7830	0,4997	0,5003	0,4393	0,5607	1,27

Uncertainties: ΔT=0.2 K, ΔP=0.01 MPa, Δn/n=1%

Table 7.4: CGran Adsorption data for each component of the CH_4/CO_2 equimolar mixture at 303 K

CGran								
P (MPa)	**n_{exc} CH_4 (mol kg^{-1})**	**n_{exc} CO_2 (mol kg^{-1})**	**n_{exc} TOT (mol kg^{-1})**	y_{CH4}	y_{CO2}	x_{CH4}	x_{CO2}	F.S.
0,2741	0,6353	0,7634	1,3987	0,5458	0,4542	0,4542	0,5458	1,44
0,4953	0,7355	1,4022	2,1376	0,5345	0,4655	0,3441	0,6559	2,18
0,7369	0,8437	1,9722	2,8159	0,5274	0,4726	0,2996	0,7004	2,60
1,0465	0,9544	2,4035	3,3579	0,5196	0,4804	0,2842	0,7158	2,72
1,3864	1,0073	2,8711	3,8784	0,5133	0,4867	0,2597	0,7403	3,00
1,7355	0,9985	3,2955	4,2940	0,5115	0,4885	0,2325	0,7675	3,45
2,0977	0,9558	3,7111	4,6669	0,5095	0,4905	0,2048	0,7952	4,03
2,7128	0,7547	4,4094	5,1641	0,5075	0,4925	0,1461	0,8539	6,02

Uncertainties: ΔT=0.2 K, ΔP=0.01 MPa, Δn/n=1%

Table 7.5: GAC 1240 Adsorption data for each component of the CH_4/CO_2 equimolar mixture at 303 K

GAC 1240								
P (MPa)	$\mathbf{n_{exc}}$ **CH$_4$ (mol kg^{-1})**	$\mathbf{n_{exc}}$ **CO$_2$ (mol kg^{-1})**	$\mathbf{n_{exc}}$ **TOT (mol kg^{-1})**	y_{CH4}	y_{CO2}	x_{CH4}	x_{CO2}	F.S.
0,3701	1,3821	1,7658	3,1478	0,5609	0,4391	0,4391	0,5609	1,63
0,5956	1,4565	2,5465	4,0031	0,5455	0,4545	0,3639	0,6361	2,09
0,8475	1,4567	3,3044	4,7610	0,5356	0,4644	0,3060	0,6940	2,61
1,1765	1,4955	3,8565	5,3519	0,5256	0,4744	0,2794	0,7206	2,85
1,4991	1,6203	4,2295	5,8499	0,5355	0,4645	0,2770	0,7230	3,00
1,8955	1,5965	4,6456	6,2422	0,5105	0,4895	0,2558	0,7442	3,03
2,3293	1,5611	5,0742	6,6353	0,5088	0,4912	0,2353	0,7647	3,36

Uncertainties: ΔT=0.2 K, ΔP=0.01 MPa, Δn/n=1%

Table 7.6: CNR-115 Adsorption data for each component of the CH_4/CO_2 equimolar mixture at 303 K

CNR-115								
P (MPa)	$\mathbf{n_{exc}}$ **CH$_4$ (mol kg^{-1})**	$\mathbf{n_{exc}}$ **CO$_2$ (mol kg^{-1})**	$\mathbf{n_{exc}}$ **TOT (mol kg^{-1})**	y_{CH4}	y_{CO2}	x_{CH4}	x_{CO2}	F.S.
0,2161	0,8356	0,8515	1,6872	0,5047	0,4953	0,4953	0,5047	1,03
0,4545	1,1345	1,8357	2,9702	0,5245	0,4755	0,3820	0,6180	1,78
0,8097	1,6295	2,8457	4,2752	0,5335	0,4665	0,3641	0,6359	1,99
1,1745	2,0943	3,2647	5,3590	0,5142	0,4858	0,3908	0,6092	1,64
1,5724	2,5574	3,5314	6,0888	0,5005	0,4995	0,4200	0,5800	1,38
1,9456	2,8433	3,8085	6,6517	0,5005	0,4996	0,4274	0,5726	1,34
2,3211	3,1580	4,0862	7,2442	0,4997	0,5003	0,4359	0,5641	1,29

Uncertainties: ΔT=0.2 K, ΔP=0.01 MPa, Δn/n=1%

Table 7.7: ROx 0.8 Adsorption data for each component of the CH_4/CO_2 equimolar mixture at 303 K

ROx 0.8								
P (MPa)	**n_{exc} CH_4 (mol kg^{-1})**	**n_{exc} CO_2 (mol kg^{-1})**	**n_{exc} TOT (mol kg^{-1})**	y_{CH4}	y_{CO2}	x_{CH4}	x_{CO2}	F.S.
0,2702	1,4143	1,4886	2,9029	0,5128	0,4872	0,4872	0,5128	1,10
0,5465	1,7155	2,7655	4,4809	0,5257	0,4743	0,3828	0,6172	1,78
0,7958	1,8543	3,5267	5,3810	0,5364	0,4636	0,3446	0,6554	2,20
1,2156	1,6456	4,6947	6,3403	0,5315	0,4685	0,2596	0,7404	3,23
1,6161	1,4644	5,4755	6,9399	0,5305	0,4695	0,2110	0,7890	4,22
1,9901	1,3953	5,7806	7,1759	0,5256	0,4744	0,1944	0,8056	4,59
2,3297	1,3215	5,9427	7,2642	0,5111	0,4889	0,1819	0,8181	4,70

Uncertainties: ΔT=0.2 K, ΔP=0.01 MPa, Δn/n=1%

CHAPTER 8

CH_4, CO_2 AND N_2 ADSORPTION BY MODIFIED ACTIVATED CARBON

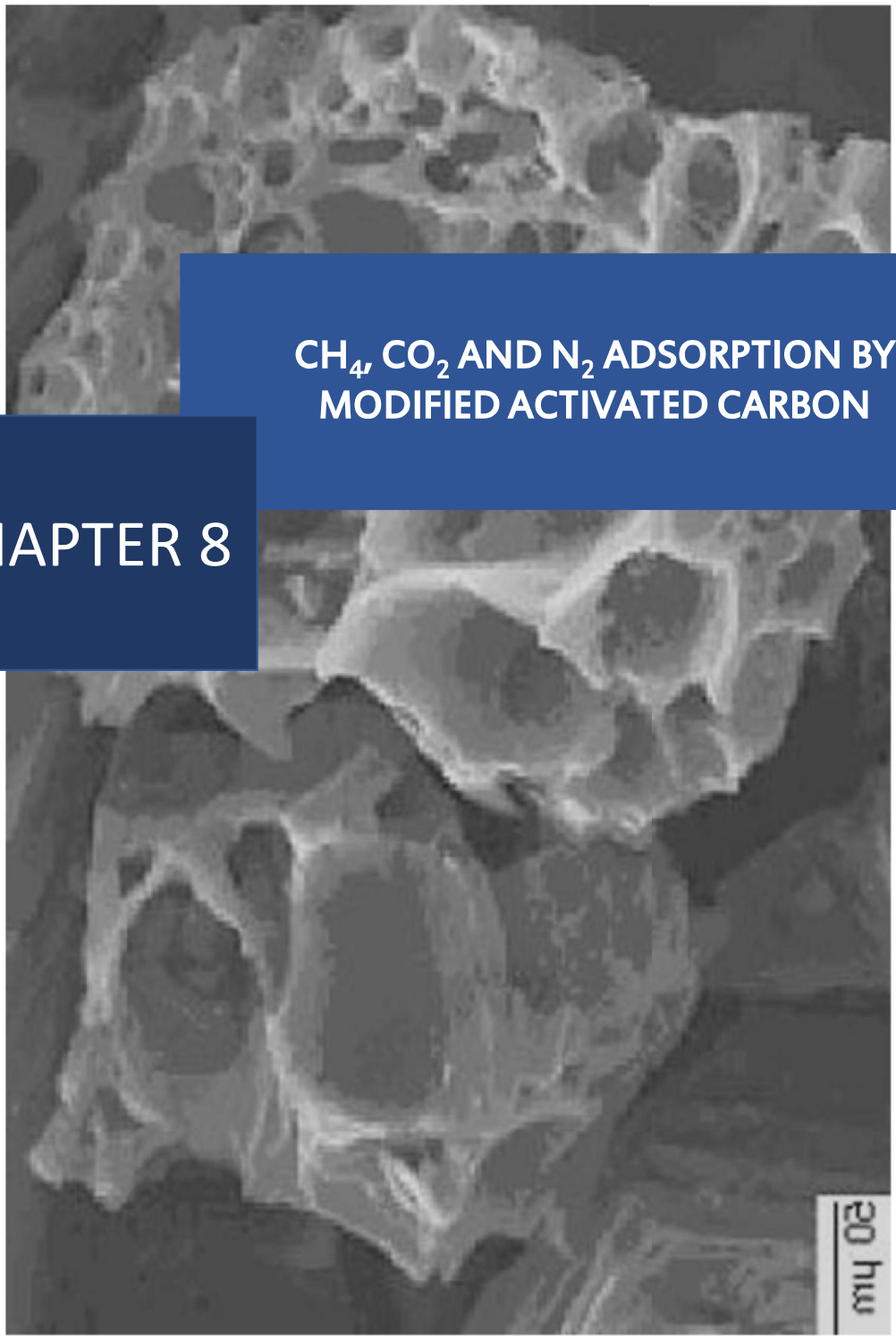

Chapter Outlook

So far, this work has highlighted the advantages of activated carbons (ACs) for CH_4 and CO_2 adsorption, they have developed textural properties and thus, high gas adsorption properties. However, the surface of pristine ACs is not vigorous enough for specific adsorbent-adsorbate interactions and for the selective adsorption of CO_2 over other gas molecules.

An additional advantage of this adsorbents is the possibility to modify their surface chemistry and porous properties by changing the activation conditions or alternatively by applying a post-synthesis treatment. In this context, surface modification processes, such as an increase of the surface basic functionalities are thought to improve the affinity between the adsorbent and carbon dioxide.

The present chapter presents preliminary results for the selective separation of CH_4/CO_2 by a modified version of activated carbon CNR-115. This activated carbon was chosen due to its high pure CO_2 adsorption capacity and developed textural properties, it also presented a low selectivity for the CH_4/CO_2 separation giving room for improvement.

The results clearly indicate an enhanced selectivity of the modified sample, reaching a CH_4/CO_2 selectivity factor of 33.

Introduction

Natural gas (NG) world consumption and production have seen a 16% and 20% increase respectively in the time period from 2006 to 2016 due to its higher energy density and lower emission of green house gases (GHG) compared with coal and oil [1, 2].

Natural gas from underground fields main component is methane (up to 95%) with a minor presence of higher molar mass hydrocarbons (C_{2+}), nitrogen (N_2) and carbon dioxide as impurities [3]. To meet the pipeline-quality requirements, nitrogen and carbon dioxide content must be under 4% and 2% respectively.

An alternative to the use of natural gas is the production of biomethane from biogas by an upgrading process consisting in bringing its methane content up to 98% by the removal of unwanted compounds such as carbon dioxide (CO_2), nitrogen (N_2) and oxygen (O_2). The obtained biomethane can then be used as a vehicular fuel or be inserted into the natural gas pipeline mix [4].

Adsorption based separation of impurities from natural gas and biogas have

advantages over other reparation techniques (e. g. water scrubbing, organic membranes and amines scrubbing) such as low investment and operation costs, low energy consumption and environmental friendliness. Its efficiency relays on the capacity of an adsorbent material to selectively retain one or more of the gas mixture component(s) [5].

Activated carbons high surface area and developed microporosity makes them excellent candidates for CO_2 capture and separation, however they present a major drawback for its application in natural gas upgrading: a low CH_4/CO_2 selectivity in comparison with other adsorbents such as zeolites and carbon molecular sieves (CMS) [6]. Nevertheless, the activated carbons surface can be manipulated through post-synthesis physical (heat treatment), chemical (acid, basic, impregnation) and biological modification (or by a mix of these) to improve their selectivity towards an specific gas [7].

Due to carbon dioxide Lewis acid behavior, the introduction of basic surface functionalities such as nitrogen (N) containing groups has been proposed as a way to increase the affinity between activated carbons and CO_2 [8, 9, 10].

The present chapter aims to study the CO_2, CH_4 and N_2 adsorption behavior of an N-modified activated carbon by a post-treatment method comprising the oxidation of the char followed by ammonia (NH_3) impregnation. To this end, the pure components and CH_4/CO_2 equimolar mixture adsorption isotherms were obtained on the pressure range of 0.1-3.0 MPa at 303 K. The presented preliminary results indicate a superior separation selectivity for the N-modified activated carbon.

8.1 Methodology

8.1.1 Activated carbon modification

Activated carbon CNR-115 has the highest surface area (1714 $m^2\ g^{-1}$) and micropore volume (0.64 $cm^3\ g^{-1}$) of the adsorbent materials analyzed in this work (see Chapter 5), its developed textural properties resulted in a poor selectivity (F.S. $<$ 2) for the CH_4/CO_2 separation (see Chapter 7). For these reasons it was chosen to undergo a surface modification process roughly consisting of oxidation with HNO_3 followed by NH_3 impregnation. The N-modified activated carbon is here labeled as CNR_{ox}.

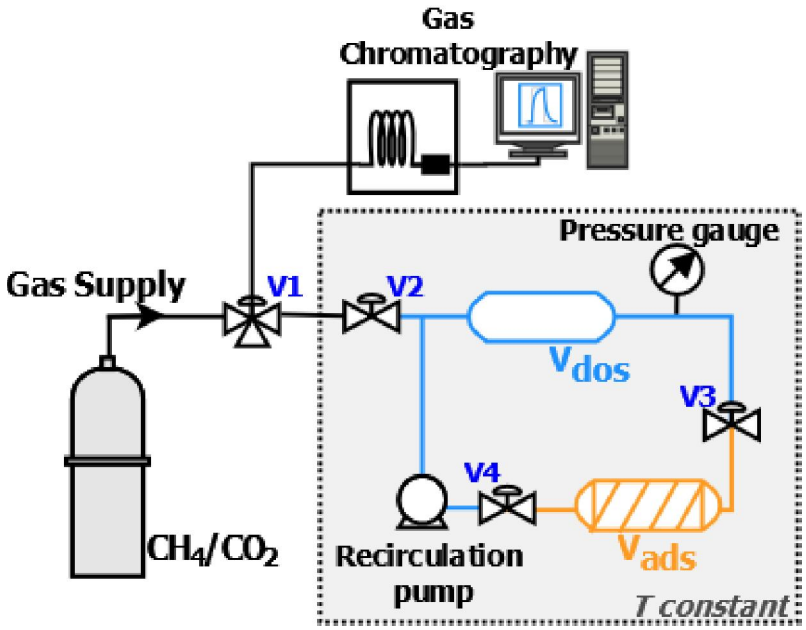

Figure 8.1: Schematization of the high pressure manometric adsorption device coupled with gas chromatography

8.1.2 Determination of adsorption isotherms

CH_4, CO_2 and N_2 pure gas adsorption isotherms were obtained following a mass balance principle based on the gas expansion from a reference volume to a volume containing the adsorbent material under isothermal conditions at 323 K on the pressure range from 0 to 3 MPa (see section 2.1 for more detail).

In addition, the gas mixture adsorption isotherms were obtained using the home-made manometric adsorption device described in section ??. The methodology roughly consisted in expanding the equimolar CH_4/CO_2 gas mixture from a dosing volume V_{dos} to an adsorption cell V_{ads} via a step-by-step method at 323 K and up to 3 MPa. The equations employed for calculating the number of adsorbed moles of each gas from the mixture can be found in section ??.

8.2 Results

The pure gas adsorption isotherms are shown in Figures 8.2-8.4. An important loss of adsorption capacity after activated carbon modification can be depicted for both carbon dioxide and methane. It has been reported that upon modification with nitrogen functional groups, the surface area and pore volume of an adsorbent material is reduced by a pore filling effect of the modifying molecule [12]. The adsorbed quantity was found to be maximal for carbon dioxide and to decreases in the order of $CO_2 > CH_4 > N_2$. It can also be noticed that the saturation of the

Table 8.1: Methane adsorbed quantity

sample	n_{ads} **at 1 MPa** **(mol kg^{-1})**	n_{ads} **at 3 MPa** **(mol kg^{-1})**
CNR - 115	3.1	4.8
CNR_{ox}	0.9	1.2

adsorbent happens at higher pressure for nitrogen ($\approx$ 2.5 MPa) than that of carbon dioxide and methane ($\approx$ 1 MPa).

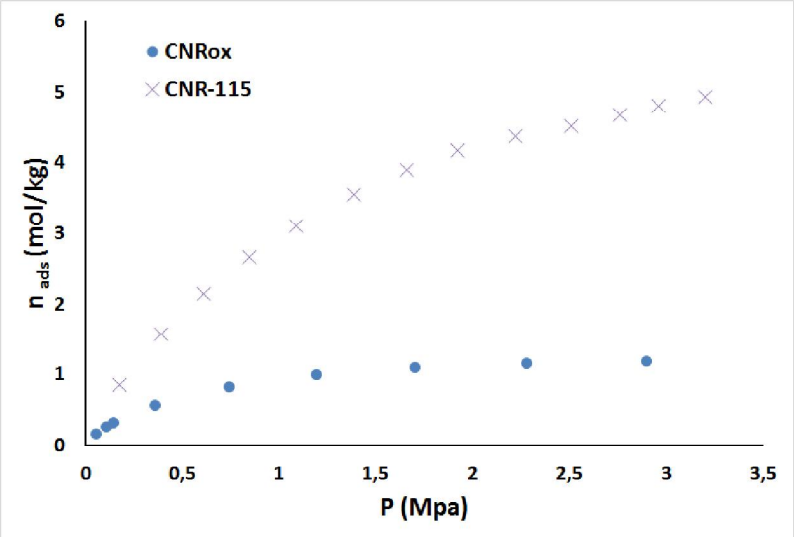

Figure 8.2: Methane adorption isotherm on N-modified activated carbon CNR_{ox} at 303 K. Methane adsorption isotherm of unmodificated activated carbon CNR-115 as shown on Chapter 5 are added as reference.

In addition, Tables 8.1 to 8.3 display the gas adsorbed quantities at near atmospheric pressure (1 MPa) and at high pressure (3 MPa). The difference in the adsorbed amount between the virgin CNR-115 and the N-modified CNR_ox is higher for methane than for carbon dioxide, e.g. at high pressure the adsorption of methane is reduce 4 times, while that of carbon dioxide is reduced by a factor of $\times$ 3, indicating a gain of selectivity towards CO_2 of the adsorbent by the surface modification process.

Table 8.2: Carbon dioxide adsorbed quantity

sample	n_{ads} **at 1 MPa** **(mol kg^{-1})**	n_{ads} **at 3 MPa** **(mol kg^{-1})**
CNR - 115	7.01	12.2
CNR_{ox}	3.0	4.1

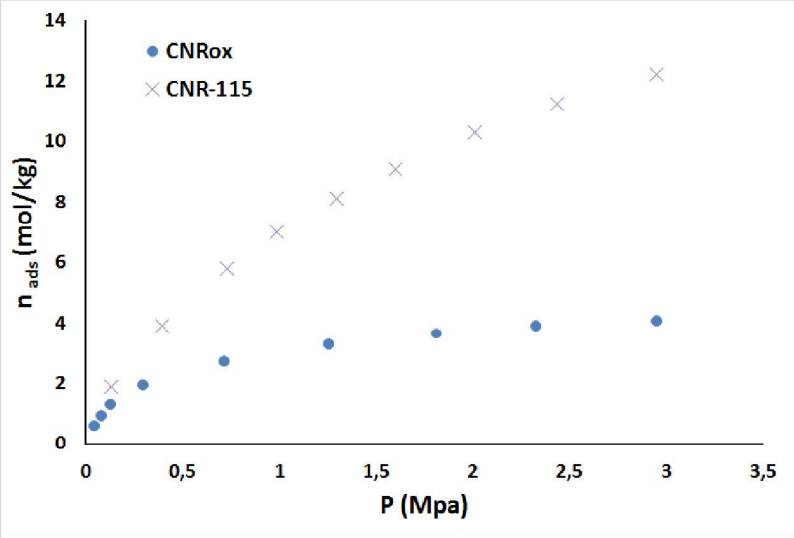

Figure 8.3: Carbon dioxide adorption isotherm on N-modified activated carbon CNR_{ox} at 303 K. Carbon dioxide adsorption isotherm of unmodificated activated carbon CNR-115 as shown on Chapter 5 are added as reference.

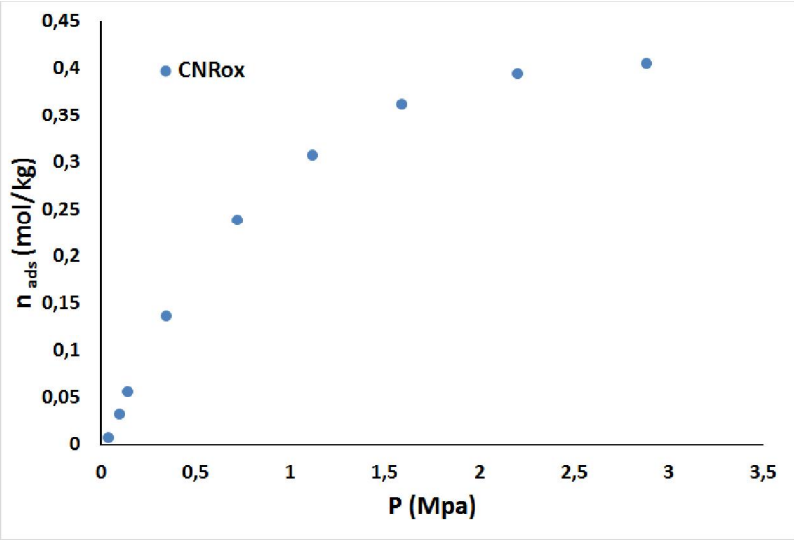

Figure 8.4: Nitrogen adorption isotherm on modified activated carbon CNR_{ox} at 303 K.

The equimolar CH_4/CO_2 adsorption for N-modified AC CNR_{ox} is represented in

Table 8.3: Nitrogen adsorbed quantity

sample	n_{ads} at 1 MPa (mol kg^{-1})	n_{ads} at 3 MPa (mol kg^{-1})
CNR_{ox}	0.28	0.4

Figure 8.5. Although Figure 8.3 shows a prominent decrease of the carbon dioxide pure gas adsorption capacity, the carbon dioxide adsorption from the gas mixture saw an increment from the unmodified sample. On the other hand, the adsorption of methane from the equimolar mixture was found to be negligible for CNR_{ox} indicating that even though the total adsorption capacity was reduced upon surface modification, the vast majority of adsorbed gas is carbon dioxide resulting in an increased CO_2 adsorption capacity from the mixture from the one found for the unmodified sample. The CH_4/CO_2 was calculated to be 33 at 1 MPa for the N-modified activated carbon, a huge improvement from the selectivity of the unmodified sample that showed a maximum selectivity of 2 (see Chapter 7 Fig 5.6).

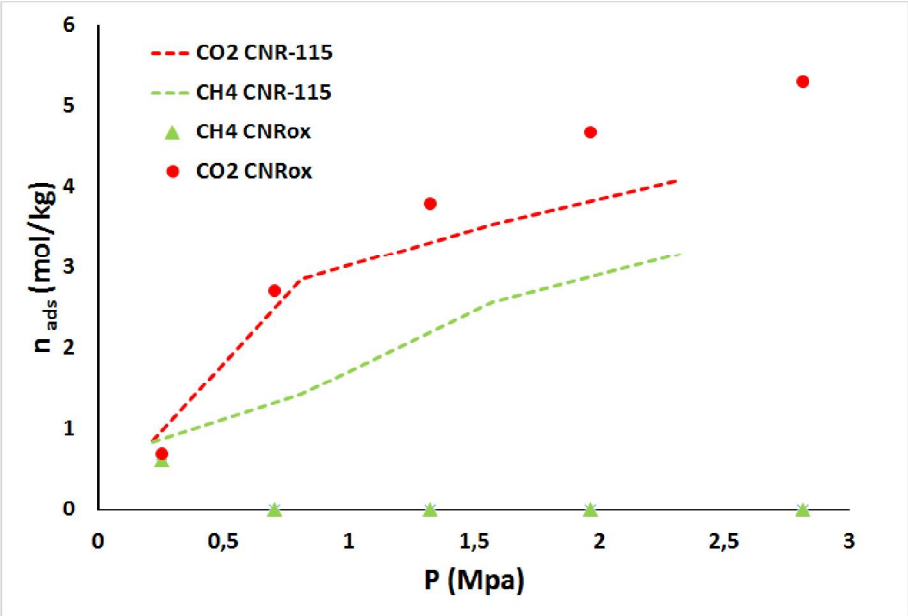

Figure 8.5: Adsorption of individual components of the CH_4/CO_2 equimolar mixture at 303 K by activated carbon CNR_{ox} at 303 K. Results for unmodificated activated carbon CNR-115 as shown on Chapter 7 are added as reference.

8.3 Conclusions

Surface modification by ammonia of activated carbon CNR-115 resulted in a loss of adsorption capacity of CH_4 and CO_2, however the modified material proved to

be highly selective for the CH_4/CO_2 separation, i.e the adsorption of methane was found to be negligible. Although the total adsorption capacity was decreased for CNR***ox***, the adsorption of carbon dioxide from the gas mixture was found to increase with respect to the unmodified sample. The results here shown are very promising, a continuation of the work on modified activated carbons (modification of other ACs, characteriwation of the modified material and dynamic adsorption mesurements) is foreseen for the following months after the presentation for evaluation of this thesis project.

8.4 Bibliography

[1] International Energy Agency. Statistics. Global energy data at your fingertips., 2019.

[2] Jiyeon Lim, Wonjung Choi, Junghoon Mok, and Yongwon Seo. Kinetic CO_2 selectivity in clathrate-based CO_2 capture for upgrading CO_2-rich natural gas and biogas. *Chemical Engineering Journal*, 369(January):686–693, 2019.

[3] Simone Cavenati, Carlos A. Grande, and Alírio E. Rodrigues. Adsorption Equilibrium of Methane, Carbon Dioxide, and Nitrogen on Zeolite 13X at High Pressures. *Journal of Chemical & Engineering Data*, 49(4):1095–1101, 2004.

[4] Diego Curto and Mariano Martín. Renewable based biogas upgrading. *Journal of Cleaner Production*, 224:50–59, 2019.

[5] Carlos A. Grande, Simon Roussanaly, Rahul Anantharaman, Karl Lindqvist, Prachi Singh, and Jasmin Kemper. CO_2 Capture in Natural Gas Production by Adsorption Processes. *Energy Procedia*, 114(1876):2259–2264, 2017.

[6] Zoltán Bacsik, Ocean Cheung, Petr Vasiliev, and Niklas Hedin. Selective separation of CO_2 and $\boldsymbol{CH_4}$ for biogas upgrading on zeolite NaKA and SAPO-56. *Applied Energy*, 162:613–621, 2016.

[7] Nor Adilla Rashidi and Suzana Yusup. An overview of activated carbons utilization for the post-combustion carbon dioxide capture. *Journal of CO2 Utilization*, 13:1–16, 2016.

[8] Gayatri Yadavalli, Hanwu Lei, Yi Wei, Lei Zhu, Xuesong Zhang, Yupeng Liu, and Di Yan. Carbon dioxide capture using ammonium sulfate surface modified activated biomass carbon. *Biomass and Bioenergy*, 98:53–60, 2017.

[9] Rebeca A. Azpiri Solares, Douglas Soares dos Santos, Andrew Ingram, and Joseph Wood. Modelling and parameter estimation of breakthrough curves for

amine-modified activated carbons under pre-combustion carbon capture conditions. *Fuel*, 253(May):1130–1139, 2019.

[10] Xiong Zhang, Shihong Zhang, Haiping Yang, Ye Feng, Yingquan Chen, Xianhua Wang, and Hanping Chen. Nitrogen enriched biochar modified by high temperature CO 2 -ammonia treatment: Characterization and adsorption of CO 2. *Chemical Engineering Journal*, 257:20–27, 2014.

[11] U.S. Secretary of Commerce. Isothermal Properties for Carbon Dioxide, 2017.

[12] P D Jadhav, R V Chatti, R B Biniwale, N K Labhsetwar, S Devotta, and S S Rayalu. Monoethanol Amine Modified Zeolite 13X for CO 2Adsorption at Different Temperatures. *Energy and Fuels*, 21(6):3555–3559, 2007.

GENERAL CONCLUSIONS

CHAPTER 9

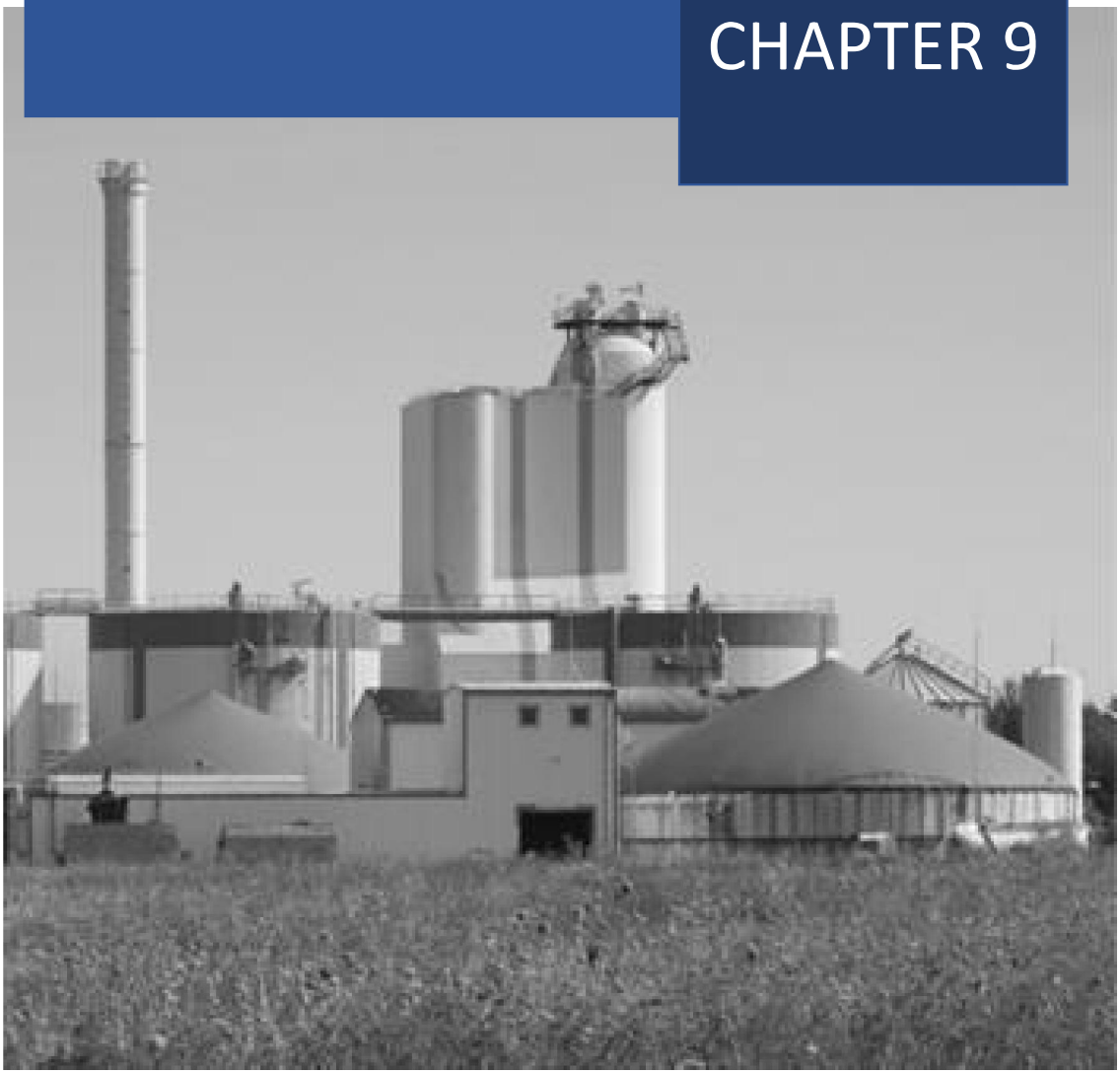

Conclusions

Activated carbons are highly versatile materials, presenting a wide range of surface areas (up to 3000 m^2 g^{-1}) and tunable pore size distribution that makes them suitable for numerous adsorption applications. They have been proposed as promising materials for the separation of CH_4/CO_2 in the framework of biogas upgrading, a process that results in the production of biomethane, a highly purified methane gas stream used as a renewable source of natural gas and vehicular fuels.

A series of adsorption experimental works aiming for the study of the two first adsorption performance indicators (adsorption capacity and selectivity) for the CH_4 and CO_2 adsorption by activated carbons are compiled in this manuscript.

The pure gas adsorption experiments carried out using both commercial and non-commercial biomass-based activated carbons (Chapters 5 and 6) allowed us to establish the factors affecting the maximum adsorption capacity of the adsorbents. In this context the effect of the activation method, textural properties and surface chemistry was depicted, mainly:

- A high surface area and micropore volume in activated carbons enhance the methane and carbon dioxide pure gas adsorption.
- There is no direct relationship between the presence of mesopores in the adsorbent and the adsorption properties, however their presence is necessary for the diffusion of the gas molecules into the smaller pores.
- The presence of basic surface functionalities improves the CO_2 adsorption capacity due to the presence of a quadrupole moment on the gas molecule that gives it a lewis acid behavior.
- The textural and chemical properties that determine the adsorption capacity of activated carbons can be modified by changing the activation method and/or activation conditions, which allows to produce adsorbent materials with the specific properties to increase the adsorption of a given compound.
- AC's can be produce of any carbonaceous material with high carbon percentage and low ash content such as agricultural by-products in a process that allows the production of cheap environmentally-friendly adsorbent materials while reducing the disposal of wastes.

Once that the pure gas adsorption influencing factors were characterized, Chapter 7 follows with the study of the CH_4/CO_2 separation selectivity indicator of the gas separation performance of the samples. The main conclusion obtained from this research are:

- When the two gases are present simultaneously a high surface area and developed porosity allow higher adsorption capacity in exchange, they reduce the separation performance of activated carbons, i.e. a higher volume of both gases is adsorbed with low selectivity factors.

The culmination of this work, and its main scientific contribution lays on its proposition of a new adsorbent material with enhanced adsorption properties presented on Chapter 8. Based on the results obtained on the previous sections, a commercial activated carbon was successfully modified by a post-synthesis treatment consisting in the oxidation of the sample using HNO_3 followed by NH_3 treatment. The results indicate an important rise on the AC CH_4/CO_2 selectivity reaching a remarkable value of 33 (selectivity factor). This value is in fact, between the highest reported values found in the literature for activated carbons.

This work presents highly promising results on the field of adsorption based upgrading of biogas which rise the needs for future work, mainly on the following areas:

- Reproducibility test of the surface modification method by the study of different activated carbons.
- Determination of the influence of humidity on the adsorption capacity and selectivity of the adsorbents.
- Design of an adsorption device coupled with calorimetry measurements for calculating the heat of adsorption of each process and thus the regeneration energy costs.

Conclusions Générales

Les charbons actifs sont des matériaux très polyvalents, avec une large gamme de surfaces spécifiques (variant de 500 à 3000 $m^2\ g^{-1}$) et une distribution de taille de pores adaptable à différents besoins ce qui en font des adsorbants appropriés pour de multiples applications et notamment la séparation du dioxyde de carbone dans les mélanges CH_4/CO_2 constitutifs du biogaz.

A l'issue de ce travail de thèse mené sur des charbons commerciaux et sur des charbons synthétisés à partir de biomasse et activés à partir de différents procédés, les principales conclusions concernant la capacité de stockage des corps purs sont les suivantes :

- une surface spécifique élevée et une microporosité développée s'avèrent être les contributions majeures à l'adsorption du CH_4 et du CO_2 purs ;
- si la présence de mésopores n'a pas influencé directement l'adsorption de ces deux gaz, cependant, un volume mésoporeux minimal est nécessaire pour faciliter la diffusion des molécules de gaz dans les pores de tailles plus petites ;
- en plus des propriétés texturales, la présence de fonctionnalités basiques sur la surface des charbons actifs (CAs) favorise l'interaction avec le moment quadripolaire du CO_2 et se traduit par une affinité plus élevée et de fait une capacité d'adsorption en CO_2 sensiblement augmentée ;
- les propriétés chimiques et texturales qui déterminent la capacité d'adsorption des charbons actifs sont modifiables par le changement de méthode d'activation et/ou des conditions d'activation. Ce qui permet la synthèse de matériaux adsorbants adaptés à chaque application ;
- de plus, ces adsorbants peuvent être fabriqués à partir de toutes matières contenant un pourcentage élevé de carbone et une faible teneur en cendres, ce qui rend l'utilisation de sous-produits agricoles intéressante car elle est peu coûteuse et écologique.

L'étude de mélanges équimolaires CH_4/CO_2 a permis de dresser les conclusions suivantes :

- en présence du mélange, comme dans le cas des corps, les propriétés texturales (l'aire superficielle BET) favorisent l'adsorption CO_2/CH_4, sans modifier la sélectivité de manière notoire. Les sélectivités obtenues pour les différents charbons, oscillant entre 3 et 5, représentent la principale limitation des CAs ;

- la fonctionnalisation du CA avec un procédé d'oxidation et imprégnation à l'ammoniaque a permis d'augmenter la sélectivité jusqu'à des valeurs de 30 qui sont parmi les meilleures reportées dans la littérature pour des charbons actifs. Il s'agit, à notre sens, d'un résultat original qui représente l'apport scientifique majeur de cette thèse ;
- ce procédé de fonctionnalisation diminue l'adsorption de CH_4 sans affecter celle de CO_2 ce qui permet l'augmentation de la sélectivité.

Ce travail ouvre des perspectives prometteuses de travail, parmi lesquelles on mentionnera prioritairement les lignes de travail suivantes :

- la reproductibilité du procédé de fonctionnalisation à partir de l'étude de plusieurs échantillons de charbons ;
- l'influence de la teneur en eau sur les capacités d'adsorption et sur les sélectivités ;
- la détermination des enthalpies d'adsorption afin d'évaluer la coût de régénération.